Enzyme-inspired metal-organic framework materials for supramolecular catalysis

by

Kanchana Prabodhani Samarakoon

B.S., University of Peradeniya, 2014

AN ABSTRACT OF A DISSERTATION

submitted in partial fulfillment of the requirements for the degree

DOCTOR OF PHILOSOPHY

Department of Chemistry
College of Arts and Sciences

KANSAS STATE UNIVERSITY
Manhattan, Kansas

2022

Abstract

This thesis describes to methods for generating multifunctional, enzyme-inspired metal-organic frameworks (MOF) catalysts:

1. Synthesis of a modifiable homochiral MOF material by incorporating a well-known solution phase catalyst
2. Use of a uniform post-synthetic modification strategy to introduce different chemical functionalities, one being a catalytic group.

In Chapter 2, using an established mixed-linker pillared MOF synthesis strategy, we incorporated a solution phase catalyst BINAPO (2,2′-bis(diphenylphosphoryl)-1,1′-binaphthyl) and a modifiable ligand, BDC-NH_2 (2-amino-1,4-benzenedicarboxalic acid) into a modifiable homochiral MOF. We successfully modified the free -NH_2 groups of the modifiable MOF with cyclic anhydrides proving our material is modifiable. We then used both materials as the catalysts for the cyanosilylation of benzaldehyde. Our materials exhibited modest catalytic activity but our efforts at synthesizing a modifiable homochiral material were successful.

For the second method, we introduced two proofs of concept with respect to the generation of uniformly multifunctionalized MOF pores. In Chapter 3 we demonstrated the uniform covalent bifunctionalization of a well-defined MOF, **KSU-1,** to achieve uniformly multifunctionalized confined spaces, which was the first example of uniform covalent functionalization of a MOF. In Chapter 4, we extended our work to orthogonal functionalization which allowed us to generate a uniformly multifunctionalized MOF, not only through multiple paths, but also in a simultaneous one-pot reaction. Finally, in Chapter 5 we used the methods we developed in Chapter 3 and 4 to construct enzyme inspired chiral Brønsted acid MOF catalysts to use in asymmetric epoxide ring opening. Using our unique strategy of uniform independent bifunctionalization, we successful

installed a Brønsted acid catalyst and a chiral group into a well-defined MOF, **KSU-1,** to obtain our desired catalyst.

Enzyme-inspired metal-organic framework materials for supramolecular catalysis

by

Kanchana Prabodhani Samarakoon

B.S., University of Peradeniya, 2014

A DISSERTATION

submitted in partial fulfillment of the requirements for the degree

DOCTOR OF PHILOSOPHY

Department of Chemistry
College of Arts and Sciences

KANSAS STATE UNIVERSITY
Manhattan, Kansas

2022

Approved by:

Major Professor
Dr. Tendai Gadzikwa

Copyright

© Kanchana Prabodhani Samarakoon 2022.

Abstract

This thesis describes to methods for generating multifunctional, enzyme-inspired metal-organic frameworks (MOF) catalysts:

3. Synthesis of a modifiable homochiral MOF material by incorporating a well-known solution phase catalyst
4. Use of a uniform post-synthetic modification strategy to introduce different chemical functionalities, one being a catalytic group.

In Chapter 2, using an established mixed-linker pillared MOF synthesis strategy, we incorporated a solution phase catalyst BINAPO (2,2′-bis(diphenylphosphoryl)-1,1′-binaphthyl) and a modifiable ligand, BDC-NH_2 (2-amino-1,4-benzenedicarboxalic acid) into a modifiable homochiral MOF. We successfully modified the free -NH_2 groups of the modifiable MOF with cyclic anhydrides proving our material is modifiable. We then used both materials as the catalysts for the cyanosilylation of benzaldehyde. Our materials exhibited modest catalytic activity but our efforts at synthesizing a modifiable homochiral material were successful.

For the second method, we introduced two proofs of concept with respect to the generation of uniformly multifunctionalized MOF pores. In Chapter 3 we demonstrated the uniform covalent bifunctionalization of a well-defined MOF, **KSU-1,** to achieve uniformly multifunctionalized confined spaces, which was the first example of uniform covalent functionalization of a MOF. In Chapter 4, we extended our work to orthogonal functionalization which allowed us to generate a uniformly multifunctionalized MOF, not only through multiple paths, but also in a simultaneous one-pot reaction. Finally, in Chapter 5 we used the methods we developed in Chapter 3 and 4 to construct enzyme inspired chiral Brønsted acid MOF catalysts to use in asymmetric epoxide ring opening. Using our unique strategy of uniform independent bifunctionalization, we successful

installed a Brønsted acid catalyst and a chiral group into a well-defined MOF, **KSU-1,** to obtain our desired catalyst.

Table of Contents

List of Figures xii
Acknowledgements xvi
Dedication xviii
Chapter 1 - Introduction 1
1.1. Supramolecular chemistry 1
1.2. Supramolecular catalysis 2
1.3. Metal-organic framework materials 6
1.4. MOFs for supramolecular catalysis 8
1.5. Thesis overview 9
1.6. References 10
Chapter 2 - Enzyme-Inspired Metal-Organic Material for Asymmetric Catalysis 16
2.1. Introduction 16
2.2. Reactions of interest 19
2.3. Synthetic strategy to obtain modifiable homochiral MOF material 19
2.4 Synthesis of modifiable MOF with a chiral ligand 22
2.5. Post-synthetic modification of Zn/DiPyBINAPO/BDC-NH_2MOF 25
2.6. Catalysis experiments 28
2.7. Conclusion 30
2.8. Experimental 30
Material 30
Synthetic procedures 31
Synthesis of (*R*)-4,4 -BINAPO (1) 31
Synthesis of (*R*)-4,4 -DibromBINAPO (2) 31
Synthesis of (*R*)-4,4 -DiPyBINAPO (3) 32
Synthesis of the Zn/DiPyBINAPO/BDC-NH_2 MOF 33
Post-synthetic functionalization of Zn/DiPyBINAPO/BDC-NH_2 MOF with Succinic anhydride 33
Catalysis experiment 33
2.8. Characterization 34

Powder X-ray diffraction (PXRD) 34
Thermogravimetric analysis (TGA) 34
Proton nuclear magnetic resonance (^{1}H NMR) 34
Electrospray Ionization Mass Spectrometry (ESI) 34
2.9. References 35
Chapter 3 - Uniform, Binary Functionalization of a Metal−Organic Framework Material 39
3.1. Introduction 39
3.2. Synthetic strategy for uniformly multifunctionalizing MOF material 41
3.3. Post-synthesis modification of KSU-1 to obtain uniformly bifunctional MOF material. . 43
3.4. Conclusion 48
3.4. Experimental 49
Materials 49
Synthetic procedures 49
Synthesis of KSU-1 49
General Procedure for the reaction of KSU-1 with butyric anhydride (Synthesis of KSU-1_{mono}). 50
General Procedure for the nucleophilic ring-opening of succinic anhydride by KSU-1mono (Synthesis of KSU-1_{bi}) 50
3.5. Characterization 51
Powder X-ray diffraction (PXRD) 51
Nitrogen gas adsorption/desorption 51
Thermogravimetric analysis (TGA) 52
Proton nuclear magnetic resonance (^{1}H NMR) 52
Electrospray Ionization Mass Spectrometry (ESI) 52
3.6. References 52
Chapter 4 - Uniform and Simultaneous Orthogonal Functionalization of a Metal-Organic Framework Material 55
4.1. Introduction 55
4.2. Synthetic strategy for uniform orthogonally functionalizing MOF material 56
4.3. Uniform orthogonal multipath and simultaneous functionalization of KSU-2 58
4.4. Conclusion 66

4.5. Experimental 67
Materials 67
Synthetic Procedures 67
Synthesis of BDC-N_3. 67
Synthesis of KSU-2 68
General Procedure for the CuAAC reaction of MOF materials with phenyl acetylene. .. 68
CuAAC of KSU-2 (Synthesis of KSU-$2_{triazole}$). 68
CuAAC of KSU-$2_{carbamate}$ (Synthesis of KSU-$2_{bi\text{-}Path1}$). KSU-$2_{carbamate}$ 69
General Procedure for the reaction of MOF materials with isopropyl isocyanate 69
Reaction of KSU-2 with isopropyl isocyanate (Synthesis of KSU-$2_{carbamate}$). KSU-2..... 69
Procedure for the simultaneous reaction of KSU-2 with phenyl acetylene and isopropyl isocyanate (Synthesis of KSU-$2_{bi\text{-}Sim}$). 70
4.6. Characterization 70
Powder X-ray diffraction (PXRD) 70
Proton nuclear magnetic resonance (^{1}H NMR) 70
Nitrogen gas adsorption/desorption 71
Thermogravimetric analysis (TGA) 71
Fourier-transform infrared spectroscopy (FTIR) 71
Electrospray Ionization Mass Spectrometry (ESI) 71
Single-crystal X-ray crystallography analysis for KSU-2. 72
4.6. References 76
Chapter 5 - Enzyme-inspired Metal-Organic Framework Materials Based Chiral Brønsted Acid Catalysts 78
5.1. Introduction 78
5.2. Synthetic strategy 80
5.3. Post-synthesis modification of KSU-1 to generate chiral Brønsted acid catalyst 81
5.4. Catalytic activity of Brønsted acid catalyst 87
5.5. Conclusion 90
5.6. Experimental 90
5.7. Characterization 92
Powder X-ray diffraction (PXRD) 92

Thermogravimetric analysis (TGA) 93
Proton nuclear magnetic resonance (^{1}H NMR) 93
5.8. References 93

List of Figures

Figure 1.1. Different supramolecular structures designed for various applications. Reproduced with permission from Ref[16] with permission from the Royal Chemical Society..... 1
Figure 1.2. Key structural features involved in enzyme activity. 2
Figure 1.3. A. Raymond's catalyst. B. Nazarov cyclization reaction catalyzed by the capsule. Adapted with permission from REF[28]. Copyright 2022 American Chemical Society. 4
Figure 1.4. Hydroformylation catalysts based on non-covalent secondary interactions. Copyright 2022 Wiley. Used with permission from Ref[35]..... 5
Figure 1.5. A. Acyl transfer reaction. B. Catalytic porphyrin trimer. Reprinted with permission from REF[36]. Copyright 2022 American Chemical Society. 5
Figure 1.6. Schematic representation of MOF synthesis. 7
Figure 1.7. Different post-synthetic modification methods. 8
Figure 1.8. Enzymatic strategies and how we intend to introduce them into MOF pores. 9
Figure 2.1. Chiral privileged ligands. 17
Figure 2.2. Tartaric acid derived bridging ligand and the resultant MOF structure. 17
Figure 2.3. BINOL-based MOF catalyst. Reprinted with permission from REF[11].Copyright 2022 American Chemical Society..... 18
Figure 2.4. Reaction schemes A. Hydroamination of alkenes B. Cyanosilylation of Benzaldehyde. 19
Figure 2.5. Schematic representation of the synthesis of a pillared mixed-linker MOF. 20
Figure 2.6. MOF ligands A. ligands forming the 2D sheets in the *xy*-plane ligand. B. ligands that pillar the sheets along the *z*-axis. 21
Figure 2.7. Synthesis of DiPyBINAPO ligand. 22
Figure 2.8. Crystal structure of DiPyBINAPO lignad (CCDC 2126199)[28,29.]..... 23
Figure 2.9. A. Reaction scheme for the synthesis of the Zn/DiPyBINAPO/BDC-NH_2 MOF..... 23
Figure 2.10. ^{1}H-NMR of digested Zn/DiPyBINAPO/BDC-NH_2 MOF sample in d_6-DMSO/D_2SO_4 mixture. 24
Figure 2.11. ESI-MS of a sample of the Zn/DiPyBINAPO/BDC-NH_2 MOF sample digested in a solution of DABCO in DMSO..... 25
Figure 2.12. PXRD and TGA data for the Zn/DiPyBINAPO/BDC-NH_2 MOF. 25

Figure 2.13. Post-synthetic modification of the Zn/DiPyBINAPO/BDC-NH_2 MOF using succinic anhydride. 26
Figure 2.14. ^{1}H-NMR of Zn/DiPyBINAPO/BDC-NH_2 MOF functionalized with succinic anhydride, digested in d_6-DMSO/D_2SO_4. 27
Figure 2.15. ESI-MS of Zn/DiPyBINAPO/BDC-NH_2 MOF functionalized with succinic anhydride sample digested in a solution of DABCO in DMSO (Left: Negative mode, Right: Positive mode). 28
Figure 2.16. Cyanosilyaltion of benzaldehyde. 28
Figure 2.17. ^{1}H-NMR of cyanosilylation of Benzaldehyde. 28
Figure 2.18. Catalysis data. 29
Figure 2.19. Reaction between phosphine oxide and TMSCN. 29
Figure 3.1. Seven step post synthetic modification of MTV-IRMOF-74-III. Reprinted with permission from REF [1].Copyright 2022 American Chemical Society. 40
Figure 3.2. Multivariate MOF from non-uniformly arranged linkers with (A) One type of reactive group and, (B) Orthogonal reactivities. Reprinted with permission from REF.[15] Copyright 2022 American Chemical Society. 41
Figure 3.3. Generation of a uniformly multifunctionalized MOF material from well-defined mixed linker MOF. Reprinted with permission from REF.[15] Copyright 2022 American Chemical Society. 42
Figure 3.4. (A) Independently reactive linkers with orthogonal coordination chemistry. (B) KSU-1 viewed down the *c*-axis. (C) Network unit of KSU-1 and its schematic representation. Reprinted with permission from REF.[51] Copyright 2022 American Chemical Society. 43
Figure 3.5. Functionalization of KSU-1 with butyric anhydride. 44
Figure 3.6. (A) ^{1}H NMR spectra of each material in the functionalization sequence digested in a solution of d_6-DMSO/D_2SO_4. (B) ^{1}H NMR of KSU-1_{bi} digested in DABCO/d_6-DMSO. 44
Figure 3.7. Functionalization of KSU-1_{mono} with succinic anhydride. 45
Figure 3.8. ^{1}H-NMR spectrum for KSU-1_{bi} digested in DABCO/d_6-DMSO. 46
Figure 3.9. High-resolution electrospray ionization mass spectrometry (ESI-MS) of KSU-1 (bottom), KSU-1_{mono} (middle), and KSU-1_{bi} (top) in negative (left) and positive (right) mode. 47

Figure 3.10. PXRD and TGA of KSU-1, KSU-1_{mono}, and KSU-1_{bi}. 47
Figure 3.11. Left: N_2 gas adsorption for KSU-1, KSU-1_{mono}, and KSU-1_{bi}. Right: Pore size distribution for KSU-1, KSU-1_{mono}, and KSU-1_{bi}..... 48
Figure 4.1. The use of orthogonally reactive linkers to generate a uniformly functionalized MOF material. Reproduced from Ref.[7] with permission from the Royal Society of Chemistry. .. 56
Figure 4.2. KSU-2 MOF A. Linkers used for KSU-2 MOF synthesis B. Single crystal structure of KSU-2 viewed along the *c*-axis C. Unit cell of KSU-2 D. Schematic representation of KSU-2. 57
Figure 4.3. ^{1}H-NMR of KSU-2 digested in d_6-DMSO/D_2SO_4 mixture. 58
Figure 4.4. Multipath uniform functionalization of KSU-2. 59
Figure 4.5. Stacked ^{1}H-NMRs of KSU-2 functionalized through multiple paths. 60
Figure 4.6. Stacked FT-IRs of KSU-2 functionalized through multiple paths. 61
Figure 4.7. High resolution ESI-MS of positive mode of KSU-$2_{traizole}$ and KSU-$2_{bi\text{-}path1.}$ 62
Figure 4.8. High resolution, ESI-MS positive mode of KSU-$2_{carbamate}$ and KSU-$2_{bi\text{-}path2.}$ 63
Figure 4.9. N_2 gas adsorption measurements KSU-2 functionalized through multiple paths (Closed: Adsorption, Open: Desorption). 64
Figure 4.10. PXRDs and TGA data of KSU-2 functionalized through multiple paths. 65
Figure 4.11. One-pot multifunctionalization of KSU-2 A. Reaction scheme. B. ^{1}H-NMR of digested sample in d_6-DMSO/D_2SO_4 mixture C. ESI-MS of digested sample in a DABCO solution. 66
Figure 5.1 Pool of chiral Brønsted acids.[15] 79
Figure 5.2. Synthetic strategy to introduce a Brønsted acid and a chiral group to KSU-1. 80
Figure 5.3 Pool of A. Cyclic anhydrides B. Chiral isocyanates. 81
Figure 5.4. Installation of Brønsted acids into KSU-1 through cyclic anhydride ring opening reactions. 82
Figure 5.5. ^{1}H-NMR of KSU-1_{acid} after digesting the MOF samples in d_6-DMSO/D_2SO_4 mixture 82
Figure 5.6. Functionalization of KSU-1 with a chiral isocyanate. 83
Figure 5.7. ^{1}H-NMR of KSU-$1_{R\text{-}carbamate}$ digested in d_6-DMSO/D_2SO_4 mixture. 84
Figure 5.8. Functionalization of KSU-$1_{R\text{-}carbamate}$ with cyclic anhydrides. 85
Figure 5.9. ^{1}H-NMRs of series of KSU-$1_{R\text{-}BA}$ digested in a d_6-DMSO/D_2SO_4 mixture. 85

Figure 5.10. PXRD data for functionalized KSU-1 materials. 86
Figure 5.11. TGA data for functionalized KSU-1 materials..... 87
Figure 5.12. Methanolysis of *cis* 2,3-epoxybutane. 87
Figure 5.13. Partial ^{1}H-NMR of aliquots from the catalytic reaction diluted in $CDCl_3$. 89
Figure 5.14. Average conversions with each catalyst after 24 h at RT. 89

Acknowledgements

I would like to express my sincere gratitude to my supervisor Dr. Tendai Gadzikwa for giving me the opportunity to join her lab as one of the first graduate students. I acknowledge her patience, valuable guidance, and support through my PhD. I am indebted for her constant motivation and encouragement to do my level best and I could not ask for a better supervisor and a mentor for my PhD.

I also want to thank my committee members, Dr. Christer Aakeroy, Dr. Ryan Rafferty, Dr. Thimothy Durrett, Dr. Keith Hohn (former) and Dr. Om Prakash for agreeing to be on my committee and for providing a valuable insight to move forward with my research work.

I would like to thank all the SupraCatLab members both present and the past for being there for me and creating lovely memories at K-State. I also want to thank all the undergraduates who helped me throughout my projects.

I am absolutely grateful to the Department of Chemistry, Kansas State University for providing me this valuable opportunity to pursue my dream and providing a friendly and supportive environment. I would like to pass my gratitude to Michael Hinton, for his help to do my teaching duties smoothly and without any issues. I also want to thank NMR manager Dr. Simon Sham for his continuous support with the NMR experiments and maintaining the instrument in good condition. I am grateful to Ron Jackson for helping me setting up the lab, solving all the lab issues and especially being such a wonderful friend. I also want to thank Mr. Tobe Eggers, Mr. James Hodgson and Mr. Bart Bath for helping me every way they can to move forward with my work. I am thankful to all the staff members, Ms. Marry Dooly, Ms. Kim Ross and Ms. Kathy Roeser for helping with all the documentation work and for making sure everything went smoothly.

I want to acknowledge Dr. Manomi Perera and Mr. Sisira Lenagala for being wonderful friends and helping me and my husband settling in Manhattan when we first arrived to US. Also, all my friends in the Department of Chemistry and Manhattan for making my time at K-State memorable.

I want to pass foremost gratitude to my Mother Ms. Menike Samarakoon, Father Mr. Samarakoon and my brother Mr. Arjuna Samarakoon for encouraging me to pursue my dream and believe in me.

Lastly, I am thankful to my husband, Mr. Buddhika Aththanayaka for being my shadow and stood by my side to be successful in this journey.

Dedication

To my husband Buddhika, my son Thinuka, and my parents

Chapter 1 - Introduction

1.1. Supramolecular chemistry

Supramolecular chemistry is the study of chemical systems that are formed from multiple small molecular entities.[1] Small molecules are held together through weak and reversible non-covalent interactions such as metal-coordination, hydrogen bonding, halogen bonding, hydrophobic forces, and Van der Waals forces.[2] Supramolecular chemistry is greatly inspired by Nature and uses Natures' examples to develop more efficient and complex artificial molecular structures. Due to its great importance, supramolecular chemistry was recognized through the Nobel Prize in 1987,[3] which was awarded to Donald J. Cram, Jean-Marie Lehn and Charles J. Pedersen for their equal contribution for the development of host-guest chemistry.[4] Supramolecular chemistry has been used to develop new materials (Figure **1.1**)[5,6] with a wide range of potential applications such as sensing,[7] molecular imaging,[8] metal extraction,[9] drug delivery,[10] chromatography,[11] separation and purification,[12] solar energy conversion,[13] crystal engineering[14] and catalysis.[15] This thesis is focused on applying supramolecular chemistry to the construction of more efficient and selective synthetic catalysts.

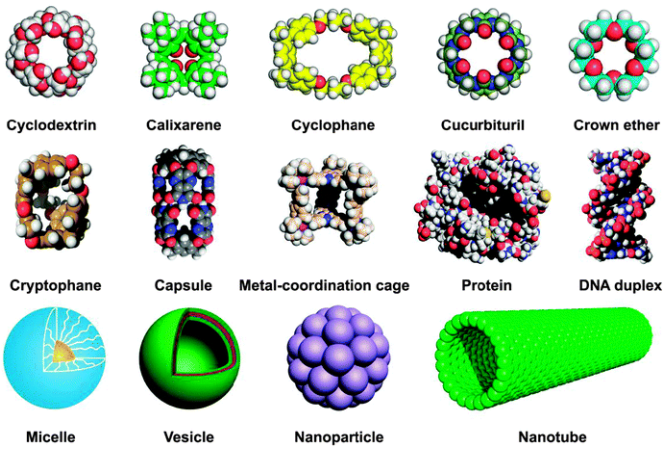

Figure 1.1. Different supramolecular structures designed for various applications. Reproduced with permission from Ref[16] with permission from the Royal Chemical Society.

1.2. Supramolecular catalysis

Supramolecular catalysis involves borrowing strategies from enzymes to design more efficient and selective synthetic catalysts.[17] Enzymes are the fastest and most selective catalysts from Nature and they can catalyze reactions up to 10^6 s^{-1} while they typically result in selectivities of >99% enantiomeric excess (ee).[18,19] Therefore, supramolecular chemists' primary goal is to develop synthetic catalysts that can mimic the mode of action of natural enzymes. This area of research has gained enormous attention due to its practical applications. For example, multiple attempts have been taken to design synthetic catalyst that mimic a class of enzymes, phosphotriesterase which are capable of nerve gas agent hydrolysis. In the field soldiers use gas masks to trap those nerve gases and supramolecular chemists are developing synthetic catalysts to not only to trap those molecules, but to also break them down into non-toxic substances. [20,21]

To explain the excellent reactivity and selectivity of enzymes it is important to identify the key structural features involved in enzymatic systems. They are (Figure **1.2**):[22–25]

i) confinement of the active site,

ii) multiple functional groups within the active site and,

iii) flexibility of the active site.

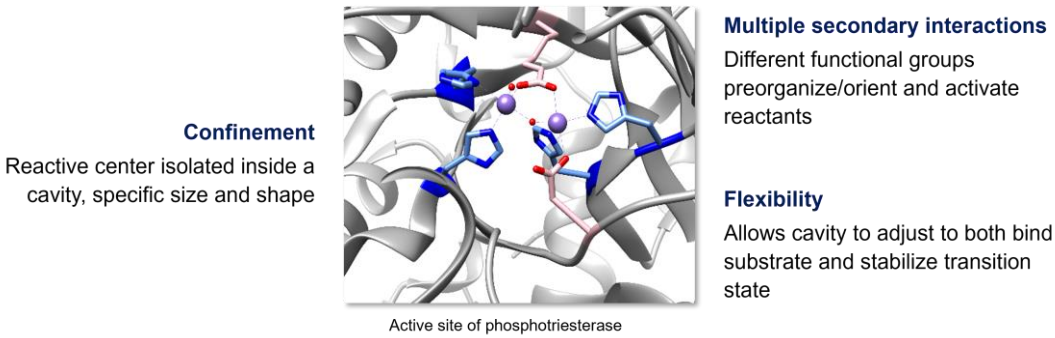

Figure 1.2. Key structural features involved in enzyme activity.

The catalytic sites of enzymes are confined to cavities that have specific size and shape.[26] These cavities ensure reactants with specific shape and size can bind, and confinement increases the local concentration of the reactants. Thereby, it enhances both reaction rate and selectivity. Multiple functional groups at the catalytic site help to pre-organize, activate, and stabilize reactants and intermediates through non-covalent interactions. Flexibility of the catalytic pocket allows it to undergo small adjustments during the reaction ensuring favorable interactions to stabilize reactants and transition states. Collectively all three structural properties make enzymes the most selective and fastest catalysts. Therefore, supramolecular chemists have spent decades attempting to synthesize catalysts that display these enzymatic features.

In their efforts to achieve confinement, chemists have assembled rigid molecular capsules with specific size and shapes.[26] For example Raymond, Bergman, Toste and co-workers have synthesized a variety of molecular cages,[27–29] including a capsule that performs at a rate of 2.1×10^6 times faster than the uncatalyzed reaction (Figure **1.3**). While there are a number of other molecular structures that have been developed to show the importance of encapsulation of active sites into confined spaces.[26,30–33] This work was the first to achieve rate enhancement similar to what is seen in enzymes

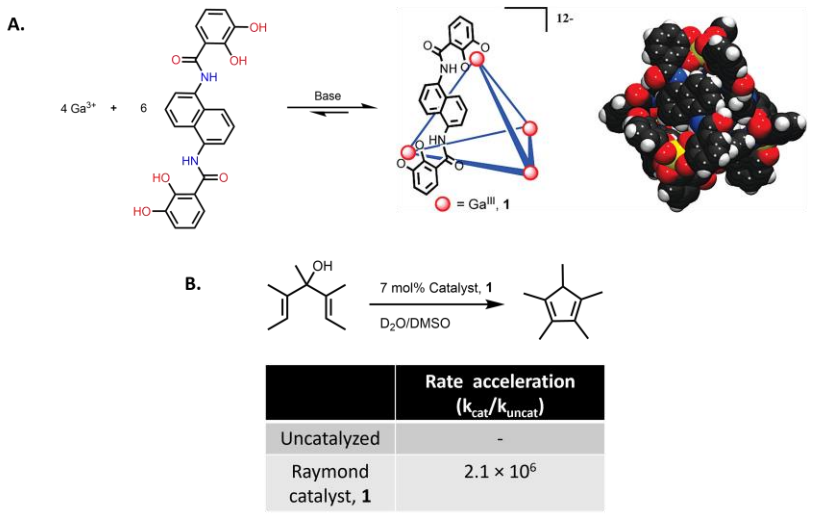

Figure 1.3. A. Raymond's catalyst. B. Nazarov cyclization reaction catalyzed by the capsule. Adapted with permission from REF[28]. Copyright 2022 American Chemical Society.

On the other hand, molecular assemblies that are capable of forming multiple secondary interactions to activate and/or orient substrates have also been studied. For example, the supramolecular assembly that was designed by Reek and co-workers with a bisphosphine ligand and an anion recognition site for the regioselective rhodium-based hydroformylation (Figure **1.4**) [34] exemplifies the importance of having secondary interaction sites to facilitate reaction selectivity.[35] They demonstrated that the binding pocket interacts with anionic alkene substrates resulting in preferential carbonylation of one sp^2 carbon, due to its distance it is from the Rh metal center.

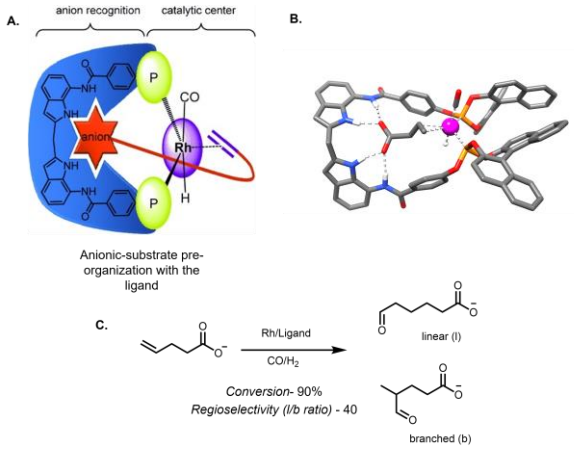

Figure 1.4. Hydroformylation catalysts based on non-covalent secondary interactions. Copyright 2022 Wiley. Used with permission from Ref[35].

To demonstrate the importance of the flexibility of the catalytic pocket different approaches have also been designed. For example, Lindsey et al. demonstrated that the acid catalyzed acyl transfer reaction was accelerated by the presence of Lewis acidic porphyrin trimer assemblies (Figure **1.5**)[36]. They showed that the reaction proceeds through a tightly bound tetrahedral intermediate and suggested that the porphyrin trimer provides a single cavity for the binding of both substrates simultaneously, while they observed a 16-fold increase in the catalytic reaction in the presence of the trimer.

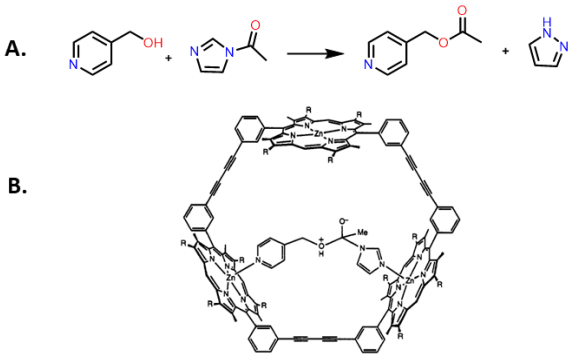

Figure 1.5. A. Acyl transfer reaction. B. Catalytic porphyrin trimer. Reprinted with permission from REF[36]. Copyright 2022 American Chemical Society.

While these enzymatic properties have had some success when applied separately, difficulties arise when attempts are made to combine all three into a one molecular structure. That is because the functional groups that participate in the assembly of supramolecular capsules might have overlapping characteristics with the functional groups that are necessary for having multiple secondary interactions in the cavity. Also, molecular capsules tend to be rigid and rigidity can hinder the catalytic activity through weak substrate binding and poor transition state stabilization.[37] Therefore it is clear that adequate enzyme mimics should possess all three features of the enzyme active site.

Because of the incompatibility of capsule assembly with the functional groups that are necessary for forming secondary interactions, as well as the rigidity of most molecular capsules, designing an enzyme-mimic with active site: i) that have specific size and shape, ii) that are surrounded by multiple chemical functionalities to facilitate substrate activation, iii) that are flexible, has been a daunting process. In order to address this issue, this current thesis work demonstrates how we can use metal-organic frameworks (MOFs) materials as a scaffold to generate such adequate enzyme-mimics.

1.3. Metal-organic framework materials

Metal-organic frameworks (MOFs) materials are a class of porous materials with extended crystalline structure which are composed of metal centers and organic linkers (Figure **1.6**). MOFs offer unique structural diversity compared to other porous materials and their pore size and shape can be controlled with careful selection of metal centers, organic linkers and/or synthetic conditions used.[38–40] Similarly their chemical diversity can be tailored through ligand elaboration and it has been shown that simply by changing the substituents on the organic linker it is possible to synthesize MOFs with different chemical properties.[41] Another way to increase the chemical

diversity of the MOF framework is the mixed-linker pillared MOF synthesis approach where MOF linker, two different linkers are used.[42] Because of their modular nature, tunability and stability[43,44] MOFs have been used in the areas of catalysis,[45] sensing,[46] separation,[47] energy storage and conversion,[48] drug delivery,[49] etc.

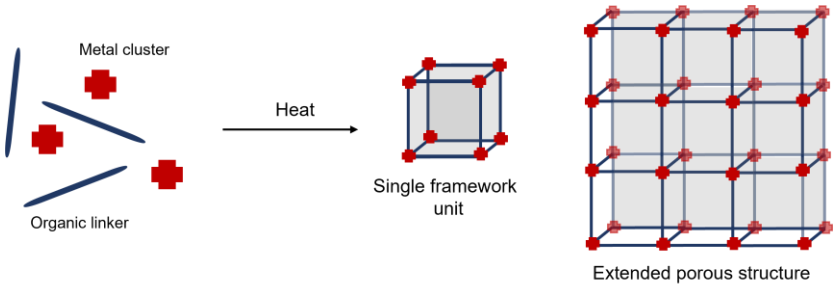

Figure 1.6. Schematic representation of MOF synthesis.

An alternative method to modulate MOF pore chemical environment is through a method called post synthesis modification (PSM) in which a MOF structure is modified without compromising its overall framework integrity. [50–53]Post-synthetic modification is an efficient and facile method not only to decorate MOF pores with different functional groups but also to get MOFs that are unattainable through traditional solvothermal conditions. PSM is not limited to chemical modifications on the organic linkers in the MOF framework, but it has been extended to modify the metal centers (i.e., transmetalation), exchange organic linkers (Solvent Assisted Linker Exchange (SALE)), etc. (Figure **1.6**).[54] PSM is a great platform to generate multifunctional MOF pores with unparalleled chemical complexity[55,56] and it will serve as the key strategy to pursue our goal of introducing enzyme-like complexity to MOFs for supramolecular catalysis.

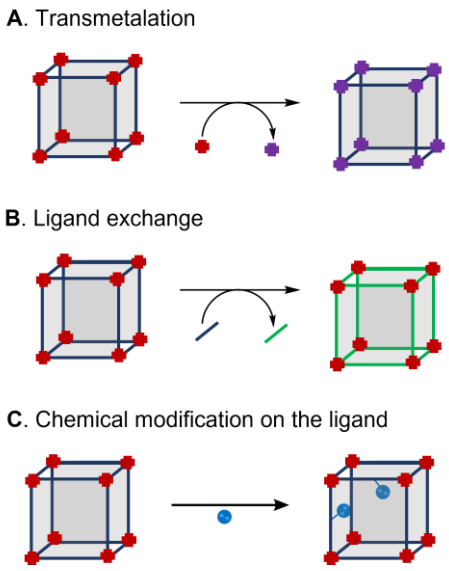

Figure 1.7. Different post-synthetic modification methods.

1.4. MOFs for supramolecular catalysis

As discussed in Section 1.2., to create an enzyme mimic it is necessary to design a synthetic catalyst in which their active site is confined, surrounded by multiple functional groups, as well as being flexible enough to undergo small adjustments during the catalytic reaction. MOFs have built-in confinement because they possess same-size pores throughout the framework and the size of the pores are in the range of small molecules (0.2-2 nm). As explained in Section 1.3., the post-synthetic modification strategy can be used to introduce chemical functionalities that can form secondary interactions (e.g., COOH), as well as to introduce flexibility (e.g., alkyl chains) (Figure **1.8**). Therefore, we believe MOFs are ideal scaffold for constructing more efficient enzyme-inspired catalysts.

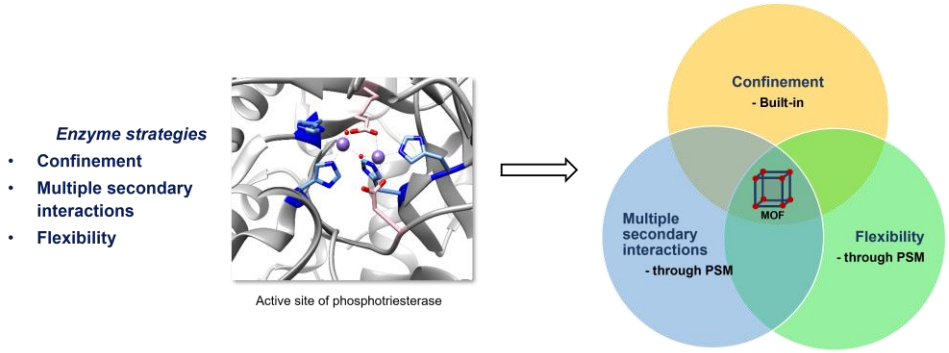

Figure 1.8. Enzymatic strategies and how we intend to introduce them into MOF pores.

1.5. Thesis overview

In order to generate enzyme-inspired catalysts using metal-organic frameworks (MOFs), this thesis describes two routes:

The synthesis of a catalytic MOF using a privileged chiral ligand and a modifiable co-ligand which can be elaborated to add enzymatic features post synthetically.

The synthesis of MOF materials with multiple independently modifiable ligands followed by post-synthetic modification to introduce both catalytic sites and key enzymatic features.

The following chapters describe our efforts in generating enzyme-inspired MOFs through these two routes. In Chapter 2, we detail the synthesis of a modifiable homochiral MOF for asymmetric catalysis by incorporating a well-known solution phase chiral privileged catalyst and a modifiable co-ligand in a MOF. Chapter 3 discusses our attempts at developing a strategy to obtain uniformly multifunctionalized MOF materials through independent covalent modification of a well-defined mixed-linker MOF material. In Chapter 4, we demonstrate a strategy for generating uniformly multifunctionalized MOF pores through both multiple paths and a simultaneous, one-pot reaction using a well-defined orthogonal MOF. In Chapter 5, we describe the use of our unique strategy of uniform independent bifunctionalization to introduce both a

Brønsted acid group and a chiral group to generate a chiral Brønsted acid catalyst for the epoxide ring opening reaction.

1.6. References

(1) Cragg, P. J. An Introduction to Supramolecular Chemistry. In *Supramolecular Chemistry: From Biological Inspiration to Biomedical Applications*; Cragg, P. J., Ed.; Springer Netherlands: Dordrecht, 2010; pp 1–48. https://doi.org/10.1007/978-90-481-2582-1_1.

(2) Mendes, A. C.; Baran, E. T.; Reis, R. L.; Azevedo, H. S. Self-Assembly in Nature: Using the Principles of Nature to Create Complex Nanobiomaterials. *WIREs Nanomedicine Nanobiotechnology* **2013**, *5* (6), 582–612. https://doi.org/10.1002/wnan.1238.

(3) The Nobel Prize in Chemistry 1987 https://www.nobelprize.org/prizes/chemistry/1987/summary/ (accessed 2022 -02 -24).

(4) Lehn, J.-M. Supramolecular Chemistry—Scope and Perspectives Molecules, Supermolecules, and Molecular Devices (Nobel Lecture). *Angew. Chem. Int. Ed. Engl.* **1988**, *27* (1), 89–112. https://doi.org/10.1002/anie.198800891.

(5) Kolesnichenko, I. V.; Anslyn, E. V. Practical Applications of Supramolecular Chemistry. *Chem. Soc. Rev.* **2017**, *46* (9), 2385–2390. https://doi.org/10.1039/C7CS00078B.

(6) Schneider, H.-J. *Applications of Supramolecular Chemistry*; CRC Press, 2012.

(7) Fabbrizzi, L.; Poggi, A. Sensors and Switches from Supramolecular Chemistry. *Chem. Soc. Rev.* **1995**, *24* (3), 197–202. https://doi.org/10.1039/CS9952400197.

(8) Lai, W.-F.; L. Rogach, A.; Wong, W.-T. Chemistry and Engineering of Cyclodextrins for Molecular Imaging. *Chem. Soc. Rev.* **2017**, *46* (20), 6379–6419. https://doi.org/10.1039/C7CS00040E.

(9) Li, A.; Zhai, H.; Li, J.; He, Q. Practical Applications of Supramolecular Extraction with Macrocycles. *Chem. Lett.* **2020**, *49* (10), 1125–1135. https://doi.org/10.1246/cl.200409.

(10) J. Webber, M.; Langer, R. Drug Delivery by Supramolecular Design. *Chem. Soc. Rev.* **2017**, *46* (21), 6600–6620. https://doi.org/10.1039/C7CS00391A.

(11) Ciogli, A.; Kotoni, D.; Gasparrini, F.; Pierini, M.; Villani, C. Chiral Supramolecular Selectors for Enantiomer Differentiation in Liquid Chromatography. In *Differentiation of*

Enantiomers I; Schurig, V., Ed.; Topics in Current Chemistry; Springer International Publishing: Cham, 2013; pp 73–105. https://doi.org/10.1007/128_2013_452.

(12) Nabeel, F.; Rasheed, T.; Bilal, M.; Li, C.; Yu, C.; Iqbal, H. M. N. Bio-Inspired Supramolecular Membranes: A Pathway to Separation and Purification of Emerging Pollutants. *Sep. Purif. Rev.* **2020**, *49* (1), 20–36. https://doi.org/10.1080/15422119.2018.1500919.

(13) Keijer, T.; Bouwens, T.; Hessels, J.; H. Reek, J. N. Supramolecular Strategies in Artificial Photosynthesis. *Chem. Sci.* **2021**, *12* (1), 50–70. https://doi.org/10.1039/D0SC03715J.

(14) Moulton, B.; Zaworotko, M. J. From Molecules to Crystal Engineering: Supramolecular Isomerism and Polymorphism in Network Solids. *Chem. Rev.* **2001**, *101* (6), 1629–1658. https://doi.org/10.1021/cr9900432.

(15) Olivo, G.; Capocasa, G.; Giudice, D. D.; Lanzalunga, O.; Stefano, S. D. New Horizons for Catalysis Disclosed by Supramolecular Chemistry. *Chem. Soc. Rev.* **2021**, *50* (13), 7681–7724. https://doi.org/10.1039/D1CS00175B.

(16) Dong, Z.; Luo, Q.; Liu, J. Artificial Enzymes Based on Supramolecular Scaffolds. *Chem. Soc. Rev.* **2012**, *41* (23), 7890–7908. https://doi.org/10.1039/C2CS35207A.

(17) Wiley-VCH - Supramolecular Catalysis https://www.wiley-vch.de/en/areas-interest/natural-sciences/supramolecular-catalysis-978-3-527-32191-9 (accessed 2022 -03 -09).

(18) Donaldson, T. L.; Quinn, J. A. Kinetic Constants Determined from Membrane Transport Measurements: Carbonic Anhydrase Activity at High Concentrations. *Proc. Natl. Acad. Sci.* **1974**, *71* (12), 4995–4999. https://doi.org/10.1073/pnas.71.12.4995.

(19) Koeller, K. M.; Wong, C.-H. Enzymes for Chemical Synthesis. *Nature* **2001**, *409* (6817), 232–240. https://doi.org/10.1038/35051706.

(20) Letort, S.; Mathiron, D.; Grel, T.; Albaret, C.; Daulon, S.; Djedaïni-Pilard, F.; Gouhier, G.; Estour, F. The First 2IB,3IA-Heterodifunctionalized β-Cyclodextrin Derivatives as Artificial Enzymes. *Chem. Commun.* **2015**, *51* (13), 2601–2604. https://doi.org/10.1039/C4CC09189B.

(21) Pan, J.; Liu, S.; Jia, H.; Yang, J.; Qin, M.; Zhou, T.; Chen, Z.; Jia, X.; Guo, T. Rapid Hydrolysis of Nerve Agent Simulants by Molecularly Imprinted Porous Crosslinked

Polymer Incorporating Mononuclear Zinc(II)-Picolinamine-Amidoxime Module. *J. Catal.* **2019**, *380*, 83–90. https://doi.org/10.1016/j.jcat.2019.10.023.

(22) Ringe, D.; Petsko, G. A. How Enzymes Work. *Science* **2008**, *320* (5882), 1428–1429. https://doi.org/10.1126/science.1159747.

(23) Pompliano, D. L.; Peyman, A.; Knowles, J. R. Stabilization of a Reaction Intermediate as a Catalytic Device: Definition of the Functional Role of the Flexible Loop in Triosephosphate Isomerase. *Biochemistry* **1990**, *29* (13), 3186–3194. https://doi.org/10.1021/bi00465a005.

(24) Fujihashi, M.; Ishida, T.; Kuroda, S.; Kotra, L. P.; Pai, E. F.; Miki, K. Substrate Distortion Contributes to the Catalysis of Orotidine 5′-Monophosphate Decarboxylase. *J. Am. Chem. Soc.* **2013**, *135* (46), 17432–17443. https://doi.org/10.1021/ja408197k.

(25) Lüdtke, S.; Neumann, P.; Erixon, K. M.; Leeper, F.; Kluger, R.; Ficner, R.; Tittmann, K. Sub-Ångström-Resolution Crystallography Reveals Physical Distortions That Enhance Reactivity of a Covalent Enzymatic Intermediate. *Nat. Chem.* **2013**, *5* (9), 762–767. https://doi.org/10.1038/nchem.1728.

(26) Mouarrawis, V.; Plessius, R.; van der Vlugt, J. I.; Reek, J. N. H. Confinement Effects in Catalysis Using Well-Defined Materials and Cages. *Front. Chem.* **2018**, *6*.

(27) Hart-Cooper, W. M.; Clary, K. N.; Toste, F. D.; Bergman, R. G.; Raymond, K. N. Selective Monoterpene-like Cyclization Reactions Achieved by Water Exclusion from Reactive Intermediates in a Supramolecular Catalyst. *J. Am. Chem. Soc.* **2012**, *134* (43), 17873–17876. https://doi.org/10.1021/ja308254k.

(28) Hastings, C. J.; Pluth, M. D.; Bergman, R. G.; Raymond, K. N. Enzymelike Catalysis of the Nazarov Cyclization by Supramolecular Encapsulation. *J. Am. Chem. Soc.* **2010**, *132* (20), 6938–6940. https://doi.org/10.1021/ja102633e.

(29) Hastings, C. J.; Backlund, M. P.; Bergman, R. G.; Raymond, K. N. Enzyme-like Control of Carbocation Deprotonation Regioselectivity in Supramolecular Catalysis of the Nazarov Cyclization. *Angew. Chem. Int. Ed.* **2011**, *50* (45), 10570–10573. https://doi.org/10.1002/anie.201105325.

(30) Donaldson, T. L.; Quinn, J. A. Kinetic Constants Determined from Membrane Transport Measurements: Carbonic Anhydrase Activity at High Concentrations. *Proc. Natl. Acad. Sci.* **1974**, *71* (12), 4995–4999. https://doi.org/10.1073/pnas.71.12.4995.

(31) Gaeta, C.; Talotta, C.; De Rosa, M.; La Manna, P.; Soriente, A.; Neri, P. The Hexameric Resorcinarene Capsule at Work: Supramolecular Catalysis in Confined Spaces. *Chem. – Eur. J.* **2019**, *25* (19), 4899–4913. https://doi.org/10.1002/chem.201805206.

(32) Koblenz, T. S.; Wassenaar, J.; Reek, J. N. H. Reactivity within a Confined Self-Assembled Nanospace. *Chem. Soc. Rev.* **2008**, *37* (2), 247–262. https://doi.org/10.1039/B614961H.

(33) Dong, Z.; Luo, Q.; Liu, J. Artificial Enzymes Based on Supramolecular Scaffolds. *Chem. Soc. Rev.* **2012**, *41* (23), 7890–7908. https://doi.org/10.1039/C2CS35207A.

(34) Dydio, P.; Reek, J. N. H. Supramolecular Control of Selectivity in Transition-Metal Catalysis through Substrate Preorganization. *Chem. Sci.* **2014**, *5* (6), 2135–2145. https://doi.org/10.1039/C3SC53505C.

(35) Dydio, P.; Dzik, W. I.; Lutz, M.; de Bruin, B.; Reek, J. N. H. Remote Supramolecular Control of Catalyst Selectivity in the Hydroformylation of Alkenes. *Angew. Chem. Int. Ed.* **2011**, *50* (2), 396–400. https://doi.org/10.1002/anie.201005173.

(36) Mackay, L. G.; Wylie, R. S.; Sanders, J. K. M. Catalytic Acyl Transfer by a Cyclic Porphyrin Trimer: Efficient Turnover without Product Inhibition. J. Am. Chem. Soc.1994, 116(7), 3141–3142 DOI: 10.1021/ja00086a061.

(37) Hong, C. M.; Kaphan, D. M.; Bergman, R. G.; Raymond, K. N.; Toste, F. D. Conformational Selection as the Mechanism of Guest Binding in a Flexible Supramolecular Host. *J. Am. Chem. Soc.* **2017**, *139* (23), 8013–8021. https://doi.org/10.1021/jacs.7b03812.

(38) Banerjee, R.; Furukawa, H.; Britt, D.; Knobler, C.; O'Keeffe, M.; Yaghi, O. M. Control of Pore Size and Functionality in Isoreticular Zeolitic Imidazolate Frameworks and Their Carbon Dioxide Selective Capture Properties. *J. Am. Chem. Soc.* **2009**, *131* (11), 3875–3877. https://doi.org/10.1021/ja809459e.

(39) Eddaoudi, M.; Kim, J.; Rosi, N.; Vodak, D.; Wachter, J.; O'Keeffe, M.; Yaghi, O. M. Systematic Design of Pore Size and Functionality in Isoreticular MOFs and Their Application in Methane Storage. *Science* **2002**, *295* (5554), 469–472. https://doi.org/10.1126/science.1067208.

(40) Yaghi, O. M.; O'Keeffe, M.; Ockwig, N. W.; Chae, H. K.; Eddaoudi, M.; Kim, J. Reticular Synthesis and the Design of New Materials. *Nature* **2003**, *423* (6941), 705–714. https://doi.org/10.1038/nature01650.

(41) Gadzikwa, T.; Zeng, B.-S.; Hupp, J. T.; Nguyen, S. T. Ligand-Elaboration as a Strategy for Engendering Structural Diversity in Porous Metal–Organic Framework Compounds. *Chem. Commun.* **2008**, No. 31, 3672–3674. https://doi.org/10.1039/B714160B.

(42) Ma, B.-Q.; Mulfort, K. L.; Hupp, J. T. Microporous Pillared Paddle-Wheel Frameworks Based on Mixed-Ligand Coordination of Zinc Ions. *Inorg. Chem.* **2005**, *44* (14), 4912–4914. https://doi.org/10.1021/ic050452i.

(43) Kalmutzki, M. J.; Hanikel, N.; Yaghi, O. M. Secondary Building Units as the Turning Point in the Development of the Reticular Chemistry of MOFs. *Sci. Adv. 4* (10), eaat9180. https://doi.org/10.1126/sciadv.aat9180.

(44) Systematic Design of Pore Size and Functionality in Isoreticular MOFs and Their Application in Methane Storage https://www.science.org/doi/10.1126/science.1067208?url_ver=Z39.88-2003&rfr_id=ori:rid:crossref.org&rfr_dat=cr_pub%20%200pubmed (accessed 2021 -09 -28).

(45) Wang, Q.; Yang, G.; Fu, Y.; Li, N.; Hao, D.; Ma, S. Nanospace Engineering of Metal-Organic Frameworks for Heterogeneous Catalysis. *ChemNanoMat* **2022**, *8* (1), e202100396. https://doi.org/10.1002/cnma.202100396.

(46) Lei, J.; Qian, R.; Ling, P.; Cui, L.; Ju, H. Design and Sensing Applications of Metal–Organic Framework Composites. *TrAC Trends Anal. Chem.* **2014**, *58*, 71–78. https://doi.org/10.1016/j.trac.2014.02.012.

(47) Li, J.-R.; Kuppler, R. J.; Zhou, H.-C. Selective Gas Adsorption and Separation in Metal–Organic Frameworks. *Chem. Soc. Rev.* **2009**, *38* (5), 1477–1504. https://doi.org/10.1039/B802426J.

(48) Zhou, J.; Wang, B. Emerging Crystalline Porous Materials as a Multifunctional Platform for Electrochemical Energy Storage. *Chem. Soc. Rev.* **2017**, *46* (22), 6927–6945. https://doi.org/10.1039/C7CS00283A.

(49) He, C.; Liu, D.; Lin, W. Nanomedicine Applications of Hybrid Nanomaterials Built from Metal–Ligand Coordination Bonds: Nanoscale Metal–Organic Frameworks and Nanoscale

Coordination Polymers. *Chem. Rev.* **2015**, *115* (19), 11079–11108. https://doi.org/10.1021/acs.chemrev.5b00125.

(50) Deria, P.; Mondloch, J. E.; Karagiaridi, O.; Bury, W.; Hupp, J. T.; Farha, O. K. Beyond Post-Synthesis Modification: Evolution of Metal–Organic Frameworks via Building Block Replacement. *Chem. Soc. Rev.* **2014**, *43* (16), 5896–5912. https://doi.org/10.1039/C4CS00067F.

(51) Garibay, S. J.; Wang, Z.; Tanabe, K. K.; Cohen, S. M. Postsynthetic Modification: A Versatile Approach Toward Multifunctional Metal-Organic Frameworks. *Inorg. Chem.* **2009**, *48* (15), 7341–7349. https://doi.org/10.1021/ic900796n.

(52) Kalaj, M.; Cohen, S. M. Postsynthetic Modification: An Enabling Technology for the Advancement of Metal–Organic Frameworks. *ACS Cent. Sci.* **2020**, *6* (7), 1046–1057. https://doi.org/10.1021/acscentsci.0c00690.

(53) Wang, Z.; Cohen, S. M. Postsynthetic Covalent Modification of a Neutral Metal−Organic Framework. *J. Am. Chem. Soc.* **2007**, *129* (41), 12368–12369. https://doi.org/10.1021/ja074366o.

(54) Mandal, S.; Natarajan, S.; Mani, P.; Pankajakshan, A. Post-Synthetic Modification of Metal–Organic Frameworks Toward Applications. *Adv. Funct. Mater.* **2021**, *31* (4), 2006291. https://doi.org/10.1002/adfm.202006291.

(55) Kalaj, M.; Cohen, S. M. Postsynthetic Modification: An Enabling Technology for the Advancement of Metal–Organic Frameworks. *ACS Cent. Sci.* **2020**, *6* (7), 1046–1057. https://doi.org/10.1021/acscentsci.0c00690.

(56) Tanabe, K. K.; Cohen, S. M. Postsynthetic Modification of Metal–Organic Frameworks—a Progress Report. *Chem. Soc. Rev.* **2011**, *40* (2), 498–519. https://doi.org/10.1039/C0CS00031K.

Chapter 2 - Enzyme-Inspired Metal-Organic Material for Asymmetric Catalysis

2.1. Introduction

Metal-organic frameworks (MOFs) materials have drawn much attention as a scaffold for catalysis due to their well-defined and tunable porous structure.[1–3] Our primary goal is to utilize MOFs as a solid support to generate more efficient and selective enzyme-inspired catalysts. As discussed in Chapter 1, enzymes are the fastest and most selective catalysts because of their catalytic sites' unique physical characteristics and the strategies that they employ. Enzymes' active sites are; i) confined to small cavities ii) rich with multiple functionalities to form secondary interactions and iii) flexible to undergo small adjustments to facilitate the catalytic reaction. We believe it is possible to design efficient synthetic catalysts using MOFs by incorporating enzymes' unique features. Because:

i) they have pores in the dimensions of small molecules, i.e. confinement

ii) their pores can be decorated with multiple functional groups that can form secondary interactions with reactants and/or intermediates, and

iii) flexibility can also be introduced post-synthetically.

In order to make such catalysts, one strategy is to immobilize previously known solution-phase catalysts into the MOF framework. This method is attractive as it can provide homogenous distribution and high loading of the catalytic ligand. It also allows us to heterogenize homogenous catalysts and take the advantage of both homogenous and heterogenous catalysts.[4] But it is challenging because of the high unpredictability in MOF synthesis.[5]

Recently the generation of asymmetric heterogenous MOF (homochiral MOF) catalysts has become an important area of research because it results in enantiomerically enriched products.[6]

Homochiral MOFs can be synthesized using building blocks that are totally racemic components (self-resolved during crystal growth)[7–9] or by using readily available chiral ligands (e.g. chiral privileged ligands (Figure **2.1.**). The second approach is more prominent and widely used.

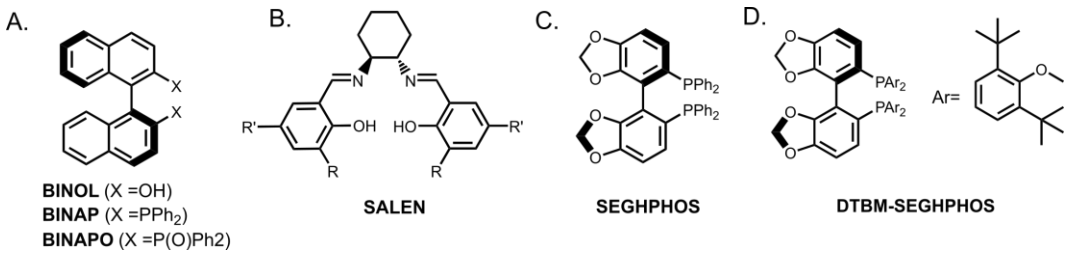

Figure 2.1. Chiral privileged ligands.

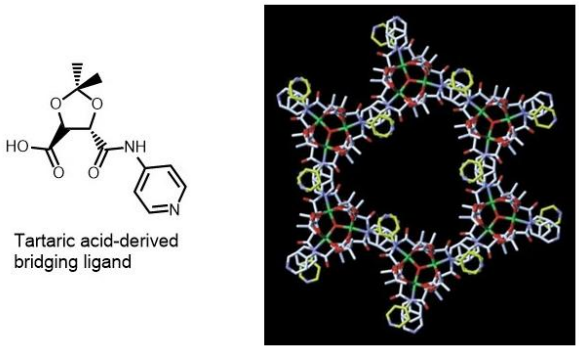

Figure 2.2. Tartaric acid derived bridging ligand and the resultant MOF structure**.**

The earliest reported catalytically active MOF was synthesized by Kim et al. using an enantiopure tartaric acid-derived bridging ligand with free pyridine groups for asymmetric transesterification.[10] The enantiomeric excess (ee) values were very low due to the substantial distances between the catalytic site and chiral environment (Figure **2.2.**). Therefore later, Wenbin Lin and co-workers introduced a new strategy to synthesize homochiral MOFs through post-synthetic modification.[11] They synthesized a homochiral cadmium based MOF using 1,1′-bi-2-naphthol (BINOL), modified with two pyridyl groups. The primary function of the pyridyl groups was to provide the coordination sites to the metal centers to form the framework and each pore environment was identical throughout the structure. Catalytic sites were created by reacting the

BINOL -OH groups with $Ti(O^iPr)_4$ (Figure **2.3.**). The synthesized heterogenous catalyst was used for the addition of diethyzinc to aromatic aldehydes to afford chiral secondary alcohols achieving ees of up to 93%. This work demonstrated that the successful post-synthetic modification of a chiral MOF synthesized with chiral bridging ligand could have a huge impact on catalytic activity.

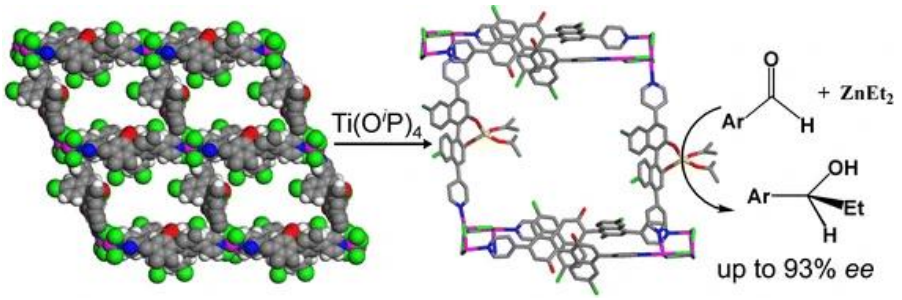

Figure 2.3. BINOL-based MOF catalyst. Reprinted with permission from REF[11].Copyright 2022 American Chemical Society**.**

A related approach to attain chiral MOFs is to use already metalated chiral bridging ligands to synthesize the MOF. In order to incorporate these homogenous catalysts into MOF frameworks, ligands are modified with metal coordinating groups. The very first example was reported by Wenbin Lin and co-workers where they modified Ru-BINAP ligands with phosphonate groups and synthesized a zirconium MOF for asymmetric hydrogenation catalysis.[12] Introducing the BINAP ligand into a MOF framework was quite challenging due to the difficulty of synthesizing the bridging BINAP ligand and the phosphine groups were sensitive to the MOF crystallization conditions.[5]

Later on Salen,[13–15] BINOL[13] and BINAPO (2,2′-bis(diphenylphosphoryl)-1,1′-binaphthyl)[12] ligands were used to synthesize different chiral catalytic MOFs for various chemical reactions.[16] Some of these were mixed-linker MOFs but the second linker was merely for structural purposes only. Our goal is to apply these strategies we learned from literature to make better enzyme-mimics using MOF structures. In this chapter we discuss our attempt to create a

modifiable mixed-linker homochiral MOFs for application in asymmetric catalysis. With careful selection of the second linker, we envisioned that we would be able to systematically modify the environment around the chiral catalyst. Thereby we can finetune the catalytic activity of the chiral MOF.

2.2. Reactions of interest

To demonstrate the utility of modifiable, mixed linker homochiral MOFs, our initial idea was to construct MOFs catalysts for the hydroamination of unbiased aliphatic amines (Figure **2.4**). Chiral aliphatic amines have been identified as one of the important moieties in the biologically relevant molecules.[17] Because of the challenges associated with this reaction, at the beginning we decided to focus on a much simpler yet synthetically important reaction to test the catalytic activity of the MOF. We will test the newly synthesized MOF in the cyanosilylation of benzaldehyde to produce cyanohydrins. Cyanohydrins are important intermediates in the synthesis of α-aminonitriles, α-hydroxyketones, α-hydroxyacids and many more important pharmaceutical ingediatents.[18] Trimethylsilyl cyanide (TMSCN) is used as the cyanide source due to its ease of handling and the low dissociation energy of the Si-C bond.[18]

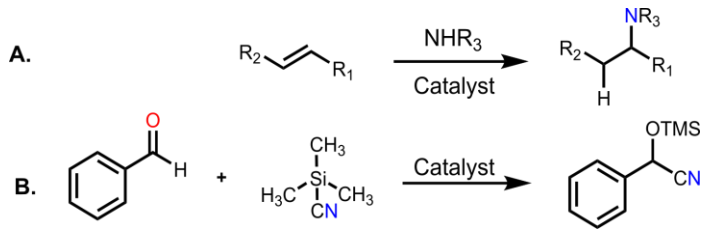

Figure 2.4. Reaction schemes A. Hydroamination of alkenes B. Cyanosilylation of Benzaldehyde**.**

2.3. Synthetic strategy to obtain modifiable homochiral MOF material

As discussed in Section 2.1, our intention is to develop an enzyme-inspired homochiral MOF to perform asymmetric catalysis. To construct the homochiral MOF material we chose the

well-established mixed-linker, pillared MOF synthesis method.[19,20] The desired MOF is synthesized with the combination of a bridging chiral privileged ligand and a modifiable co-ligand (Figure **2.5**). The modifiable ligand, which is a dicarboxylate creates 2D sheets in the *xy*-plane of the MOF and the chiral ligand, the dipyridyl is along the *z*-axis connecting the 2D sheets to form the MOF framework. This results in a catalytic MOF in which each unit cell has a chiral catalytic ligand and a modifiable co-ligand.

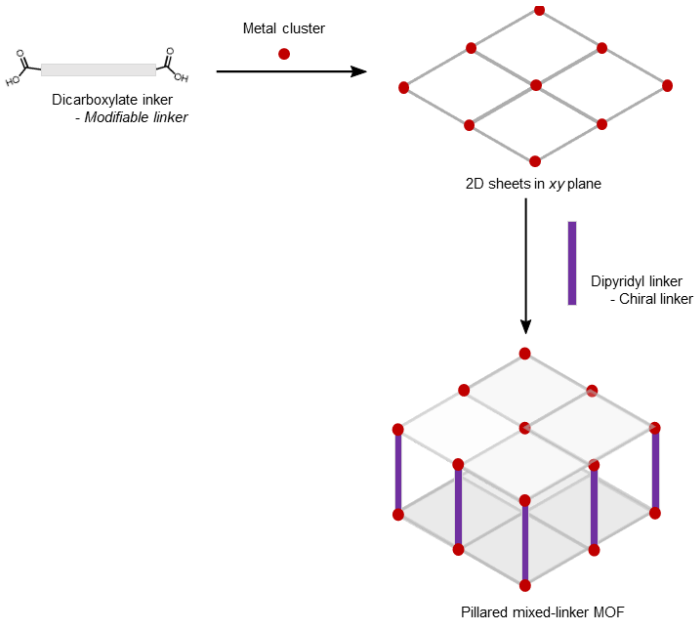

Figure 2.5. Schematic representation of the synthesis of a pillared mixed-linker MOF**.**

Buchwald and co-workers have demonstrated, a chiral diphosphine ligand DTBM-SEGPHOS (5,5'-Bis[di(3,5-ditert-butyl-4-methoxyphenyl) phosphino]-4,4'-bi-1,3-benzodioxole) as an effective catalyst in the conversion of *symmetric* alkenes into their aliphatic amines.[17]In the presence of *asymmetric* alkenes, they achieved very high enantioselectivity but poor activity. According to the recent mechanistic study it was revealed that:[21,22]

i) the higher catalytic activity of the DTBM-SEPHOS is a result of ligand-substrate dispersive interactions (interactions through space) caused by the bulky t-butyl groups

ii) the presence of a chiral ligand is import for the enantioselectivity.

Therefore, we envisioned that by incorporating a chiral catalyst into a confined space i.e. MOF material could result higher enantioselectivity, regioselectivity while modifiable ligand can used to introduce groups that can influence activity by the providing dispersive interactions.

To construct the chiral MOF materials, we chose two different chiral privileged hydroamination ligands, DTBM-SEGHPHOS and BINAP (Figure **2.6**). In addition to the DTBM-SEGPHOS catalyst, we chose the BINAP because we hoped to demonstrate how we can use the co-ligand to introduce appropriate secondary functionality to tune its catalytic activity. As the modifiable ligand we choose commercially available 2-amino-1,4-benzenedicarboxalic acid (BDC-NH_2) (Figure **2.6**). Therefore, we can use the nucleophilic -NH_2 group to introduce either an activating co-catalyst or to enhance the bulkiness around the catalyst site.[23–26]

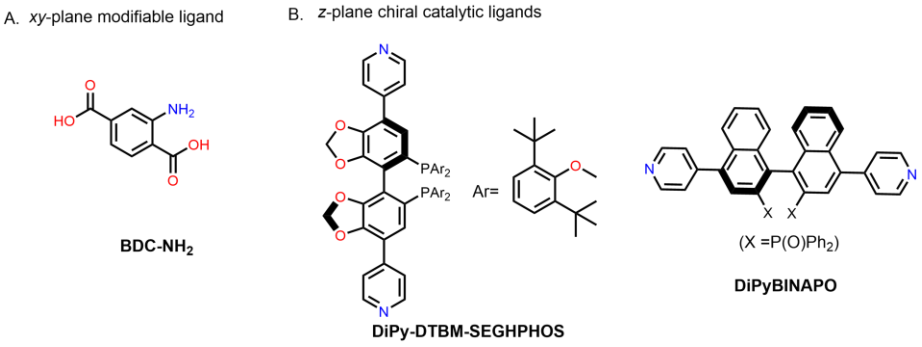

Figure 2.6. MOF ligands A. ligands forming the 2D sheets in the *xy*-plane ligand. B. ligands that pillar the sheets along the *z*-axis.

2.4 Synthesis of modifiable MOF with a chiral ligand

The synthesis of both the modified DTBM-SEGHPOS (DiPy-DTBM-SEGHPHOS) and BINAPO (DiPyBINAPO) ligands with axial pyridine groups were attempted following modified literature procedures.[27]The synthesis of DiPy-DTBM-SEGHPHOS was not successful due to a few challenging synthetic steps but DiPyBINAPO was successfully synthesized on a gram scale (Figure **2.7**). The final product was confirmed by proton nuclear resonance spectroscopy (^{1}H-NMR) and by single crystal X-ray crystallography **(**Figure **2.8)**.[28,29]

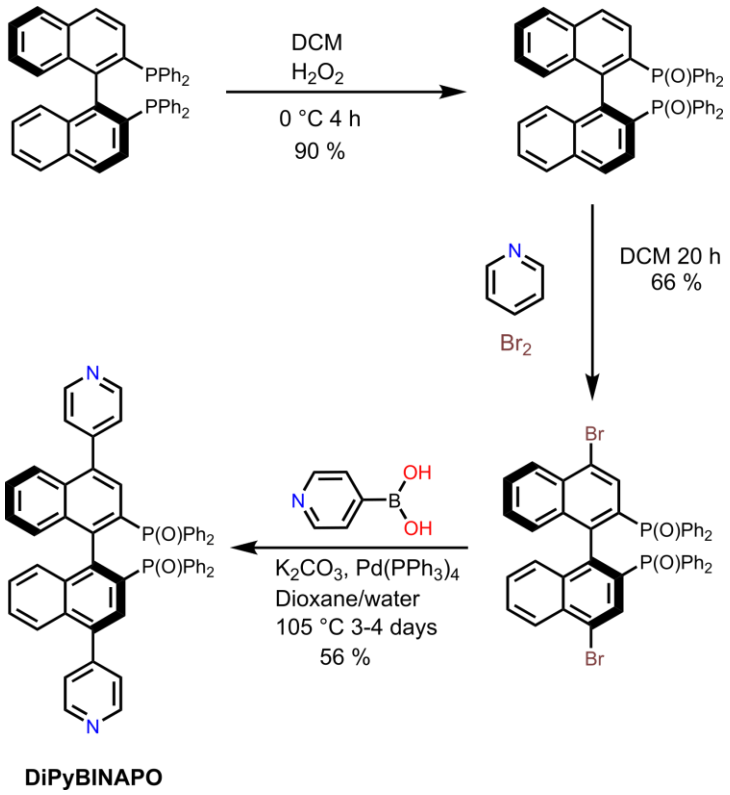

Figure 2.7. Synthesis of DiPyBINAPO ligand.

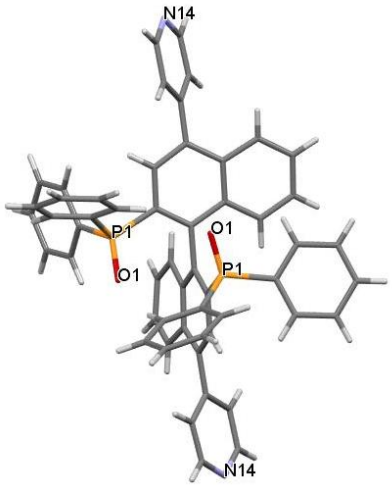

Figure 2.8. Crystal structure of DiPyBINAPO lignad (CCDC 2126199)[28,29.]

In order to synthesize the single crystals of the MOF $Zn(NO_3)_2.6H_2O$, BDC-NH_2 and DiPyBINAPO ligands were mixed combinatorially under a variety of solvothermal conditions **(Figure 2.9)**. From dozens of experiments, one sample formed a crystalline powder, but I was unable to grow single crystals that are suitable for single crystal data collection, but crystalline powder was analyzed using ^{1}H-NMR, powder x-ray crystallography (PXRD), and thermogravimetric analysis (TGA) to confirm the composition, crystallinity, and solvent accessible pore volume respectively.

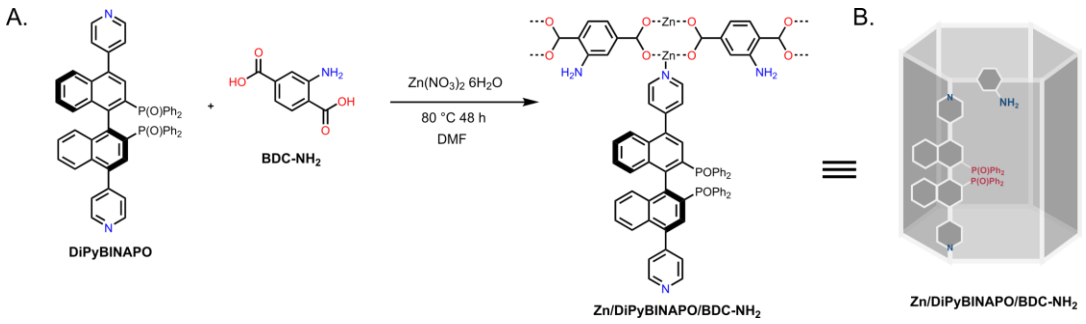

Figure 2.9. A. Reaction scheme for the synthesis of the **Zn/DiPyBINAPO/BDC-NH_2** MOF. B. Schematic representation of the MOF.

^{1}H-NMR showed that the crystalline powder consists of a 1:2 ratio of DiPyBINAPO, BDC-NH_2 (Figure **2.10)** and ESI-MS confirmed that the material has both DiPyBINAPO, BDC-NH_2 ligands (Figure **2.11)**. PXRD confirmed that material was crystalline (Figure **2.12)** and TGA analysis showed that the material lost about ~40% of its weight as the DMF (Figure **2.12)**. All these characterizations concluded the successful synthesis of a mixed-ligand MOF solvothermally. But efforts are continuing to synthesize single crystals of the MOF to determine its structure.

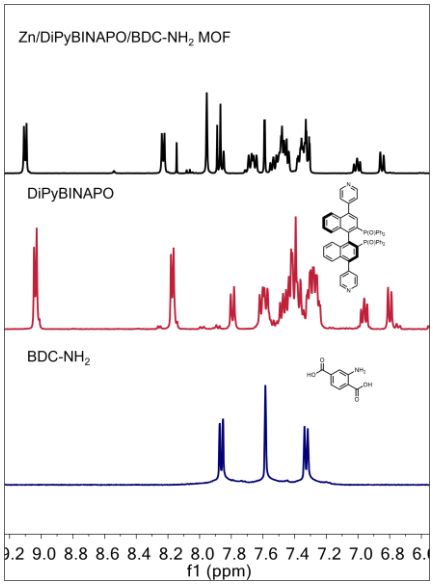

Figure 2.10. ^{1}H-NMR of digested **Zn/DiPyBINAPO/BDC-NH_2** MOF sample in d_6-DMSO/D_2SO_4 mixture.

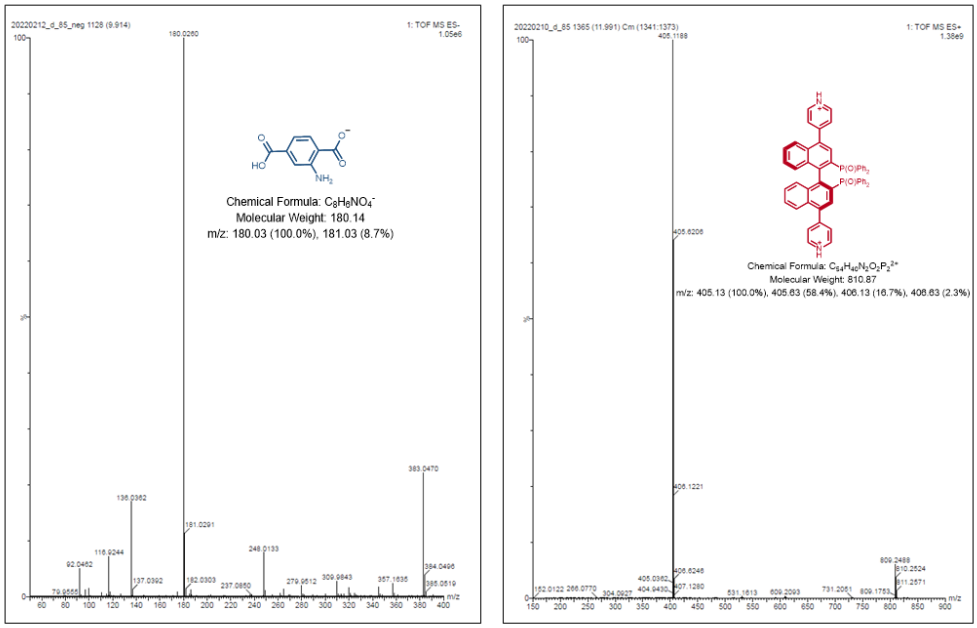

Figure 2.11. ESI-MS of a sample of the **Zn/DiPyBINAPO/BDC-NH$_2$** MOF sample digested in a solution of DABCO in DMSO

(Left: Negative mode, Right: Positive mode).

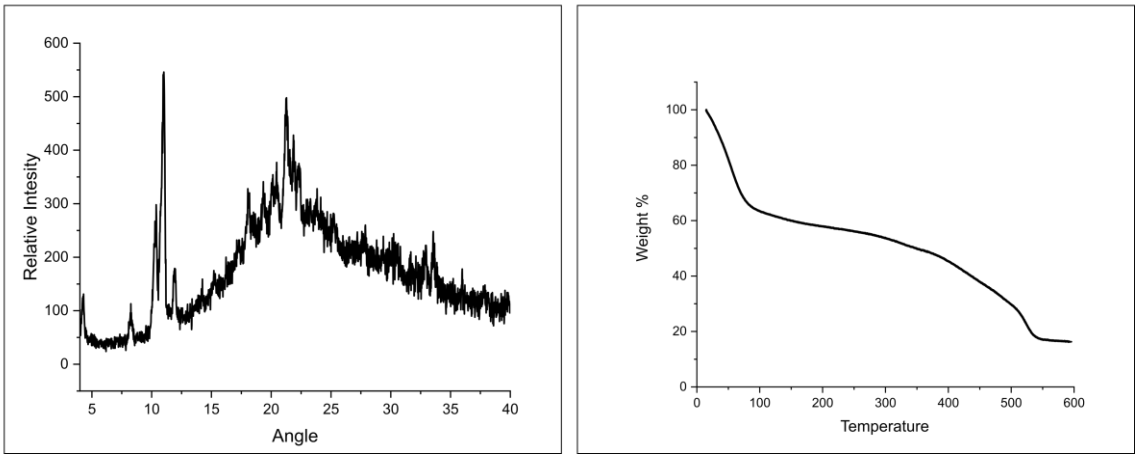

Figure 2.12. PXRD and TGA data for the Zn/DiPyBINAPO/BDC-NH$_2$ MOF**.**

2.5. Post-synthetic modification of Zn/DiPyBINAPO/BDC-NH$_2$MOF

After the full characterization of the crystalline powder of the **Zn/DiPyBINAPO/BDC-NH$_2$** MOF the next step was to confirm that the modifiable linker BDC-NH$_2$ was synthetically accessible, allowing us to modify the chemical environment of the MOF pore (Figure **2.13**). As

explained the Section 2.3, catalytic activity of the chiral catalyst can be fine-tuned by introducing a group that can form dispersive interactions with the substrate or with an activating co-catalyst. Therefore, as the first attempt, we reacted the -NH_2 group with a linear anhydride, butyric anhydride to introduce a linear aliphatic chain into the MOF. But our attempt was unsuccessful even after multiple trials. After that, succinic anhydride, a cyclic anhydride was reacted with the -NH_2 groups to give free -COOH groups attached to the MOF through amide linkages. The MOF material was soaked in a 0.2 M solution of succinic anhydride in DMF at 80 °C on the shaker. After 4 days the reaction had gone to competition and all of the peaks corresponding to parent BDC-NH_2 had shifted in the ^{1}H-NMR (Figure **2.14**) (**Zn/diPyBINAPO/BDC-$NH_{succinic}$**). ESI-MS of the digested material in a solution of DABCO revealed masses corresponding to [BDC-NH-COOH-H^+] further confirmed the successful reaction (Figure **2.15**). The reaction was relatively slow which could be due to steric effects from the phenyl substituents of the phosphine oxides blocking the MOF cavities.

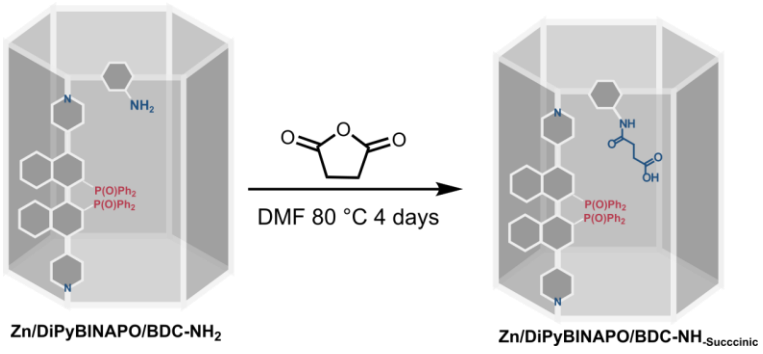

Figure 2.13. Post-synthetic modification of the **Zn/DiPyBINAPO/BDC-NH_2** MOF using succinic anhydride.

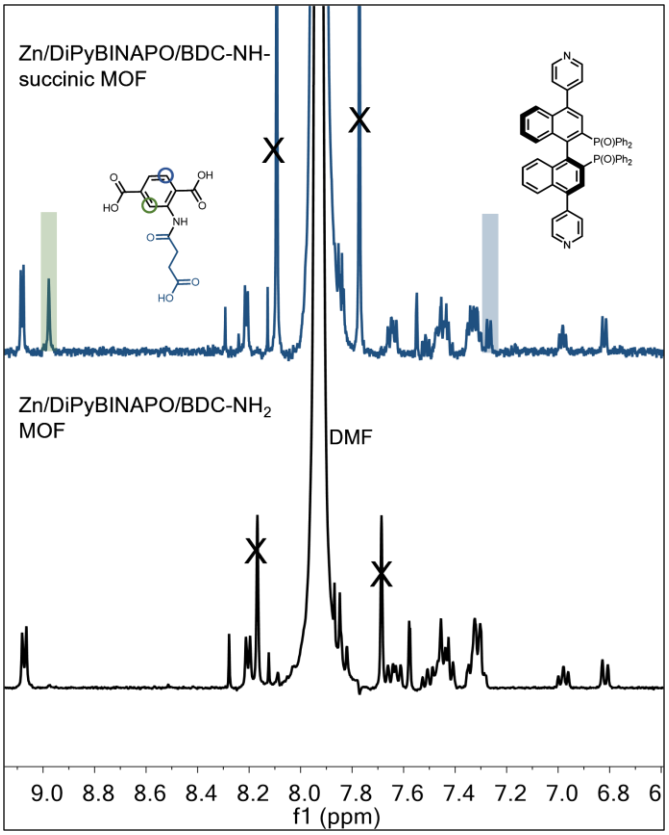

Figure 2.14. ^{1}H-NMR of **Zn/DiPyBINAPO/BDC-NH$_2$** MOF functionalized with succinic anhydride, digested in d_6-DMSO/D_2SO_4.

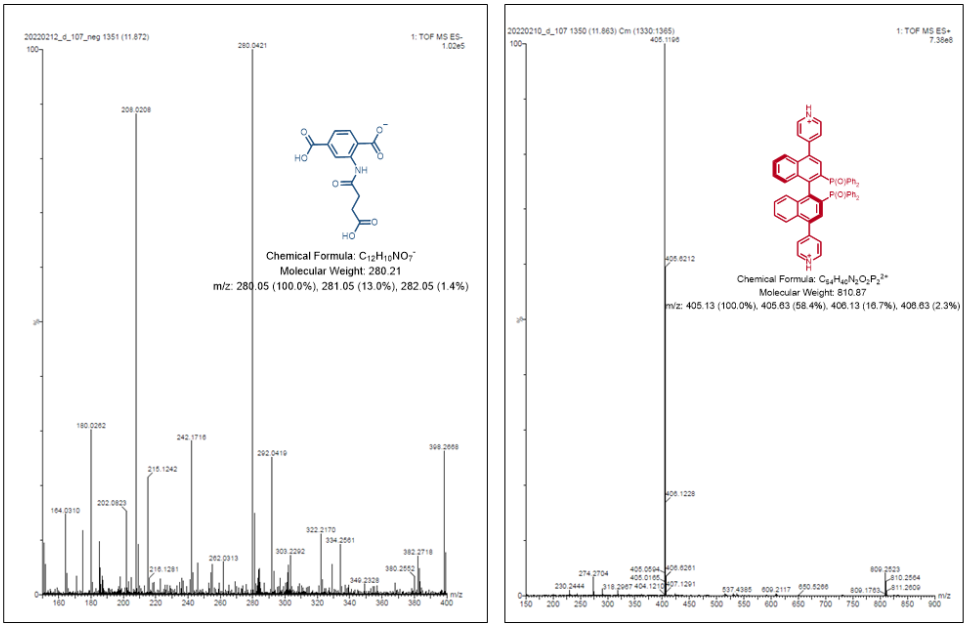

Figure 2.15. ESI-MS of **Zn/DiPyBINAPO/BDC-NH$_2$** MOF functionalized with succinic anhydride sample digested in a solution of DABCO in DMSO (Left: Negative mode, Right: Positive mode).

2.6. Catalysis experiments

The catalytic behavior of the **Zn/BDC-NH$_2$/diPyBINAPO** MOF and **Zn/diPyBINAPO/BDC-NH$_{succinic}$** MOF was tested using the cyanosilylation of benzaldehyde (Figure **2.16**). In a typical experiment, 5 mol% of MOF material was added to a 4 ml scintillation vial charged with TMSCN in neat benzaldehyde and left on the shaker at room temperature for up to 24 hours. Aliquots were analyzed by ^{1}H-NMR after diluting the sample in $CDCl_3$ (Figure **2.17**).

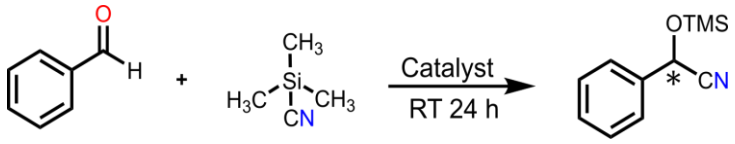

Figure 2.16. Cyanosilyaltion of benzaldehyde.

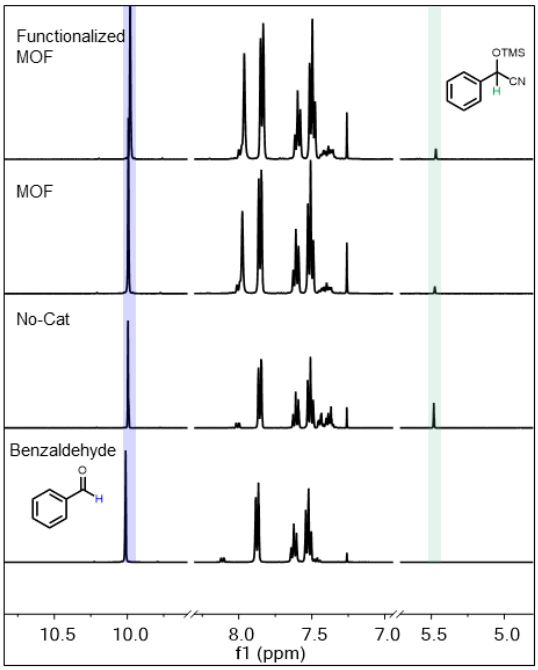

Figure 2.17. ^{1}H-NMR of cyanosilylation of Benzaldehyde.

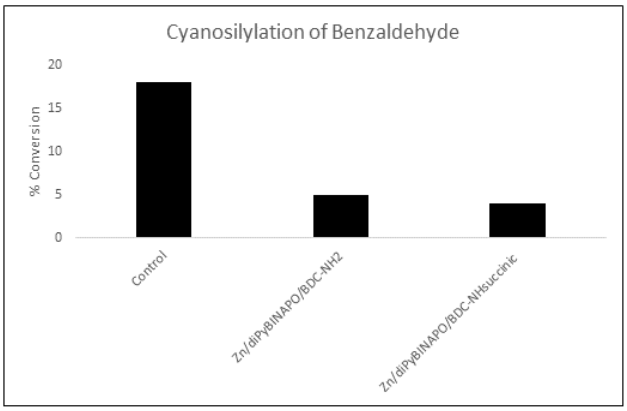

Figure 2.18. Catalysis data.

A control reaction in the absence of catalyst showed 18% conversion and the conversion in the presence of **Zn/diPyBINAPO/BDC-NH$_2$** was only about 5%. Surprisingly the presence of catalyst lowered the reaction conversion (Figure **2.18**). When the modified **Zn/diPyBINAPO/BDC-NH$_{succinic}$** material was used as the catalyst, the percent conversion was almost same as before. During the catalytic reaction phosphine oxide acts as a Lewis base to activate TMSCN. TMSCN reacts with Phosphine oxide to form the respective isocyanide (Figure **2.19**).[30] Therefore, we suspect that the MOF pore might be too crowded after the formation of isocyanide causing slower diffusion of benzaldehyde molecules and resulting low reaction conversions. But in both cases, since we used a chiral MOF linker, we anticipate achieving some enantioselectivity. Therefore, it is necessary to perform chiral HPLC or chiral GC to determine the %ee of the reaction.

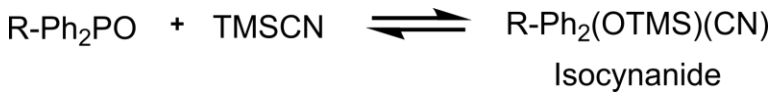

Figure 2.19. Reaction between phosphine oxide and TMSCN**.**

2.7. Conclusion

In conclusion we attempted to synthesize a modifiable homochiral metal-organic framework material for asymmetric catalysis. The well-known chiral privileged ligand, BINAPO was functionalized with dipyridyl anchoring groups and immobilized together with the commercially available BDC-NH_2, in a mixed-linker MOF. Even though we were unable to grow single crystals suitable for structure elucidation, crystalline powder of the MOF material was successfully synthesized and characterized to confirm the composition, crystallinity and accessible pore volume. The newly synthesized MOF was further functionalized post-synthetically to introduce additional functional groups in an attempt to demonstrate the utility of the modifiable ligand in the MOF. Even though material showed very low catalytic activity during the cyanosilylation of Benzaldehyde reaction, the concept of developing modifiable homochiral MOF was successful. Upon further optimization it will be possible to improve the reaction conversion.

Further studies will be carried out, to synthesize single crystals that are suitable for single crystal analysis, optimize reaction conditions to achieve higher conversion, chiral HPLC or chiral GC analysis to determine the enantioselectivity of the products and finally modify the MOF material to use as a catalyst to perform the hydroamination reaction.

2.8. Experimental

Material

All chemicals were used as received from commercial sources unless otherwise noted. Sulfuric acid-d_2 (D_2SO_4, 98 wt.% in D_2O, 99.5+% atom D) and (R)-BINAP purchased from Acros Organics. *N*,*N*-dimethylformamide (DMF), tetrahydrofuran (THF), Acetonitrile (MeCN), Methanol (MeOH), $NaHSO_3$, $NaHCO_3$, anhydrous Na_2SO_4, $MgSO_4$, H_2O_2 were purchased from Fisher Scientific, and zinc nitrate hexahydrate from Strem Chemicals. Chloroform ($CHCl_3$),

Methylene chloride (DCM) 2-aminoterephthalic acid (**BDC-NH_2**), Bromine, Pyridine and Succinic anhydride were purchased from Sigma Aldrich. 1,4-Diazabicyclo[2.2.2]octane (DABCO) were purchased from Oakwood Products. Dimethyl sulfoxide-d_6 (d_6-DMSO, 99.9 atom % D) and $CDCl_3$ were purchased from Cambridge Isotopes Laboratories.

Synthetic procedures

Synthesis of (*R*)-4,4 -BINAPO (1)

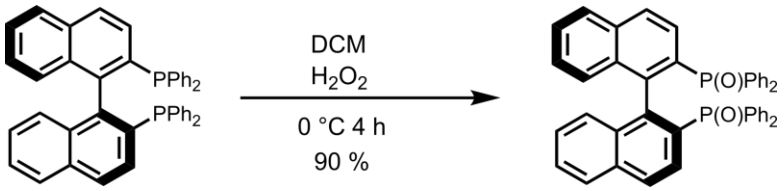

Followed a modified literature procedure.[31] In a 250 mL round bottom flask were placed (R)-BINAP (5.6g, 9 mmol) and 100 mL of DCM. The mixture was cooled to 0 °C and 10 mL of H_2O_2 (35 %) was added. The mixture was stirred for 4h. Then 100 mL of water was added. Aqueous phase was washed with 50 mL of aqueous $HaHSO_3$ solution, dried over Na_2SO_4. The solvent was removed *in vacuo* resulting in a powdered white solid. The solid was purified via two-solvent recrystallization in DCM and n-heptane. Recrystallization yielded colorless-needle like crystals (5.0 g, 7.94 mmol, 90%).

Synthesis of (*R*)-4,4 -DibromBINAPO (2)

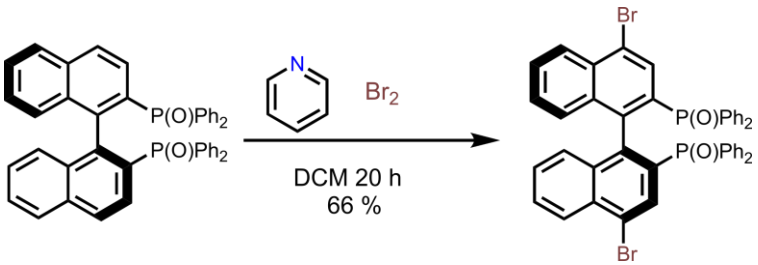

Followed a modified literature procedure.[31] To a 250 mL Schlenk flask equipped with a stir bar, added **1** (4.0 g, 6.11 mmol) and it was evacuated 3 times. Anhydrous DCM (75 mL) and anhydrous

Pyridine (0.518 mmol) were added to the flask. Then flask was transferred to the glove box and Br_2 (0.932 mL, 18.3 mmol) was slowly added to the stirred mixture. The reaction was stirred at overnight resulting a deep brown solution. The reaction was quenched with 1M $NaHSO_3$ and it was stirred until the organic layer was turned yellow. Isolated organic phase was washed with 1M $NaHSO_3$ and brine three times and finally with $NaHCO_3$ solution. Organic phase was dried with anhydrous $MgSO_4$ and removed the solvent *in vacuo* leaving a yellow-brown powder solid. To get dibrominated product above procedure was repeated two more times and progress of the reaction was monitored via TLC. Upon successful bromination, crude product was recrystallized using DCM to obtain pure product (2.64 g, 3.24 mmol, 66%).

Synthesis of (*R*)-4,4 -DiPyBINAPO (3)

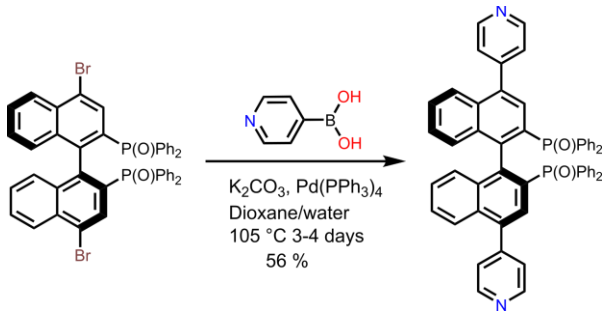

Followed a literature procedure.[27] 2 (500 mg, 0.6 mmol), 4-pyridylboronic acid (0.15g, 1.3 mmol), K_2CO_3 (3.2 g, 2.36 mmol) were added to a degassed mixture of dioxane/water (2/1, 20 mL) in a Schlenk flask and brought to reflux at 105 °C. Once heated, the catalysts [$Pd(PPh_3)_4$] (0.01 g, 0.008 mmol) was added and under N_2. The progress of the reaction was monitored through TLC after 3 days reaction was stopped. The reaction mixture was cooled to room temperature and washed with DCM (20 ml) isolated the organic phase and dried over $MgSO_4$, filtered off the drying agent and removed the solvent *in vacuo*. Left with golden yellow crude powder which was purified vial column chromatography (DCM:MeOH 97:3) (135%, 0.0182 mmol, 56 %).

Synthesis of the Zn/DiPyBINAPO/BDC-NH_2 MOF

$Zn(NO_3)_2 \cdot 6H_2O$ (95.04 mg, 0.320 mmol), **(*R*)-4,4 -DiPyBINAPO** (64.62 mg. 0.08 mmol), and DMF (4 mL) were combined in a 20 mL Scintillation vial. The vial was heated at 80 °C in a heating block until the solution became clear. A solution of **BDC-NH_2** (28.80 mg, 0.160 mmol) in DMF (2 mL) was added, and the flask incubated at 80 °C. After 48 h, the vial was removed from the heating block. Light brown crystalline powder was collected by filtration and washed with DMF 2-3 times. Stored in DMF until further use.

Post-synthetic functionalization of Zn/DiPyBINAPO/BDC-NH_2 MOF with Succinic anhydride

Following a modified literature procedure,[32] **MOF** (15-20 mg, 0.0173 mmol, ca. 0.0347mmol equiv of $-NH_2$) was transferred into a into a 20 mL scintillation vial. The vial was charged with 8 mL of a 0.2 M solution of Succinic anhydride (46 equiv.) in DMF (stored in 3Å molecular sieves), and the mixture was left at 80 °C for 4 days with continuous mixing on a Corning LSE Low Speed Orbital Shaker. The MOF material was then transferred to a new scintillation vial containing fresh DMF and mixed for ~30 min. The DMF was exchanged with fresh DMF 3 times, and then fresh DMF a further 3 times and stored under DMF.

Catalysis experiment

Followed a modified literature procedure.[33] 5 mol% of the **MOF** catalyst was weighed and transferred to a 4 ml vial charged with Benzaldehyde (0.5 mmol, 50.84 µL) and TMSCN (1/5 mmol, 187.5 µL). Vial was left on the shaker for 24 hours at room temperature and liquot was taken and diluted in $CDCl_3$ before the ^{1}H-NMR analysis.

2.8. Characterization

Powder X-ray diffraction (PXRD)

Powder patterns were recorded on a Bruker AXS D8 Advance Phaser diffractometer with Cu Kα radiation (λ = 1.5418 Å) over a range of 5° < 2θ < 40° in 0.02° steps with a 0.5 s counting time per step. Samples were collected from the bottom of the reaction vial as a thick suspension in DMF and spread on a Si-Einkristalle plate immediately before PXRD measurements.

Thermogravimetric analysis (TGA)

TGA was performed on a TGA-Q50 interfaced with a PC using TA Universal Analysis software. Samples were heated at a rate of 10 ºC/min under a nitrogen atmosphere. All samples were extensively solvent exchanged with fresh DMF prior to analysis.

Proton nuclear magnetic resonance (^{1}H NMR)

Spectra were recorded on a Brucker 400MHz NMR spectrometer (400 MHz for ^{1}H). NMR chemical shifts are reported in ppm against a residual solvent resonance as the internal standard ($\delta(d_6\text{-DMSO}) = 2.5$ ppm or $\delta(CDCl_3) = 7.26$)). In a typical analysis, MOF materials stored in DMF were solvent exchanged with $CHCl_3$, isolated by vacuum filtration, and then evacuated in a vacuum oven at 80 °C overnight. Evacuated MOF samples (~8 mg) were transferred into an NMR tube and d_6-DMSO (0.6 mL) was added. Subsequently, D_2SO_4 (0.010 mL, 98% w/w in D_2O) was also added. The tubes were capped and sonicated until all the solid was dissolved (~ 1 min).

Electrospray Ionization Mass Spectrometry (ESI)

MOF samples (~5mg) were placed in a solution of DABCO (10 mg) and 0.25ml of DMSO in a 2-dram vial. The vial was sonicated for ~ 1 min then heated at 80 °C overnight. A small amount of residue was filtered out and resulting solution was sent for ESI-MS analysis at the Dr. Ping Li's lab at Kansas State University.

2.9. References

(1) Alhumaimess, M. S. Metal–Organic Frameworks and Their Catalytic Applications. *J. Saudi Chem. Soc.* **2020**, *24* (6), 461–473. https://doi.org/10.1016/j.jscs.2020.04.002.

(2) Pascanu, V.; González Miera, G.; Inge, A. K.; Martín-Matute, B. Metal–Organic Frameworks as Catalysts for Organic Synthesis: A Critical Perspective. *J. Am. Chem. Soc.* **2019**, *141* (18), 7223–7234. https://doi.org/10.1021/jacs.9b00733.

(3) Yang, D.; Gates, B. C. Catalysis by Metal Organic Frameworks: Perspective and Suggestions for Future Research. *ACS Catal.* **2019**, *9* (3), 1779–1798. https://doi.org/10.1021/acscatal.8b04515.

(4) C. Collis, A. E.; T. Horváth, I. Heterogenization of Homogeneous Catalytic Systems. *Catal. Sci. Technol.* **2011**, *1* (6), 912–919. https://doi.org/10.1039/C1CY00174D.

(5) Zhang, H.; Lou, L.-L.; Yu, K.; Liu, S. Advances in Chiral Metal–Organic and Covalent Organic Frameworks for Asymmetric Catalysis. *Small* **2021**, *17* (22), 2005686. https://doi.org/10.1002/smll.202005686.

(6) Ma, L.; Abney, C.; Lin, W. Enantioselective Catalysis with Homochiral Metal–Organic Frameworks. *Chem. Soc. Rev.* **2009**, *38* (5), 1248–1256. https://doi.org/10.1039/B807083K.

(7) Ezuhara, T.; Endo, K.; Aoyama, Y. Helical Coordination Polymers from Achiral Components in Crystals. Homochiral Crystallization, Homochiral Helix Winding in the Solid State, and Chirality Control by Seeding. *J. Am. Chem. Soc.* **1999**, *121* (14), 3279–3283. https://doi.org/10.1021/ja9819918.

(8) Deng, S.-Q.; Mo, X.-J.; Cai, S.-L.; Zhang, W.-G.; Zheng, S.-R. Homochiral Cu(I) Coordination Polymers Based on a Double-Stranded Helical Building Block from Achiral Ligands: Symmetry-Breaking Crystallization, Photophysical and Photocatalytic Properties. *Inorg. Chem.* **2019**, *58* (21), 14660–14666. https://doi.org/10.1021/acs.inorgchem.9b02341.

(9) Wu, S.-T.; Zhang, Y.-S.; Zhang, B.; Hu, X.-L.; Huang, X.-H.; Huang, C.-C.; Zhuang, N.-F. Viedma Ripening of Chiral Coordination Polymers Based on Achiral Molecules. *Cryst. Growth Des.* **2019**, *19* (5), 2537–2541. https://doi.org/10.1021/acs.cgd.9b00235.

(10) Seo, J. S.; Whang, D.; Lee, H.; Jun, S. I.; Oh, J.; Jeon, Y. J.; Kim, K. A Homochiral Metal–Organic Porous Material for Enantioselective Separation and Catalysis. *Nature* **2000**, *404* (6781), 982–986. https://doi.org/10.1038/35010088.

(11) Wu, C.-D.; Hu, A.; Zhang, L.; Lin, W. A Homochiral Porous Metal−Organic Framework for Highly Enantioselective Heterogeneous Asymmetric Catalysis. *J. Am. Chem. Soc.* **2005**, *127* (25), 8940–8941. https://doi.org/10.1021/ja052431t.

(12) Falkowski, J. M.; Sawano, T.; Zhang, T.; Tsun, G.; Chen, Y.; Lockard, J. V.; Lin, W. Privileged Phosphine-Based Metal–Organic Frameworks for Broad-Scope Asymmetric Catalysis. *J. Am. Chem. Soc.* **2014**, *136* (14), 5213–5216. https://doi.org/10.1021/ja500090y.

(13) Bogaerts, T.; Deyne, A. V. Y.-D.; Liu, Y.-Y.; Lynen, F.; Speybroeck, V. V.; Voort, P. V. D. Mn-Salen@MIL101(Al): A Heterogeneous, Enantioselective Catalyst Synthesized Using a 'Bottle around the Ship' Approach. *Chem. Commun.* **2013**, *49* (73), 8021–8023. https://doi.org/10.1039/C3CC44473B.

(14) Ma, L.; Falkowski, J. M.; Abney, C.; Lin, W. A Series of Isoreticular Chiral Metal–Organic Frameworks as a Tunable Platform for Asymmetric Catalysis. *Nat. Chem.* **2010**, *2* (10), 838–846. https://doi.org/10.1038/nchem.738.

(15) Song, F.; Wang, C.; Falkowski, J. M.; Ma, L.; Lin, W. Isoreticular Chiral Metal−Organic Frameworks for Asymmetric Alkene Epoxidation: Tuning Catalytic Activity by Controlling Framework Catenation and Varying Open Channel Sizes. *J. Am. Chem. Soc.* **2010**, *132* (43), 15390–15398. https://doi.org/10.1021/ja1069773.

(16) Sharifzadeh, Z.; Berijani, K.; Morsali, A. Chiral Metal–Organic Frameworks Based on Asymmetric Synthetic Strategies and Applications. *Coord. Chem. Rev.* **2021**, *445*, 214083. https://doi.org/10.1016/j.ccr.2021.214083.

(17) Yang, Y.; Shi, S.-L.; Niu, D.; Liu, P.; Buchwald, S. L. Catalytic Asymmetric Hydroamination of Unactivated Internal Olefins to Aliphatic Amines. *Science* **2015**, *349* (6243), 62–66. https://doi.org/10.1126/science.aab3753.

(18) Tiago, G. A. O.; Mahmudov, K. T.; Guedes da Silva, M. F. C.; Ribeiro, A. P. C.; Branco, L. C.; Zubkov, F. I.; Pombeiro, A. J. L. Cyanosilylation of Aldehydes Catalyzed by Ag(I)- and Cu(II)-Arylhydrazone Coordination Polymers in Conventional and in Ionic Liquid Media. *Catalysts* **2019**, *9* (3), 284. https://doi.org/10.3390/catal9030284.

(19) Qin, J.-S.; Yuan, S.; Wang, Q.; Alsalme, A.; Zhou, H.-C. Mixed-Linker Strategy for the Construction of Multifunctional Metal–Organic Frameworks. *J. Mater. Chem. A* **2017**, *5* (9), 4280–4291. https://doi.org/10.1039/C6TA10281F.

(20) Bitzer, J.; Kleist, W. Synthetic Strategies and Structural Arrangements of Isoreticular Mixed-Component Metal–Organic Frameworks. *Chem. – Eur. J.* **2019**, *25* (8), 1866–1882. https://doi.org/10.1002/chem.201803887.

(21) Lu, G.; Liu, R. Y.; Yang, Y.; Fang, C.; Lambrecht, D. S.; Buchwald, S. L.; Liu, P. Ligand–Substrate Dispersion Facilitates the Copper-Catalyzed Hydroamination of Unactivated Olefins. *J. Am. Chem. Soc.* **2017**, *139* (46), 16548–16555. https://doi.org/10.1021/jacs.7b07373.

(22) Bandar, J. S.; Pirnot, M. T.; Buchwald, S. L. Mechanistic Studies Lead to Dramatically Improved Reaction Conditions for the Cu-Catalyzed Asymmetric Hydroamination of Olefins. *J. Am. Chem. Soc.* **2015**, *137* (46), 14812–14818. https://doi.org/10.1021/jacs.5b10219.

(23) Cohen, S. M. Postsynthetic Methods for the Functionalization of Metal–Organic Frameworks. *Chem. Rev.* **2012**, *112* (2), 970–1000. https://doi.org/10.1021/cr200179u.

(24) Garibay, S. J.; Wang, Z.; Tanabe, K. K.; Cohen, S. M. Postsynthetic Modification: A Versatile Approach Toward Multifunctional Metal-Organic Frameworks. *Inorg. Chem.* **2009**, *48* (15), 7341–7349. https://doi.org/10.1021/ic900796n.

(25) K. Tanabe, K.; M. Cohen, S. Postsynthetic Modification of Metal–Organic Frameworks—a Progress Report. *Chem. Soc. Rev.* **2011**, *40* (2), 498–519. https://doi.org/10.1039/C0CS00031K.

(26) Kim, M.; Cahill, J. F.; Prather, K. A.; Cohen, S. M. Postsynthetic Modification at Orthogonal Reactive Sites on Mixed, Bifunctional Metal–Organic Frameworks. *Chem. Commun.* **2011**, *47* (27), 7629–7631. https://doi.org/10.1039/C1CC12101D.

(27) Lestari, W. W.; Zaake-Hertling, H.; Lönnecke, P.; Hey-Hawkins, E. 4, 4′- and 5, 5′-Functionalized (S)- and (R)-2, 2′-Bis(Diphenylphosphanyl)-1, 1′-Binaphthyl Oxide Derivatives. *Z. Für Anorg. Allg. Chem.* **2013**, *639* (14), 2589–2596. https://doi.org/10.1002/zaac.201300278.

(28) Samarakoon, Kanchana; Averkiev, Boris; Gadzikwa, Tendai. CCDC 2126200: Experimental Crystal Structure Determination. https://doi.org/10.5517/CCDC.CSD.CC29CH39.

(29) Samarakoon, Kanchana; Averkiev, Boris; Gadzikwa, Tendai. CCDC 2126199: Experimental Crystal Structure Determination. https://doi.org/10.5517/CCDC.CSD.CC29CH28.

(30) Ryu, D. H.; Corey, E. J. Highly Enantioselective Cyanosilylation of Aldehydes Catalyzed by a Chiral Oxazaborolidinium Ion. *J. Am. Chem. Soc.* **2004**, *126* (26), 8106–8107. https://doi.org/10.1021/ja0475959.

(31) Wang, X.; Lu, S.; Li, J.; Liu, Y.; Li, C. Conjugated Microporous Polymers with Chiral BINAP Ligand Built-in as Efficient Catalysts for Asymmetric Hydrogenation. *Catal. Sci. Technol.* **2015**, *5* (5), 2585–2589. https://doi.org/10.1039/C5CY00038F.

(32) Garibay, S. J.; Wang, Z.; Cohen, S. M. Evaluation of Heterogeneous Metal−Organic Framework Organocatalysts Prepared by Postsynthetic Modification. *Inorg. Chem.* **2010**, *49* (17), 8086–8091. https://doi.org/10.1021/ic1011549.

(33) Lestari, W. W.; Lönnecke, P.; Streit, H. C.; Schleife, F.; Wickleder, C.; Hey-Hawkins, E. A Chiral Two-Dimensional Coordination Polymer Based on CuII and (S)-4,4′-Bis(4-Carboxyphenyl)-2,2′-Bis(Diphenylphosphinoyl)-1,1′-Binaphthyl: Synthesis, Structure, and Magnetic and Optical Properties. *Inorganica Chim. Acta* **2014**, *421*, 392–398. https://doi.org/10.1016/j.ica.2014.06.006.

Chapter 3 - Uniform, Binary Functionalization of a Metal−Organic Framework Material

Portions of this chapter appear in the following manuscript:

Samarakoon, K. P.; Satterfield, C. S.; McCoy, M. C.; Pivaral-Urbina, D. A.; Islamoglu, T.; Day, V. W.; Gadzikwa, T. Uniform, Binary Functionalization of a Metal–Organic Framework Material. *Inorg. Chem.* **2019**, *58* (14), 8906–8909

3.1. Introduction

Chapter 2 described a way to generate an enzyme-inspired MOF catalyst through solvothermal synthesis. But, as previously mentioned, MOF synthesis is highly unpredictable and standard solvothermal methods may not yield the desired porous material, or as shown in the Chapter 2, it might not yield single crystals suitable for single crystal analysis to determine the framework structure. Therefore, it is necessary to develop an alternative method to obtain the anticipated catalytic-MOF.

Because of their robust framework structure, MOF pores can be systematically decorated with chemical functionalities that are flexible and capable of forming multiple interactions.[1–8] As an example, using simple reagents Cohen and co-workers have utilized post-synthetic modification strategies to introduce a wide range of functional groups that are both flexible and have ability to form secondary interactions.[2] A similar method was used by Yagi and co-workers to introduce an enzyme-like complexity through the seven-step post functionalization of a multivariate MOF, MTV-IRMOF-74-III with an amino acid sequences (Figure **3.1**).[1] Such post assembly introduction of such multiple functionalities further increases the chemical and three-dimensional complexity

of the MOF cavities. All the attempts show how were MOF pores can be used to satisfy two of the four elements for bioinspired catalysts that were described in Chapter 1.

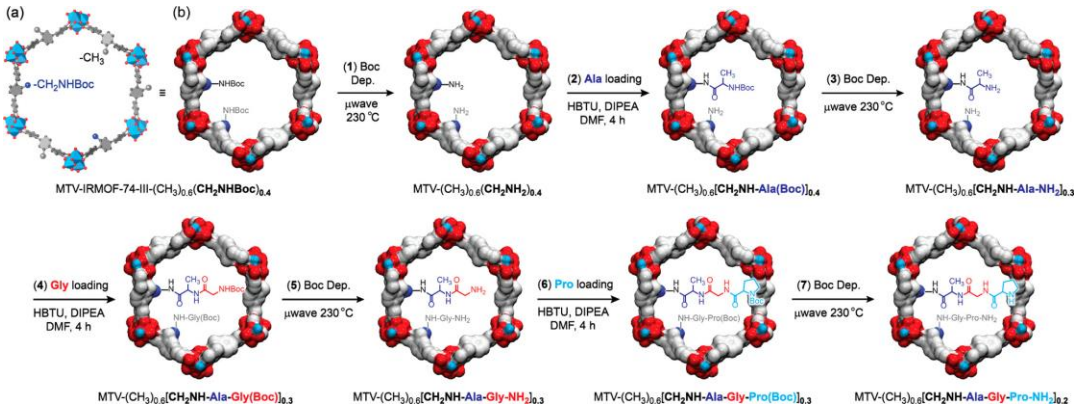

Figure 3.1. Seven step post synthetic modification of MTV-IRMOF-74-III. Reprinted with permission from REF [1].Copyright 2022 American Chemical Society.

The generation of uniformly multifunctionalized cavities has challenged MOF chemists.[1,4,9–12] Telfer and co-workers, with their unique family of 4-componet MOFs, have illustrated the ability to create confined-spaces that are uniformly multifunctionalized.[13,14] In one of their reports, they synthesized a multicomponent MOF, MUF-77 to achieve enzyme-like complexity by using an organocatalyst linker and two different modulating linkers that tune the spatial environment around the catalysts.[13] Thereby, they were able to increase the reaction rate and the enantiomeric excess of an aldol reaction. In another report by Telfer and co-workers, they successfully programmed the microenvironment around the site of catalysis by introducing secondary groups into the catalytic MOF unit.[14] Even though in those two reports they did not use post-synthetic modification strategy to modify their MOF interiors, they made us to realize that, to achieve the best enzyme-mimics, along with the multifunctionalization it is equally important to have uniformity of the catalytic groups.

3.2. Synthetic strategy for uniformly multifunctionalizing MOF material

Non-identical pores are a result of nonuniformly dispersed reactive linkers throughout the MOF material.[3,11] One of the most common ways to have nonuniformity is the post functionalization of a single linker MOF using different functional groups (Figure **3.2 A**).[2] For example, Cohen and co-workers have performed a three step functionalization of single-linker MOF, IRMOF-3 to generate non-uniformly multifunctionalized pores.[2] The same group demonstrated that the use of a multivariant mixed-linker MOF with orthogonal reactive linkers to generate bifunctional yet non-uniformly functionalized MOF(Figure **3.2 B**).[11] They synthesized a MOF that has -Br and -NH_2 functionalities but, both linkers were dicarboxylates Therefore, two orthogonal groups were non-uniformly distributed throughout the MOF resulting an inhomogenously multifunctionalized MOF In another example, Rosi and co-workers utilized a multivariant MOF with orthogonal functional groups to generate again non-uniformly multifunctionalized MOF cavities.[3] While the non-uniformity is undesirable both works provide synthetic tools for uniform multifunctionalization.

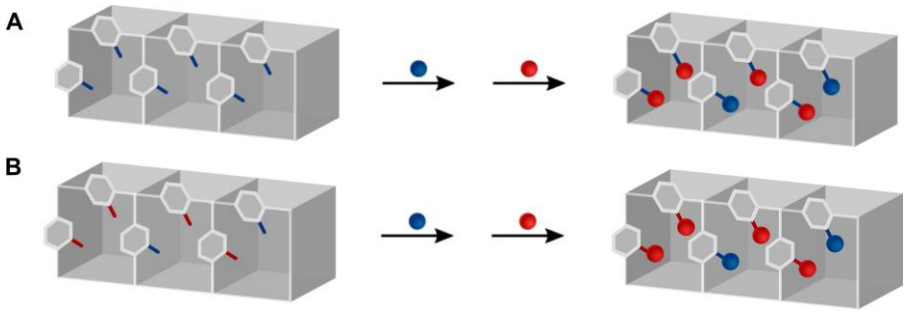

Figure 3.2. Multivariate MOF from non-uniformly arranged linkers with (A) One type of reactive group and, (B) Orthogonal reactivities. Reprinted with permission from REF.[15] Copyright 2022 American Chemical Society.

Therefore, in order to obtain a well-defined MOF it is necessary to have (Figure **3.3);**

1. Functional groups with independent reactivities, and

2. Linkers with orthogonal coordination chemistries. So that the linkers are in well-defined locations throughout the framework

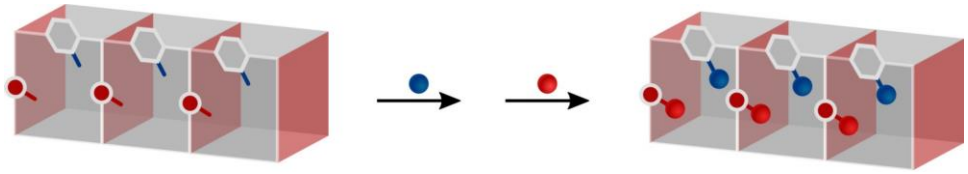

Figure 3.3. Generation of a uniformly multifunctionalized MOF material from well-defined mixed linker MOF. Reprinted with permission from REF.[15] Copyright 2022 American Chemical Society.

To achieve a well-defined mixed linker MOF, we chose amine and hydroxyl groups as the reactive functional groups and carboxylates and pyridines as the orthogonal coordination sites. During solvothermal synthesis, when linkers are heated with a M^{2+} metal salts, dicarboxylate linkers form two sheets along the *xy*-plane. These 2D-sheets then connect through the dipyridyl linkers along the *z*-axis forming the 3D MOF framework. The presence of organic linkers with orthogonal coordinating sites guarantees construction of a well-defined mixed-linker MOF. It is also known that low-temperature nucleation of the frameworks can form the rarer Kagome'-type lattice that have pores large enough for post synthesis functionalization.[17–19]

By experimenting with various solvothermal conditions, Christopher Satterfield (MS-Student-Gadzikwa Lab) was able to synthesize a well-defined MOF, **KSU-1**. 2-amino-1,4-benzenedicarboxalic acid (BDC-NH_2) and *meso*-α, β-di(4-pyridyl) glycol (DPG) were incubated with $Zn(NO_3)_2 \cdot 6H_2O$ in N,N-dimethylformamide (DMF) at 60°C for 2 days and left at room temperature for another two days. **KSU-1** was obtained as pale-yellow color, block-like crystals with Kagome lattice (Figure **3.4**).

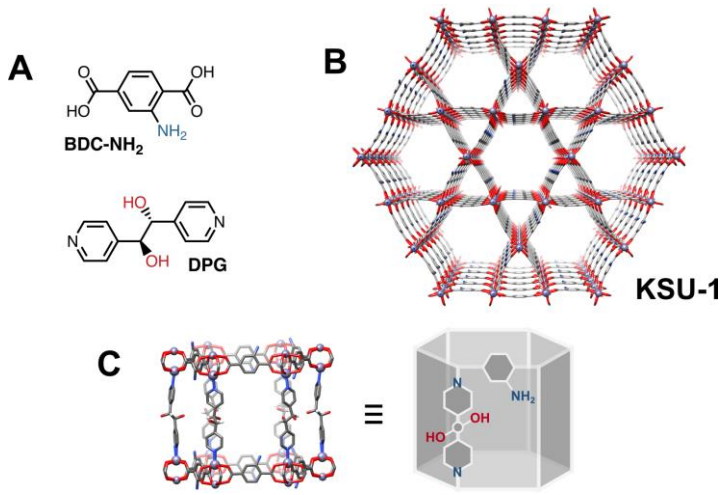

Figure 3.4. (A) Independently reactive linkers with orthogonal coordination chemistry. (B) **KSU-1** viewed down the *c*-axis. (C) Network unit of **KSU-1** and its schematic representation. Reprinted with permission from REF.[51] Copyright 2022 American Chemical Society.

3.3. Post-synthesis modification of KSU-1 to obtain uniformly bifunctional MOF material.

Having established the porosity and the purity of **KSU-1,** the next step was to investigate post synthesis modification to a obtain uniformly functionalized MOF. We hypothesized that the amine group of BDC-NH_2 is sufficiently nucleophilic to react with a linear aliphatic acid anhydride under relatively low concentrations, while the hydroxyl groups of DPG are not. Butyric anhydride was chosen as the nucleophile for the amidation reaction, which was performed following a modified literature procedure (Figure **3.5**).[2] After the MOF material was immersed in an anhydrous $CHCl_3$ solution of butyric anhydride for a total of 96 h, with constant agitation, the success of the reaction was evaluated using ^{1}H-NMR (Figure **3.6 A**). The amidation product (**KSU-1$_{mono}$**) was then thoroughly washed, evacuated and, digested in a solution of D_2SO_4 and d_6-DMSO. The ^{1}H-NMR of **KSU-1$_{mono}$** was compared with **KSU-1.** All the peaks corresponding to the initial BDC-NH_2 protons had completely shifted and new peaks corresponding to the protons of the butyryl substituents of the amide appeared in the aliphatic region (0.5-2.5 ppm). The integration ratios of

DPG: butyryl peaks were 1:2 as expected and confirmed selective and quantitative functionalization of the amine.

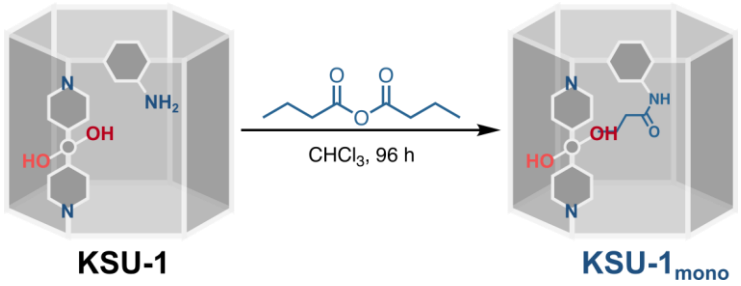

Figure 3.5. Functionalization of **KSU-1** with butyric anhydride.

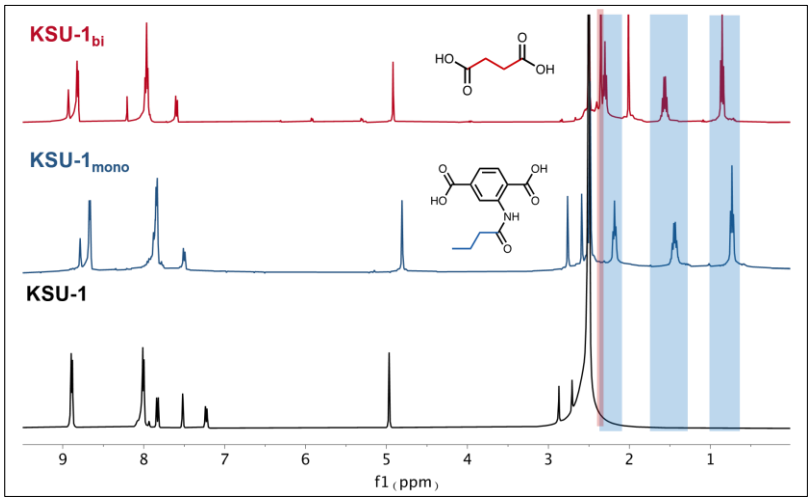

Figure 3.6. (A) ^{1}H NMR spectra of each material in the functionalization sequence digested in a solution of d_6-DMSO/D_2SO_4. (B) ^{1}H NMR of **KSU-1$_{bi}$** digested in DABCO/d_6-DMSO.

KSU-1$_{mono}$ was further characterized via high resolution electrospray ionization mass spectrometry (ESI-MS) after it was digested in a solution of 1,4-diazobicyclo[2,2,2]octane (DABCO) in DMSO (Figure **3.9**). Mass fragments revealed the presence of both BDC-amide and unreacted DPG which further confirmed the selective functionalization. Powder X-Ray Diffraction (PXRD) and Thermogravimetric analysis (TGA) of **KSU-1$_{mono}$** indicated that the material retained both its crystallinity and significant porosity, with the material loosing ~35 % of its weight as DMF (Figure **3.9**). Adsorption isotherms with N_2 at 77K revealed that the porosity of evacuated **KSU-**

1$_{mono}$ could be accessed partially with CO_2 activation (Figure **3.11**). The large solvent-accessible volume that still remained in **KSU-1$_{mono}$** indicated that the second functionalization of the MOF material is still feasible.

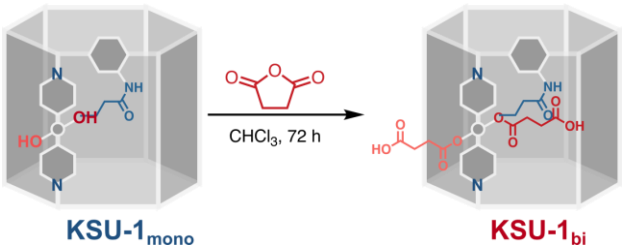

Figure 3.7. Functionalization of **KSU-1$_{mono}$** with succinic anhydride.

As the second step, **KSU-1$_{mono}$** was then subjected to the nucleophilic ring opening of succinic anhydride by the DPG linker to produce the diester product, (Figure **3.7**).[20] The MOF was immersed in a suspension of succinic anhydride in anhydrous $CHCl_3$ and agitated for 72h to produce the bifunctionalized material **KSU-1$_{bi}$.** After washing and evacuating the material, **KSU-1$_{bi}$** was digested in a solution of D_2SO_4 and d_6-DMSO (Figure **3.6**). Because of the acidity of the NMR solvent mixture,the ester bond hydrolyzed and ^{1}H-NMR of **KSU-1$_{bi}$** was expected to be identical with **KSU-1$_{mono}$** except for the presence of a new peak around 2.4 ppm corresponding to the freed succinic acid. Proton integration indicated the 1:1 ratio of succinic acid to butyric amide because the -NH_2 to -OH ratio is 1:1 in the parent material **KSU-1.** These results indicated the quantitative and independent functionalization of the BDC-NH_2 and DPG linkers.

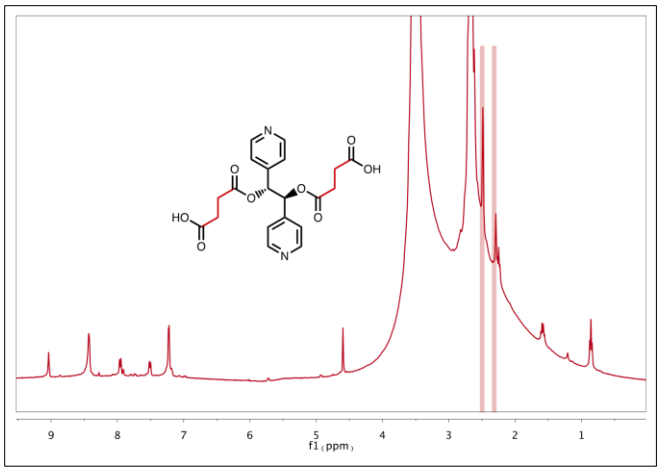

Figure 3.8. ^{1}H-NMR spectrum for **KSU-1$_{bi}$** digested in DABCO/d_6-DMSO.

To confirm that the covalent attachment of succinic acid to the DPG linker via ester linkage, **KSU-1$_{bi}$** was disassembled in a solution of DABCO prepared in d_6-DMSO. Two separate signals corresponding to the -CH_2 protons of the ester derivative were present in the ^{1}H-NMR spectrum (Figure **3.8**). Mass fragments corresponds to DPG-diester from **KSU-1$_{bi}$** were also present in the ESI-MS spectrum ((Figure **3.9**) and the absence of the mass fragments for DPG or DPG-monoester further confirmed the quantitative conversion of DPG to DPG-diester. PXRD pattern of the material confirmed that the material was still crystalline and TGA showed **KSU-1$_{bi}$** had solvent accessible volume as it lost ~25% of its weight as DMF (Figure **3.10**). Gas adsorption data again revealed partial porosity and the presence of mesoporous (Figure **3.11**).

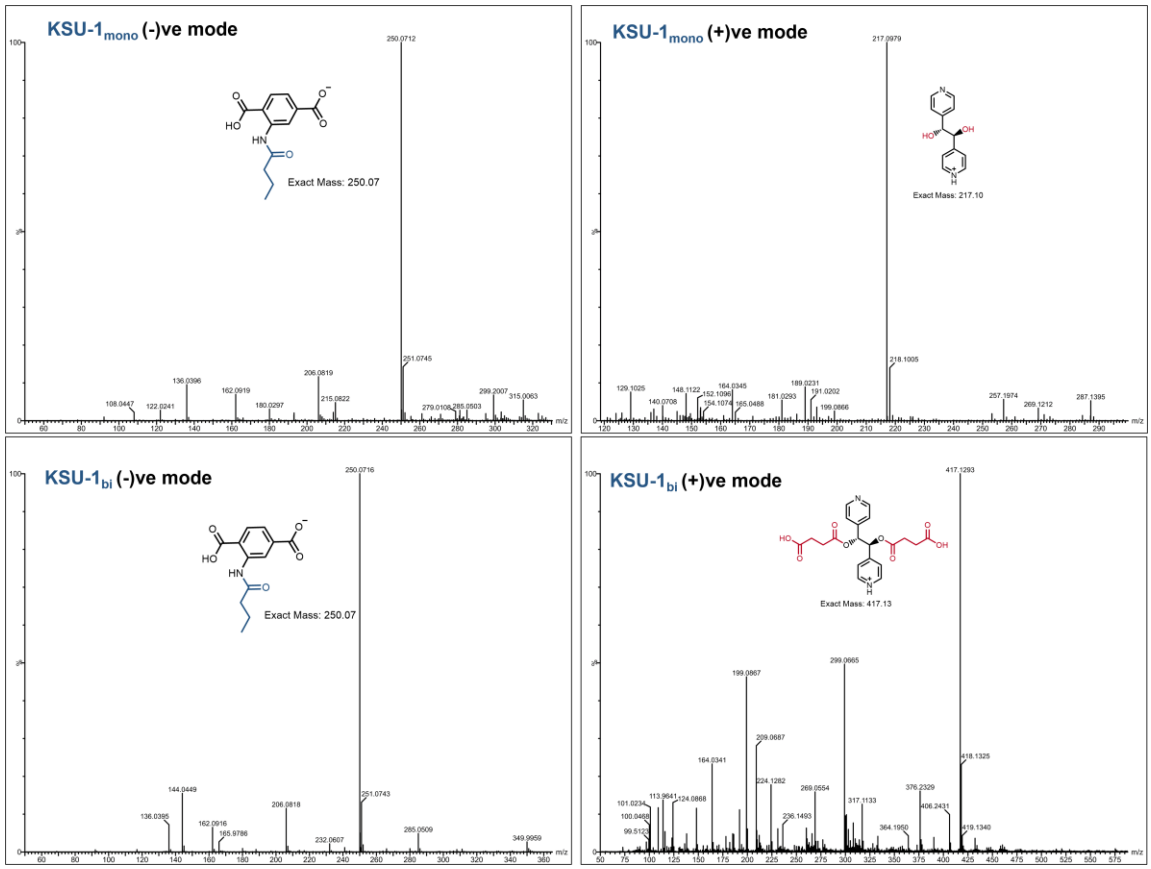

Figure 3.9. High-resolution electrospray ionization mass spectrometry (ESI-MS) of **KSU-1** (bottom), **KSU-1$_{mono}$** (middle), and **KSU-1$_{bi}$** (top) in negative (left) and positive (right) mode.

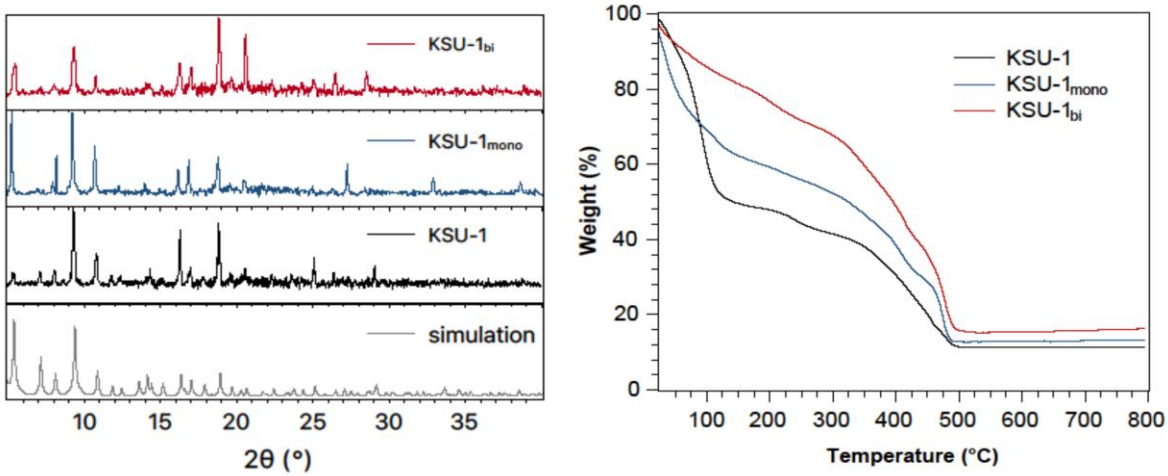

Figure 3.10. PXRD and TGA of **KSU-1**, **KSU-1$_{mono}$**, and **KSU-1$_{bi}$**.

Successful incorporation of butyryl group and the succinic group was confirmed by. both ^{1}H-NMR and mass spectra. Therefore, we can conclude two functional groups are uniformly distribute throughout the KSU-1 framework. But the presence of positional disorder of the amine group should also be considered.

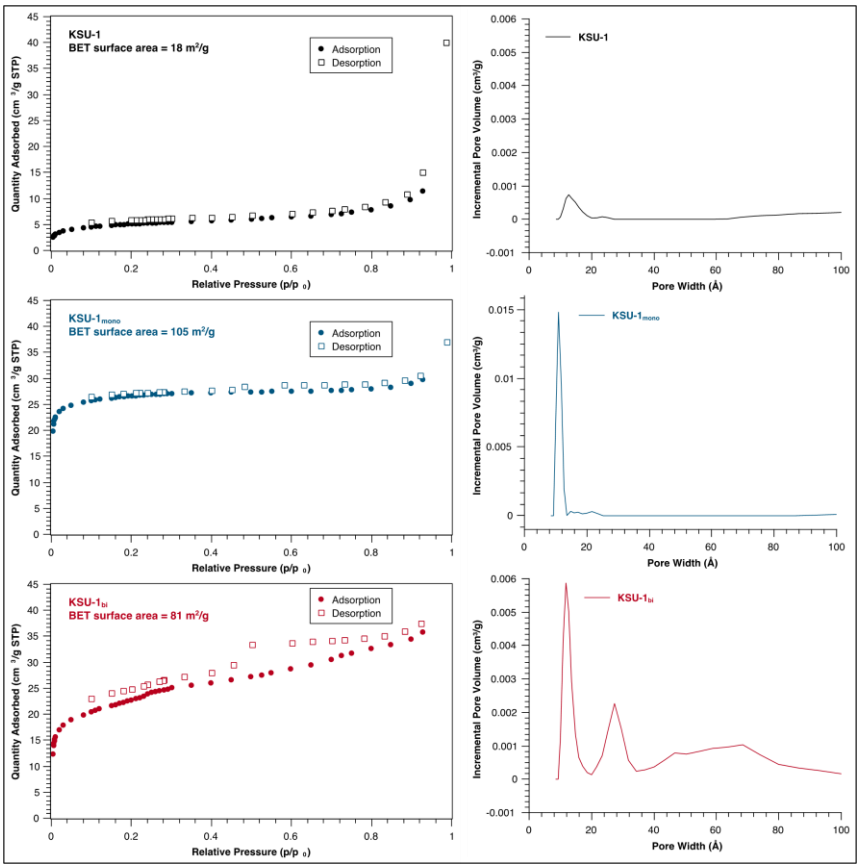

Figure 3.11. Left: N_2 gas adsorption for **KSU-1**, **KSU-1$_{mono}$**, and **KSU-1$_{bi}$**. Right: Pore size distribution for **KSU-1**, **KSU-1$_{mono}$**, and **KSU-1$_{bi}$**.

3.4. Conclusion

In conclusion, we have successfully implemented a methodology to achieve uniformly multifunctioanlized MOF material. This new strategy of MOF construction opens up exciting opportunities in the development of multifunctional MOFs. Even though, the resulting paddle wheel MOF does not possess permanent microporosity which will hinder some of its applications,

the developed method can be used as a blueprint to construct more robust materials. One can advanced this method to incorporate desired functionalities to the MOF framework to construct more complex materials for different applications. Uniform covalent functionalization of MOF framework materials will bring us one step closer to the construction of enzyme-inspired uniform and highly functionalized confined spaces.

3.4. Experimental

Materials

All chemicals were used as received from commercial sources unless otherwise noted. *Meso*-α,β-di(4-pyridyl) glycol (DPG) was purchased from TCI. Butyric anhydride and 2-aminoterephthalic acid (BDC-NH_2) were purchased from Alpha Aesar. Succinic anhydride and sulfuric acid-d_2 (D_2SO_4, 98 wt.% in D_2O, 99.5+% atom D) were purchased from Acros Organics. *N*,*N*-dimethylformamide (DMF) was purchased from Fisher Scientific, and zinc nitrate hexahydrate from Strem Chemicals. Anhydrous chloroform ($CHCl_3$) was purchased from Sigma Aldrich, and 1,4-Diazabicyclo[2.2.2]octane (DABCO) from Oakwood Products. Dimethyl sulfoxide-d_6 (d_6-DMSO, 99.9 atom % D) was purchased from Cambridge Isotopes Laboratories.

Synthetic procedures

Synthesis of KSU-1.

$Zn(NO_3)_2 \cdot 6H_2O$ (95.2 mg, 0.32 mmol), DPG (106 mg. 0.49 mmol), and DMF (80 mL) were combined in a 500 mL Florence flask. The flask was heated at 60 °C in a 500 mL heating block until the solution became clear. A solution of BDC-NH_2 (90.6 mg, 0.50 mmol) in DMF (20 mL) was added, and the flask incubated at 60 °C. After 48 h, the flask was removed from the heating block and left at room temperature for 48 h. Pale yellow crystals (40 mg, 35% yield) of the product were collected by filtration after several ~30 min washings with DMF.

General Procedure for the reaction of KSU-1 with butyric anhydride (Synthesis of KSU-1_{mono}).

Following a modified literature procedure,[2] **KSU-1** (50 mg, 0.0708 mmol, ca. 0.142 mmol equiv of $-NH_2$) was transferred into a 10 mm diameter glass exchange thimble with a frit that was placed into a 20 mL scintillation vial. The vial was charged with 10 mL of a 0.05 M solution of butyric anhydride (4 equiv.) in anhydrous $CHCl_3$, and the mixture was left at room temperature for 24 h with continuous mixing on a Corning LSE Low Speed Orbital Shaker. The glass thimble containing the MOF material was then transferred to a new scintillation with 10 mL of a 0.025 M solution of butyric anhydride (2 equiv.) in anhydrous $CHCl_3$ and left to mix for another 24 h. The reactant solution was exchanged this way 2 more times, each after 24 h. The thimble containing the MOF material was then transferred to a new scintillation vial containing fresh $CHCl_3$ and mixed for ~30 min. The $CHCl_3$ was exchanged with fresh $CHCl_3$ 3 times, and then fresh DMF a further 3 times. Pale yellow crystals were isolated from the frit (93% yield) and stored under DMF.

General Procedure for the nucleophilic ring-opening of succinic anhydride by KSU-1mono (Synthesis of KSU-1_{bi}).

Following a modified literature procedure,[20] **KSU-1mono** (50 mg, 0.0593 mmol, ca. 0.118 mmol equiv of $-OH$) was transferred into a 10 mm diameter glass exchange thimble with glass frit, that was placed into a 20 mL scintillation vial that had been charged with a suspension of succinic anhydride (80 mg, 6 equiv.) in 4 mL of anhydrous $CHCl_3$. The mixture was left at room temperature for 72 h with continuous mixing on a Corning LSE Low Speed Orbital Shaker. The thimble containing the MOF material was then transferred to a new scintillation vial containing fresh $CHCl_3$ and mixed for ~30 min. The $CHCl_3$ was exchanged with fresh $CHCl_3$ 3 more times,

and then fresh DMF a further 3 times. Pale yellow crystals were isolated from the frit (9088% yield) and stored under DMF.

3.5. Characterization

Powder X-ray diffraction (PXRD)

Powder patterns were recorded on a Bruker AXS D8 Advance Phaser diffractometer with Cu Kα radiation (λ = 1.5418 Å) over a range of 5° < 2θ < 40° in 0.02° steps with a 0.5 s counting time per step. Samples were collected from the bottom of the reaction vial as a thick suspension in DMF and spread on a Si-Einkristalle plate immediately before PXRD measurements.

Nitrogen gas adsorption/desorption

Measurements were performed on a Micromeritics Tristar II 3020 (Micromeritics, Norcross, GA) at 77 K on samples that underwent supercritical CO_2 drying. Supercritical CO_2 drying was performed using a Tousimis Samdri PVT-30 critical point dryer (Tousimis, Rockville, MD, USA). Supercritically dried samples were prepared in the following manner: MOF materials that had undergone DMF to hexanes solvent exchanges were again solvent exchanged with ethanol by two quick washes. The ethanol-dispersed samples were transferred into the sample holder with a glass pipet and allowed to settle down. Excess EtOH was pipetted out and the sample holder was placed into a Tousimis Samdri-PVT-3D supercritical CO_2 dryer. The temperature was lowered to 0 °C, and the chamber was filled with liquid CO_2 (ultrahigh grade CO_2 with a siphon from Air-Gas Inc). The sample was soaked for 8 hours total, venting for five minutes every two hours. The chamber was then heated to 40 °C, and the supercritical CO_2 was bled off at a rate of 0.25 mL/min until the chamber reached ambient pressure (typically overnight). The chamber was opened and the sample was quickly transferred into a pre-weighed glass sample tube which was sealed and quickly transferred to a system providing 10-4 torr dynamic vacuum.

Thermogravimetric analysis (TGA)

TGA was performed on a TGA-Q50 interfaced with a PC using TA Universal Analysis software. Samples were heated at a rate of 10 ºC/min under a nitrogen atmosphere. All samples were extensively solvent exchanged with fresh DMF prior to analysis.

Proton nuclear magnetic resonance (^{1}H NMR)

Spectra were recorded on a Varian 400MHz NMR spectrometer (400 MHz for ^{1}H). NMR chemical shifts are reported in ppm against a residual solvent resonance as the internal standard (δ(d_6-DMSO) = 2.5 ppm). In a typical analysis, MOF materials stored in DMF were solvent exchanged with $CHCl_3$, isolated by vacuum filtration, and then evacuated in a vacuum oven at 80 °C overnight. Evacuated MOF samples (~8 mg) were transferred into an NMR tube and d_6-DMSO (0.5 mL) was added. Subsequently, D_2SO_4 (0.05 mL, 98% w/w in D_2O) or DABCO (10 mg; 178 mM) was also added. The tubes were capped and sonicated until all the solid was dissolved (~ 1 min).

Electrospray Ionization Mass Spectrometry (ESI)

MOF samples (~5mg) were placed in a solution of DABCO (10 mg) and 0.25ml of DMSO in a 2-dram vial. The vial was sonicated for ~ 1 min then heated at 80 °C overnight. A small amount of residue was filtered out and resulting solution was sent for ESI-MS analysis at the Mass Spectrometry Laboratory at the University of Illinois, Urbana-Champaign.

3.6. References

(1) Fracaroli, A. M.; Siman, P.; Nagib, D. A.; Suzuki, M.; Furukawa, H.; Toste, F. D.; Yaghi, O. M. Seven Post-Synthetic Covalent Reactions in Tandem Leading to Enzyme-like Complexity within Metal–Organic Framework Crystals. *J. Am. Chem. Soc.* **2016**, *138* (27), 8352–8355. https://doi.org/10.1021/jacs.6b04204.

(2) Garibay, S. J.; Wang, Z.; Tanabe, K. K.; Cohen, S. M. Soso. *Inorg. Chem.* **2009**, *48* (15), 7341–7349. https://doi.org/10.1021/ic900796n.

(3) Liu, C.; Luo, T.-Y.; Feura, E. S.; Zhang, C.; Rosi, N. L. Orthogonal Ternary Functionalization of a Mesoporous Metal–Organic Framework via Sequential Postsynthetic Ligand Exchange. *J. Am. Chem. Soc.* **2015**, *137* (33), 10508–10511. https://doi.org/10.1021/jacs.5b06780.

(4) Keenan, L. L.; Hamzah, H. A.; Mahon, M. F.; Warren, M. R.; Burrows, A. D. Secondary Amine-Functionalised Metal–Organic Frameworks: Direct Syntheses versus Tandem Post-Synthetic Modifications. *CrystEngComm* **2016**, *18* (30), 5710–5717. https://doi.org/10.1039/C6CE01270A.

(5) Nath, I.; Chakraborty, J.; Verpoort, F. Metal Organic Frameworks Mimicking Natural Enzymes: A Structural and Functional Analogy. *Chem. Soc. Rev.* **2016**, *45* (15), 4127–4170. https://doi.org/10.1039/C6CS00047A.

(6) Lillerud, K. P.; Olsbye, U.; Tilset, M. Designing Heterogeneous Catalysts by Incorporating Enzyme-Like Functionalities into MOFs. *Top. Catal.* **2010**, *53* (13), 859–868. https://doi.org/10.1007/s11244-010-9518-4.

(7) Cohen, S. M. Modifying MOFs: New Chemistry, New Materials. *Chem. Sci.* **2010**, *1* (1), 32–36. https://doi.org/10.1039/C0SC00127A.

(8) Mandal, S.; Natarajan, S.; Mani, P.; Pankajakshan, A. Post-Synthetic Modification of Metal–Organic Frameworks Toward Applications. *Adv. Funct. Mater.* **2021**, *31* (4), 2006291. https://doi.org/10.1002/adfm.202006291.

(9) Burrows, A. D. Mixed-Component Metal–Organic Frameworks (MC-MOFs): Enhancing Functionality through Solid Solution Formation and Surface Modifications. *CrystEngComm* **2011**, *13* (11), 3623–3642. https://doi.org/10.1039/C0CE00568A.

(10) Kong, X.; Deng, H.; Yan, F.; Kim, J.; Swisher, J. A.; Smit, B.; Yaghi, O. M.; Reimer, J. A. Mapping of Functional Groups in Metal-Organic Frameworks. *Science* **2013**, *341* (6148), 882–885. https://doi.org/10.1126/science.1238339.

(11) Kim, M.; Cahill, J. F.; Prather, K. A.; Cohen, S. M. Postsynthetic Modification at Orthogonal Reactive Sites on Mixed, Bifunctional Metal–Organic Frameworks. *Chem. Commun.* **2011**, *47* (27), 7629–7631. https://doi.org/10.1039/C1CC12101D.

(12) Liu, H.; Xi, F.-G.; Sun, W.; Yang, N.-N.; Gao, E.-Q. Amino- and Sulfo-Bifunctionalized Metal–Organic Frameworks: One-Pot Tandem Catalysis and the Catalytic Sites http://pubs.acs.org/doi/full/10.1021/acs.inorgchem.6b01057 (accessed 2020 -03 -25). https://doi.org/10.1021/acs.inorgchem.6b01057.

(13) Liu, L.; Zhou, T.-Y.; Telfer, S. G. Modulating the Performance of an Asymmetric Organocatalyst by Tuning Its Spatial Environment in a Metal–Organic Framework. *J. Am. Chem. Soc.* **2017**, *139* (39), 13936–13943. https://doi.org/10.1021/jacs.7b07921.

(14) Zhou, T.-Y.; Auer, B.; Lee, S. J.; Telfer, S. G. Catalysts Confined in Programmed Framework Pores Enable New Transformations and Tune Reaction Efficiency and Selectivity. *J. Am. Chem. Soc.* **2019**, *141* (4), 1577–1582. https://doi.org/10.1021/jacs.8b11221.

(15) Samarakoon, K. P.; Satterfield, C. S.; McCoy, M. C.; Pivaral-Urbina, D. A.; Islamoglu, T.; Day, V. W.; Gadzikwa, T. Uniform, Binary Functionalization of a Metal–Organic Framework Material. *Inorg. Chem.* **2019**, *58* (14), 8906–8909. https://doi.org/10.1021/acs.inorgchem.9b00838.

(16) Ma, B.-Q.; Mulfort, K. L.; Hupp, J. T. Microporous Pillared Paddle-Wheel Frameworks Based on Mixed-Ligand Coordination of Zinc Ions. *Inorg. Chem.* **2005**, *44* (14), 4912–4914. https://doi.org/10.1021/ic050452i.

(17) Chun, H.; Moon, J. Discovery, Synthesis, and Characterization of an Isomeric Coordination Polymer with Pillared Kagome Net Topology. *Inorg. Chem.* **2007**, *46* (11), 4371–4373. https://doi.org/10.1021/ic070036t.

(18) Kondo, M.; Takashima, Y.; Seo, J.; Kitagawa, S.; Furukawa, S. Control over the Nucleation Process Determines the Framework Topology of Porous Coordination Polymers. *CrystEngComm* **2010**, *12* (8), 2350–2353. https://doi.org/10.1039/C004066E.

(19) Zhou, K.; Chaemchuen, S.; Wu, Z.; Verpoort, F. Rapid Room Temperature Synthesis Forming Pillared Metal-Organic Frameworks with Kagomé Net Topology. *Microporous Mesoporous Mater.* **2017**, *239*, 28–33. https://doi.org/10.1016/j.micromeso.2016.09.038.

(20) Gadzikwa, T.; Farha, O. K.; Mulfort, K. L.; Hupp, J. T.; Nguyen, S. T. A Zn-Based, Pillared Paddlewheel MOF Containing Free Carboxylic Acids via Covalent Post-Synthesis Elaboration. *Chem. Commun.* **2009**, No. 25, 3720–3722. https://doi.org/10.1039/B823392F.

Chapter 4 - Uniform and Simultaneous Orthogonal Functionalization of a Metal-Organic Framework Material

Portions of this chapter appear in the following manuscript:

Samarakoon, K.; Yazdanparast, M.; Day, V. W.; Gadzikwa, T. Uniform and Simultaneous Orthogonal Functionalization of a Metal-Organic Framework Material. **2020,** *5***,** 804-808.

4.1. Introduction

In Chapter 3, we introduced a methodology to create uniformly binary functionalized MOF cavities via the covalent post synthetic modification of a well-defined MOF, **KSU-1**.[1] While this is an efficient methodology for generating confined spaces that are both complex and uniform, the system has a drawback that limits its general use: the amine and hydroxyl reactive groups of **KSU-1** both are nucleophiles. While the -OH has poorer aptitude for nucleophilic attack compared to $-NH_2$, allowing for independent reaction, the first functionalization is restricted to reacting the $-NH_2$ with the limited range of electrophiles that will not also react with -OH. Additionally, the material cannot be modified with moieties that are better nucleophiles than the hydroxyls. Both enzymes and organocatalysts often rely on the nucleophilic activation as a mode of catalytic activity, therefore, to introduce a nucleophilic catalyst to **KSU-1**, one of the linkers must have orthogonal reactivity to nucleophiles

In synthetic chemistry orthogonality refers to 100% selectivity in chemical reactions resulting in no any cross reactivity and yielding the same product regardless of the reaction sequence.[2] These types of reactions are well studied in the construction of complex molecules like

natural products,[3] dendrimers[4] and functionalized polymers.[5] The presence of orthogonal groups in the system opens up the opportunity to carry out one-pot simultaneous reactions and it avoids traditional protection-deprotection strategies.[2]

Therefore, to address the issues associated with the **KSU-1** system, we use the concept of orthogonal chemistry, where we use chemical functionalities that have completely different reactivities to construct our MOF material. The goal of this work is to demonstrate the applicability of orthogonal chemistry in generating uniformly functionalized MOF materials.

4.2. Synthetic strategy for uniform orthogonally functionalizing MOF material

Our aim was to synthesize a new MOF that has the same topology as the **KSU-1** but with orthogonal reactivities. For the second system we modified our initial BDC-NH_2 linker to BDC-N_3 where it has an azide group. In the presence of Cu(I), azides only react with terminal alkynes, i.e. Cu(I) azide alkyne cyclo addition reactions (CuAAC).[6] These are unique reactions and CuAAC reactions do not interfered with other functionalities present in the systems (Figure **4.1**).

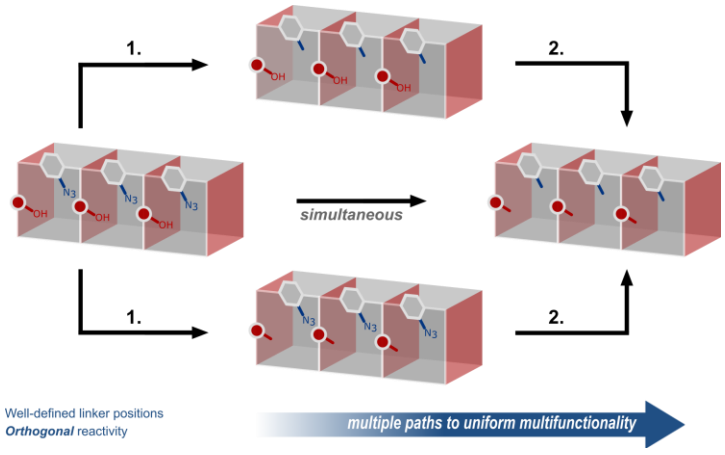

Figure 4.1. The use of orthogonally reactive linkers to generate a uniformly functionalized MOF material. Reproduced from Ref.[7] with permission from the Royal Society of Chemistry.

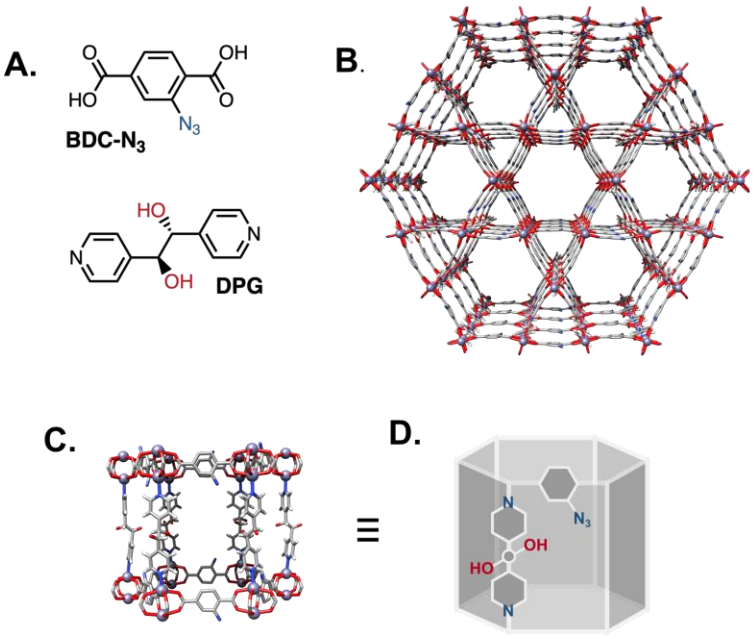

Figure 4.2. KSU-2 MOF A. Linkers used for **KSU-2** MOF synthesis B. Single crystal structure of **KSU-2** viewed along the *c*-axis C. Unit cell of **KSU-2** D. Schematic representation of **KSU-2**.

We synthesized our second MOF, **KSU-2** with 2-azido-1,4-benzenediacarboxylic acid (BDC-N_3) and *meso*-α,β-di(4-pyridyl)glycol (DPG) in the presence of Zn^{2+} as the metal salt. Organic linkers were incubated in the presence of $Zn(NO_3)_2$ $6H_2O$ at 60 °C for 24 hours on a hot plate to yield yellow color, block-like crystals (Figure **4.2**). Singal crystal data suggested that **KSU-2** has kagome type lattice as in **KSU-1** with large hexagonal shaped pores and small triangular pores. The BDC-N_3 linkers were connected by Zn-paddlewheel secondary building units (SBUs) in the *ab*-plane, forming 2D Kagome-type sheets that were pillared by DPG linkers along the *c*-axis. Phase purity of the bulk material was determined via proton nuclear magnetic resonance (^{1}H-NMR) spectroscopy of the material digested in deuterated D_2SO_4 and d_6-DMSO (Figure **4.3**) and powder x-ray diffraction (PXRD) (Figure **4.10**). The material retained very little porosity as determined by the N_2 gas adsorption (Figure **4.9**), though it possess substantial solvent accessible

volume according to the thermogravimetric analysis (TGA) analysis. It indicated that **KSU-2** had enough space for the multifunctionalization (Figure **4.9**) to generate uniformly and orthogonally functionalized MOF.

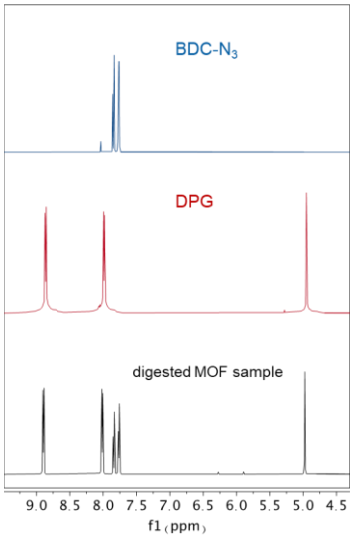

Figure 4.3. ^{1}H-NMR of **KSU-2** digested in d_6-DMSO/D_2SO_4 mixture.

4.3. Uniform orthogonal multipath and simultaneous functionalization of KSU-2

After successful synthesis of **KSU-2**, the next step was to use the material to generate a uniformly multifunctionalized MOF. The orthogonality of the reactive groups in **KSU-2** allowed us to perform both multipath functionalization and simultaneous one-pot reactions. For multifunctionalization via pathway 1, BDC-N_3 was reacted with phenyl acetylene in the presence of CuBr catalyst under a nitrogen atmosphere at 60 °C for 72 hours (Figure **4.4**). The Reaction was monitored by ^{1}H-NMR (Figure **4.5**) and Fourier transform infrared spectroscopy (FT-IR) (Figure **4.6**). Quantitative conversion of BDC-N_3 was confirmed by the disappearance of the azide peak in the FT-IR spectrum and by the presence of peaks corresponding to protons from $BDC_{triazole}$ (**KSU-2$_{triazole}$**) in the ^{1}H-NMR. Electron spray ionization-mass spectroscopy (ESI-MS) of the **KSU-2**-

$_{Triazole}$ was done after digesting the MOF material in a solution of DABCO prepared in DMSO. The presence of the mass fragment (m/z = 310) for $[BDC_{triazole}\text{-}H^{+}]^{-}$ in the negative mode and the unreacted DPG fragment (m/z = 217) in the positive mode further confirmed the successful generation of **KSU-2**$_{triazole}$ (Figure **4.7**).

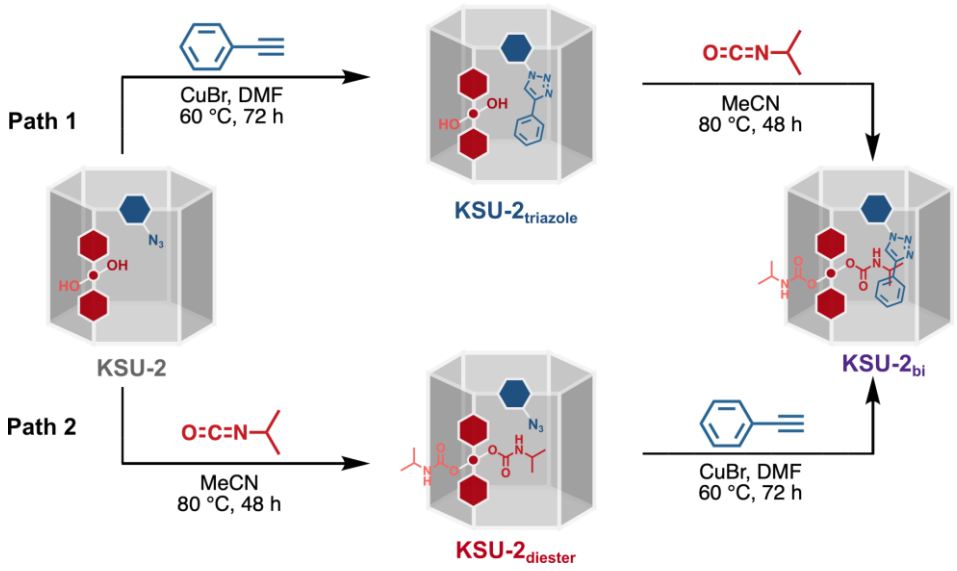

Figure 4.4. Multipath uniform functionalization of **KSU-2.**

PXRD of the material confirmed material was still crystalline. To determine how much solvent accessible pore volume had been retained after the click reaction, TGA was performed after rinsing and prolong soaking of the material in DMF. The material lost about 30% weight as DMF, and which confirming the retention of a significant amount of solvent accessible pore volume although, N_2 adsorption revealed negligible porosity after the evacuation. These results encouraged us to proceed to the functionalization of the hydroxyl groups of the DPG ligand of **KSU-2**$_{triazole}$.

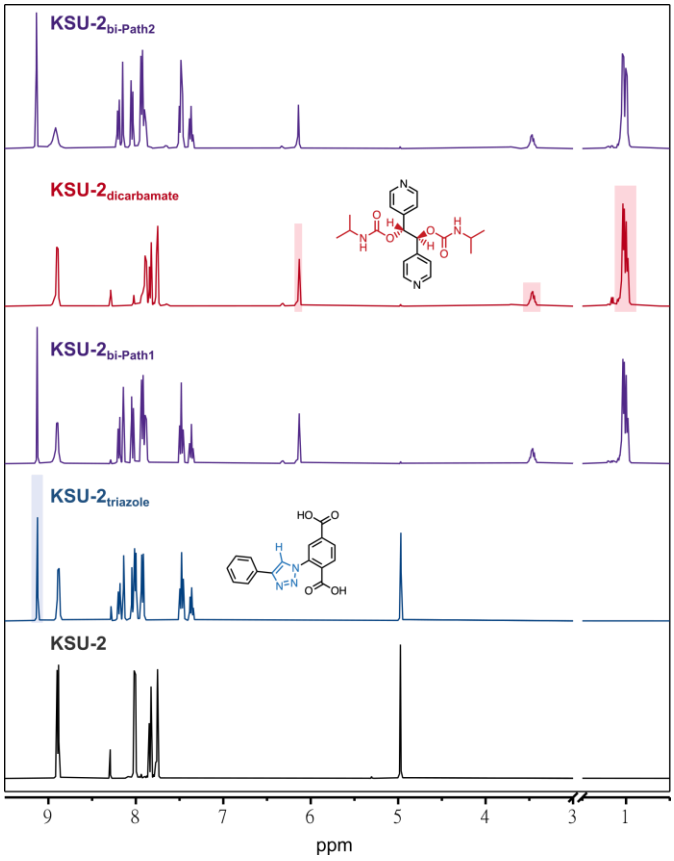

Figure 4.5. Stacked ^{1}H-NMRs of **KSU-2** functionalized through multiple paths.

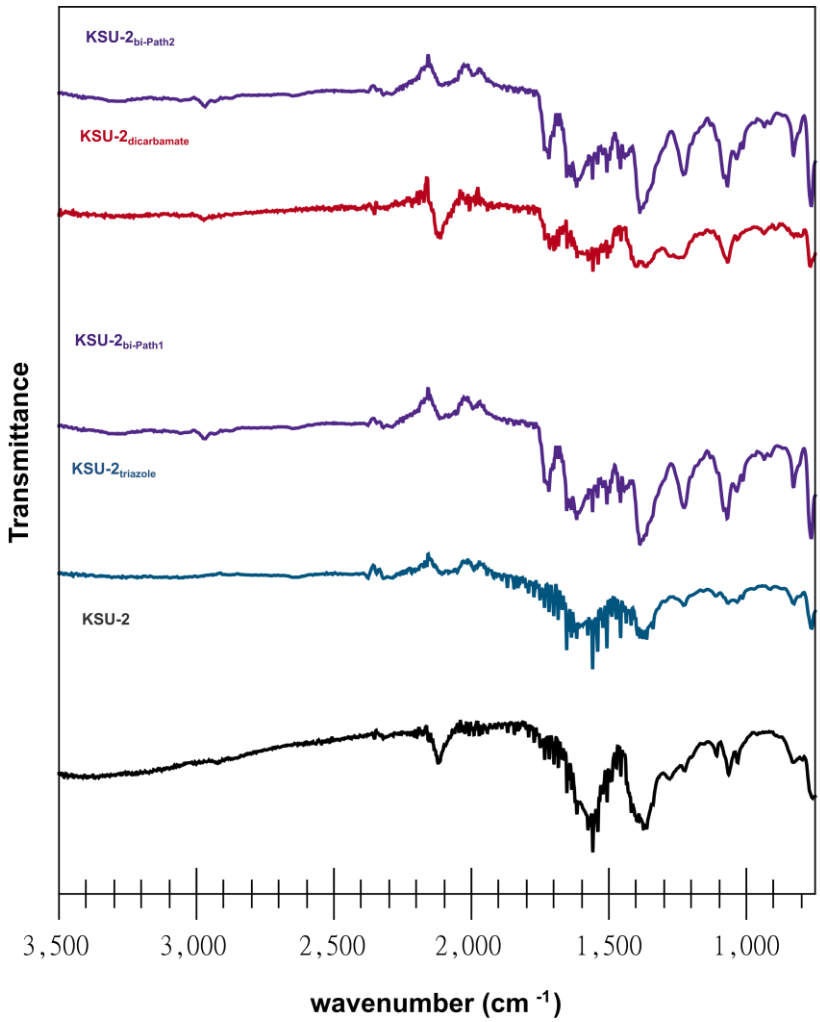

Figure 4.6. Stacked FT-IRs of **KSU-2** functionalized through multiple paths.

For the next step, the hydroxyl groups of the DPG were reacted with isocyanates. Isocyanates have been widely used to functionalize amine groups in MOFs[8–10] and we performed a similar type of reaction but with the -OH on the DPG ligand to form the dicarbamates. In Chapter 3, **KSU-1$_{mono}$** was reacted with cyclic anhydrides to form the diester which hydrolyzed in the presence of acid during NMR sample preparation leading us to perform additional characterizations to confirm covalent attachment. But dicarbamates do not hydrolyze in the presence of an acid and it made easier for characterization. Following a modified procedure,[9] **KSU-**

2$_{triazole}$ was immersed in a 0.2 M solution of isopropyl isocyanate in acetonitrile, with continuous agitation at 80 °C for 48 hours yielded **KSU-2$_{bi\ path\ 1}$** (Figure **4.4**). The complete shift of the proton alpha to the glycol in the ^{1}H-NMR confirmed the quantitative conversion of hydroxyls to carbamate (Figure **4.5**).

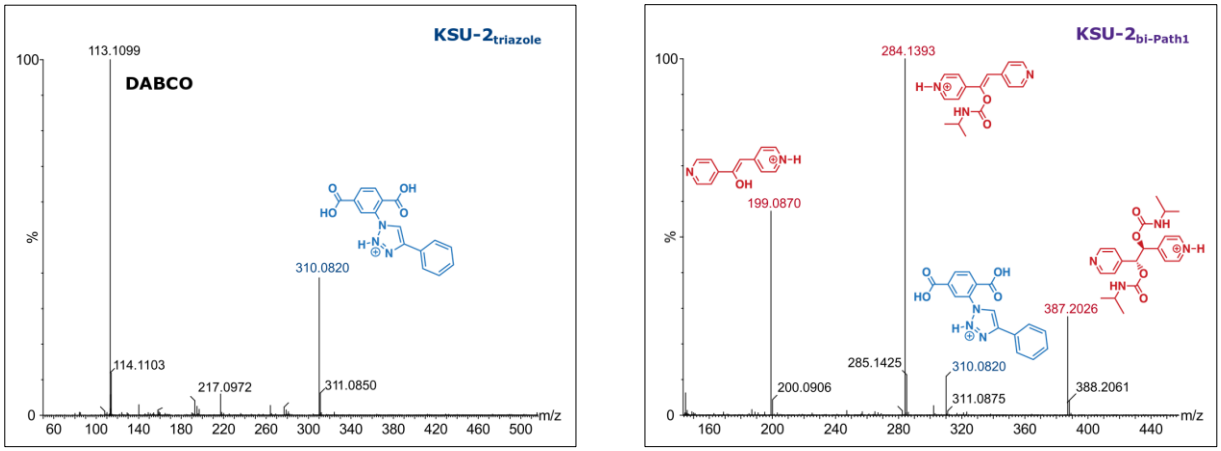

Figure 4.7. High resolution ESI-MS of positive mode of **KSU-2$_{traizole}$** and **KSU-2$_{bi\text{-}path1}$**.

Covalent functionalization was further confirmed through ESI-MS ((Figure **4.7**). **KSU-2 $_{bi\ path\ 1}$** was disassembled in a solution of DABCO in DMSO and analyzed in both positive and negative modes. Positive mode spectra revealed the presence of both BDC$_{\text{-triazole}}$ (m/z =310) and DPG-$_{\text{dicarbamate}}$ (m/z =387). Significant peaks corresponding to McLafferty rearrangement product [DPG dicarmate-CO_2-i$PrNH_2$ +H] as well as that fragment minus neutral iPrNCO were observed in the same positive mode spectrum. PXRD was done, which revealed it was crystalline. TGA confirmed that material still possessed a significant amount of solvent accessible pore volume as it lost ~20 % of weight as DMF. Having confirmed successful generation of **KSU-2 $_{bi\ path\ 1}$** via path 1 we next attempted the reverse path functionalization to get the same final product.

In the reverse path bifunctionalization of **KSU-2**, the hydroxyl groups of the DPG linker were first reacted with isopropyl isocyanate followed by the Cu-catalyzed click reaction on the

azide groups (Figure **4.4**). The same isocyanate reaction conditions were used to obtain **KSU-2** dicarbamate. The material was characterized by the ^{1}H-NMR after digesting it in a solution of D_2SO4 and d_6-DMSO. Quantitative conversion of the hydroxyls to dicarbamate was confirmed by the complete shift of the alpha protons of the glycol (Figure **4.5**). Positive mode spectra of the ESI-MS (Figure **4.8**) showed the presence of DPG-$_{\text{dicarbamate}}$ after disassembling the sample in a solution of DABCO in DMSO. Additionally, FT-IR showed the IR stretch for the unreacted azide ((Figure **4.6**). Interestingly, N_2 adsorption of the **KSU-2**-dicarbamate showed that material was slightly more stable under evacuation.

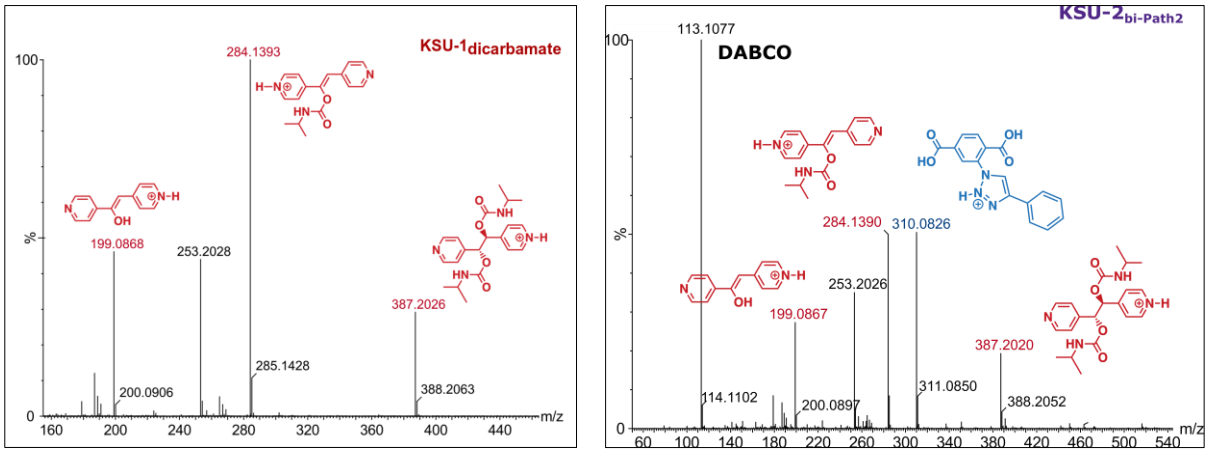

Figure 4.8. High resolution**,** ESI-MS positive mode of **KSU-2$_{\text{carbamate}}$** and **KSU-2$_{\text{bi-path2}}$**.

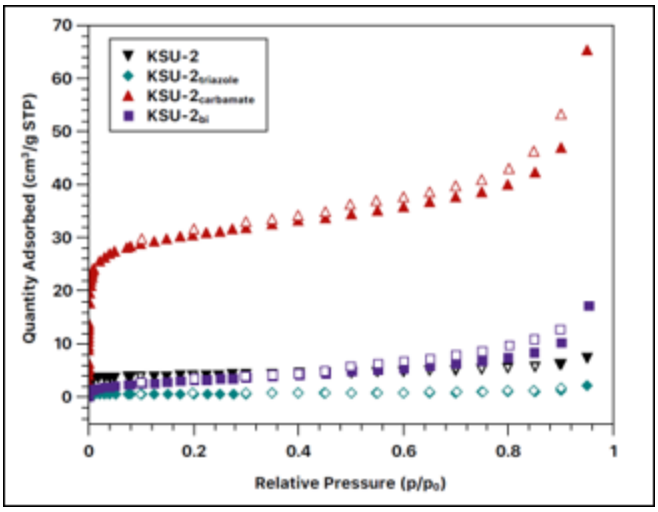

Figure 4.9. N_2 gas adsorption measurements **KSU-2** functionalized through multiple paths (Closed: Adsorption, Open: Desorption).

As the next step, **KSU-2$_{\text{dicarbamate}}$** was reacted with phenyl acetylene in the presence of Cu(I) catalyst to get the **KSU-2$_{\text{bi path 2}}$**. The same CuAAC conditions as in pathway 1 were used and the ^{1}H-NMR was identical to **KSU-2$_{\text{bi path 1}}$**, which confirmed the successful reverse path bifunctionalization of **KSU-2**. All the other characterizations were carried out and the results were well-aligned with the data from pathway 1.

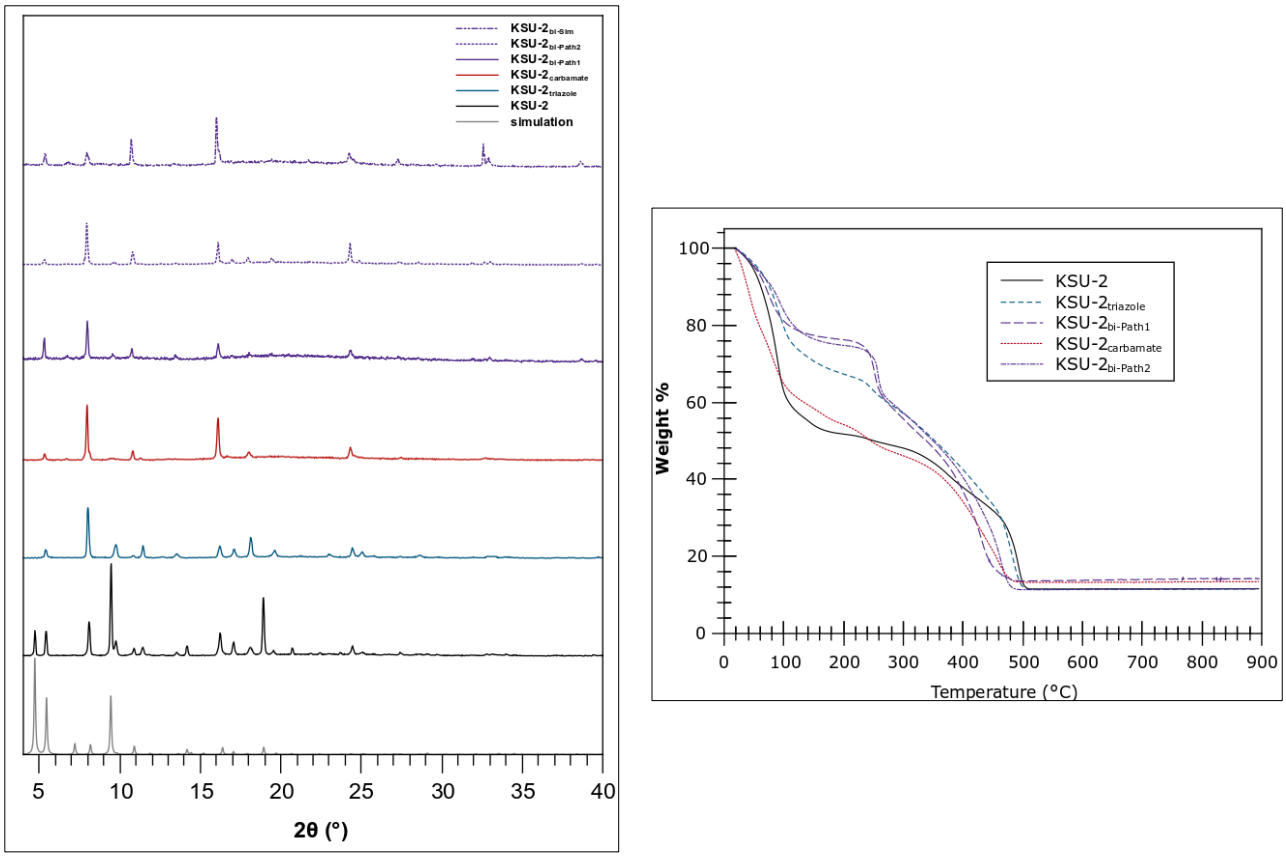

Figure 4.10. PXRDs and TGA data of **KSU-2** functionalized through multiple paths.

An additional advantage of having an orthogonal system is the ability to perform simultaneous one-pot reaction to obtain the same final product. In the one-pot functionalization, **KSU-2** was treated with a mixture of DMF: MeCN 1:1 in the presence of both phenylacetylene and isopropyl isocyanate at 60 °C. The FT-IR, ^{1}H-NMR and ESI-MS results (Figure **4.11**) were same as for **KSU-2-$_{bi}$** and confirmed the successful one-pot, independent reactions.

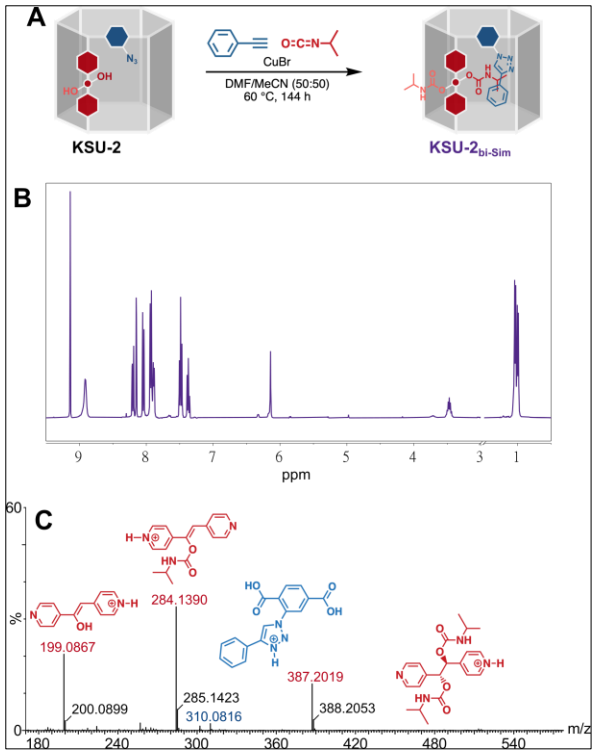

Figure 4.11. One-pot multifunctionalization of **KSU-2** A. Reaction scheme. B. ^{1}H-NMR of digested sample in d_6-DMSO/D_2SO_4 mixture C. ESI-MS of digested sample in a DABCO solution.

4.4. Conclusion

Chapter 4 demonstrated the advantage of having orthogonal reactive groups at well-defined positions in a MOF scaffold for generating uniformly multifunctionalized confined spaces. Through this work, we

i) addressed the limitations of initial **KSU-1** system

ii) attained multifunctionalized confined spaces through both multipath and one-pot/simultaneous reactions

KSU-2 has the characteristics of a biorthogonal systems which means it can be functionalized with functional groups that are found in biological systems. This strategy can be successfully used to develop actual enzyme mimics or systems which can do cooperative catalysis.

4.5. Experimental

Materials

All chemicals were used as received from commercial sources unless otherwise noted. Meso-*α*,*β*-di(4-pyridyl) glycol (**DPG**) was purchased from TCI. Sulfuric acid-d_2 (D_2SO_4, 98 wt.% in D_2O, 99.5+% atom D), Copper bromide (98%) were purchased from Acros Organics. *N*,*N*-dimethylformamide (DMF), tetrahydrofuran (THF), Acetonitrile (MeCN), *tert*-butyl nitrite (90 %) and phenyl acetylene (98%) were purchased from Fisher Scientific, and zinc nitrate hexahydrate from Strem Chemicals. Chloroform ($CHCl_3$), 2-aminoterephthalic acid (**BDC-NH$_2$**), and isopropyl isocyanate (98%) were purchased from Sigma Aldrich. 1,4-Diazabicyclo[2.2.2]octane (DABCO) and trimethylsilyl azide (95%) were purchased from Oakwood Products. Dimethyl sulfoxide-d_6 (d_6-DMSO, 99.9 atom % D) was purchased from Cambridge Isotopes Laboratories.

Synthetic Procedures

Synthesis of BDC-N$_3$.

Followed a modified literature procedure.[62] 2-aminoterephthalic acid (**BDC-NH$_2$**) (0.20 g, 1.10 mmol, 1 equiv.) was dissolved in dry THF (20 ml) and *tert*-butyl nitrite (0.39 ml, 3.3. mmol, 3 equiv.) was added at 0 °C. After stirring for 15 min trimethylsilyl azide (0.38 ml, 2.20 mmol, 2 equiv.) was added at 0 °C, the reaction mixture was slowly warmed-up to room temperature and stirred for 48 h. The reaction mixture was evaporated under reduced pressure, the solid was washed with cold THF, filtered and dried under vacuum to give **BDC-N$_3$** as a yellow solid (0.24 g ,94%).

Synthesis of KSU-2

$Zn(NO_3)_2 \cdot 6H_2O$ (297.0 mg, 0.10 mmol), DPG (246.0 mg. 1.13 mmol), and DMF (80 mL) were combined in a 500 mL Florence flask. The flask was heated at 60 °C in a 500 mL heating block until the solution became clear. A solution of BDC-N_3 (104.5 mg, 0.50 mmol) in DMF (20 mL) was added, and the flask incubated at 60 °C. After 24 h, the flask was removed from the heating block and left at room temperature for 24 h. Yellow crystals (142.7 mg, 21% yield) of the product were collected by filtration after several ~30 min washings with DMF.

General Procedure for the CuAAC reaction of MOF materials with phenyl acetylene.

Following a modified literature procedure,[63] the azide-bearing MOF (1 equiv) was transferred into a 10 mm diameter glass exchange thimble with a glass frit that was placed into a 20 mL scintillation vial. The vial was charged with phenyl acetylene (16 equiv) and enough DMF to make a 100 mM solution. This solution was degassed with bubbling N_2 gas for 60 minutes, before CuBr (10 mol%) was added. The mixture was left under N_2, at 60 °C for 72 h with continuous mixing on a Corning LSE Low Speed Orbital Shaker. The thimble containing the MOF material was then transferred to a new scintillation vial containing fresh DMF and mixed for ~30 min. The DMF was exchanged with fresh DMF, with ~30 min. mixing, 3 more times. Product crystals were isolated from the frit and stored under DMF.

CuAAC of KSU-2 (Synthesis of KSU-2$_{triazole}$).

KSU-2 (50 mg, 0.066 mmol, ca. 0.132 mmol of $-N_3$), phenyl acetylene (214 µL, 1.0 mmol), DMF (10 mL), and CuBr (14.3 mg, 0.1 mmol). Green crystals were isolated from the frit (98% yield) and stored under DMF.

CuAAC of KSU-2$_{carbamate}$ (Synthesis of KSU-2$_{bi\text{-}Path1}$). KSU-2$_{carbamate}$

(50 mg, 0.054 mmol, ca. 0.108 mmol of $-N_3$), phenyl acetylene (214 µL, ~1.0 mmol), DMF (10 mL), and CuBr (14.3 mg, 0.1 mmol). Brownish-green crystals were isolated from the frit (93% yield) and stored under DMF.

General Procedure for the reaction of MOF materials with isopropyl isocyanate

Following a modified literature procedure,[64] the DPG-containing MOF (1 equiv) was transferred into a 10 mm diameter glass exchange thimble with glass frit, that was placed into a 20 mL scintillation vial that had been charged with isopropyl isocyanate (12 equiv) and enough MeCN to make a 0.2 M solution. The mixture was left at 80 °C for 48 h with continuous mixing on a Corning LSE Low Speed Orbital Shaker. The thimble containing the MOF material was then transferred to a new scintillation vial containing fresh MeCN and mixed for ~30 min. The MeCN was exchanged with fresh MeCN, and shaken for ~30 min., 3 more times. The solvent was exchanged with fresh DMF, and shaken, a further 3 times. MOF crystals were isolated from the frit and stored under DMF.

Reaction of KSU-2 with isopropyl isocyanate (Synthesis of KSU-2$_{carbamate}$). KSU-2

(50 mg, 0.066 mmol, ca. 0.132 mmol of −OH), isopropyl isocyanate (78 µL, 0.80 mmol), and MeCN (4 mL). Reddish-brown crystals were isolated from the frit (67% yield) and stored under DMF.

Reaction of KSU-2$_{triazole}$ with isopropyl isocyanate (Synthesis of KSU-2$_{bi\text{-}Path2}$). KSU-2$_{triazole}$

(50 mg, 0.052mmol, ca. 0.104 mmol of −OH), isopropyl isocyanate (61µL, 0.62 mmol), and MeCN (4 mL). Green crystals were isolated from the frit (87% yield) and stored under DMF.

Procedure for the simultaneous reaction of KSU-2 with phenyl acetylene and isopropyl isocyanate (Synthesis of KSU-$2_{bi\text{-}Sim}$).

KSU-2 (50 mg, 0.066 mmol, ca. 0.132 mmol of $-N_3$, ca. 0.132 mmol of $-OH$) was transferred into a 10 mm diameter glass exchange thimble with a glass frit that was placed into a 20 mL scintillation vial. The vial was charged with phenyl acetylene (214 µL, 1.0 mmol), isopropyl isocyanate (196 µL, 2.0 mmol), and 10 mL of MeCN:DMF (50:50 v/v). This solution was degassed with bubbling N_2 gas for 60 minutes, before CuBr (14.3 mg, 0.1 mmol, 10 mol %) was added. The mixture was left under N_2, at 60 °C for 6 days with continuous mixing on a Corning LSE Low Speed Orbital Shaker. The thimble containing the MOF material was then transferred to a new scintillation vial containing fresh DMF:MeCN and mixed for ~30 min. The DMF was exchanged with fresh DMF, with ~30 min. mixing, 3 more times. Product crystals were isolated from the frit and stored under DMF.

4.6. Characterization

Powder X-ray diffraction (PXRD)

Powder patterns were recorded on a Bruker AXS D8 Advance Phaser diffractometer with Cu Kα radiation (λ = 1.5418 Å) over a range of $5° < 2\theta < 40°$ in 0.02° steps with a 0.5 s counting time per step. Samples were collected from the bottom of the reaction vial as a thick suspension in DMF and spread on a Si-Einkristalle plate immediately before PXRD measurements.

Proton nuclear magnetic resonance (^{1}H NMR)

Spectra were recorded on a Varian 400MHz NMR spectrometer (400 MHz for 1H). NMR chemical shifts are reported in ppm against a residual solvent resonance as the internal standard (δ(*d*$_6$-DMSO) = 2.5 ppm). In a typical analysis, MOF materials stored in DMF were solvent exchanged with $CHCl_3$, isolated by vacuum filtration, and then evacuated in a vacuum oven at 80 °C

overnight. Evacuated MOF samples (5-6 mg) were transferred into an NMR tube and d_6-DMSO (0.55 mL) was added. Subsequently, D_2SO_4 (0.09 mL, 98% w/w in D_2O) was also added. The tubes were capped and sonicated until all the solid was dissolved (~ 1 min).

Nitrogen gas adsorption/desorption

Measurements were performed on anAutosorb iQMP(Quantachrome Instruments, Anton Paar USA, Ashland VA) at 77 K.Samples were prepared in the following manner: MOF materials that had undergone DMF to hexanes solvent exchanges were again solvent exchanged with chloroformby two quick washes.Finally, the sample was washed with dichloromethane and dried under vacuum (< 10-3 torr) at 60 °C for 5 h. Using the "outgas" function of the surface area analyzer, the sample was dried again for 360 min at 80 °C to remove all residual solvent.

Thermogravimetric analysis (TGA)

TGA was performed on a TGA-Q50 interfaced with a PC using TA Universal Analysis software. Samples were heated at a rate of 10 ºC/min under a nitrogen atmosphere. All samples were extensively solvent exchanged with fresh DMF prior to analysis.

Fourier-transform infrared spectroscopy (FTIR)

Fourier-transform infrared spectroscopy was performed on a Cary 630 spectrometer. Spectra were collected on MOF samples (~1 mg) which had combined with 5 mass equivalents (~5 mg) of KBr and ground together to a fine powder.

Electrospray Ionization Mass Spectrometry (ESI)

MOF samples (~5mg) were placed in a solution of DABCO (10 mg) and 0.25ml of DMSO in a 2-dram vial. The vial was sonicated for ~ 1 min then heated at 80 °C overnight. A small amount of residue was filtered out and resulting solution was sent for ESI-MS analysis at the Mass Spectrometry Laboratory at the University of Illinois, Urbana-Champaign.

Single-crystal X-ray crystallography analysis for KSU-2.

A set of diffraction data [38465 reflections using 2290 1º-wide ω- or ϕ-scan frames with scan times of 8-20 seconds] was collected[65] for a single-domain crystal of **KSU-2** using monochromated CuKα radiation (λ = 1.54178 Å) on a Bruker Proteum Single Crystal Diffraction System with dual CCD detectors and associated Helios high-brilliance multilayer optics and a shared Bruker MicroSTAR microfocus Cu rotating anode x-ray source operating at 45kV and 60mA. Data for **KSU-2** was collected with a Platinum 135 CCD detector and a crystal-to-detector distance of 50 mm. The integrated data[66] were corrected empirically for variable absorption effects using equivalent reflections. The Bruker software package SHELXTL was used to solve the structure using "direct methods" techniques. All stages of weighted full-matrix least-squares refinement were conducted using F_o^2 data with the SHELXTL XL v2018 Version 1 software package.[67] Final crystallographic details are summarized in Table S1.

The asymmetric unit of **KSU-2** contains two Zn^{2+} cations, two 2-azidoterephthalate dianions and one neutral *meso*-*α*,*β*-di(4-pyridyl) glycol moiety. Although disorder is common and not unexpected in MOF structures, the bridging ligands in this particular system have additional potential for inherent disorder. While octahedral coordination at the Zn ions will preclude much rotational disorder of the planar terephthalate ligands about the Zn----Zn vector, each "locked" ligand can still bridge the same two Zn metals in four different ways. Since the *meso*-*α*,*β*-di(4-pyridyl) glycol ligand coordinates to a Zn atom through a single nitrogen on each end, it could have different rotational orientations about the Zn----Zn vector. The ligand could also bridge the same two metals with its two ends interchanged. Fortunately, both of the terephthalate ligands appear to have only three of the four possible orientations and the di(4-pyridyl) glycol ligands do not appear to be have significant rotational disorder about the Zn----Zn vector.

Fourier maps from the initial structure solution clearly revealed the Zn atoms, all C and O atoms of the terephthalate ligands and the pyridine rings of the di(4-pyridyl) glycol ligand. Non-structured (presumably disordered) electron density was present between the two pyridine moieties. After refining these clearly identified atoms with isotropic thermal parameters, the Zn and terephthalate carbon and oxygen atoms were refined with anisotropic thermal parameters. A difference Fourier revealed low electron density at sp^2-hybridized positions for four ortho (4- and 7-) carbons of both terephthalate ligands. It also contained a more structured region of electron density between the two coordinated pyridine ligands. The occupancy factors and isotropic thermal parameters for two (one for each terephthalate ligand) of the eight ortho (4- and 7-) nitrogens behaved erratically during refinement cycles and were eventually removed from the structural model. The remaining six nitrogens were included in the final structural model with isotropic thermal parameters and variable occupancy factors that refined to final values ranging from 0.035 to 0.110 for the two terephthalate ligands. Reasonable electron density corresponding to the second and third azide nitrogen atoms did not appear in any difference Fourier.

The published structure of *meso*-*α*,*β*-di(4-pyridyl) glycol was then used with the coordinates of the two pyridine ligands and the disordered electron density between them to derive coordinates for two bridging modes for the *meso*-*α*,*β*-di(4-pyridyl) glycol ligand in **KSU-2**. Bond lengths and angles for the atoms of these two *meso*-*α*,*β*-di(4-pyridyl) glycol bridging modes were required to have values similar to the published structure. The bond lengths and angles were restrained to idealized sp^2- or sp^3-hybridized multiples of the aromatic C=C bond length that was included in the refinement as a free variable; it refined to a final value of 1.295(2) Å. All four of the 7-atom p-methylpyridine moieties and both 10-atom terephthalate (C21-C27, N24, N26, N27;

and C31-C37, N34, N36, N37) moieties were also required to be coplanar. The normalized occupancy factors for the two *meso*-*α*,*β*-di(4-pyridyl) glycol bridging modes refined to 52%/48%.

Since the terephthalate atoms were disordered but reasonably well-defined and all of the *meso*-*α*,*β*-di(4-pyridyl) glycol nonhydrogen atoms linking the pyridine rings were disordered and not well-defined, the *meso*-*α*,*β*-di(4-pyridyl) glycol ligand nonhydrogen atoms were included in the structural model with isotropic thermal parameters. Hydrogen atoms bonded to carbon in all ligands were included in the structural model as idealized riding model atoms (assuming sp^2- or sp^3-hybridization of the carbon atoms and C-H bond lengths of 0.95 Å or 1.00 Å). Hydrogen atoms bonded to hydroxyl oxygen atoms were included as idealized riding model atoms (assuming or sp^3-hybridization of the oxygen atom and an O-H bond length of 0.84 Å) that were free to rotate about their C-O bonds in least-squares refinement cycles. The isotropic thermal parameters of idealized hydrogen atoms in all ligands were fixed at values 1.2 (bonded to C) or 1.5 (bonded to O) times the equivalent isotropic thermal parameter of the carbon or oxygen atom to which they are covalently bonded. The x coordinate of disordered glycol carbon atom C7 was fixed in the final refinement cycles and a DAMP parameter of 400 was used to aid convergence. Low residual difference Fourier electron density appearing at reasonable positions in the MOF channels was included in the structural model as disordered partial-occupancy isotropic oxygen atoms that still did not completely fill the structural voids. Refinement of racemic twinning revealed the crystal was a 69/31 racemic twin.

Table 1. Crystal and Refinement Data ***KSU-2***.

	KSU-2
Empirical formula	$C_{28.00}H_{14.00}N_{4.00}O_{16.32}Zn_{2.00}$
Formula weight	299.44
Temperature	200(2) K
Wavelength	1.54178 Å
Crystal system	Trigonal
Space group	P3 – C_3^1 (No. 143)
a	21.5814(4) Å
b	21.5814(4) Å
c	16.1592(3) Å
a	90.00°
β	90.00°
γ	120.00°
Volume	6517.9(3)Å^3
Z	3
Density (calculated)	0.610 g/cm^3
Absorption coefficient	0.956 mm^{-1}
F(000)	1202
Crystal size	0.050 x 0.050 x 0.040 mm^3
Theta range	2.36 to 70.52°
Index ranges	$-25\leq h\leq 26$, $-24\leq k\leq 26$, $-14\leq l\leq 19$
Reflections collected	85166
Independent reflections	14685 [R_{int} = 0.064]
Completeness to θ = 66°	99.9 %
Absorption correction	Multi-scan
Max. and min. transmission	1.000 and 0.756
Refinement method	Full-matrix least-squares on F^2

Data / restraints / parameters	14685 / 107 / 454
Goodness-of-fit on F^2	1.062
Final R indices [I>2σ(I)]	$R_1 = 0.108$, $wR_2 = 0.278$
R indices (all data)	$R_1 = 0.141$, $wR_2 = 0.331$
Largest diff. peak and hole	1.26 and -1.09 $e^-/Å^3$

4.6. References

(1) Samarakoon, K. P.; Satterfield, C. S.; McCoy, M. C.; Pivaral-Urbina, D. A.; Islamoglu, T.; Day, V. W.; Gadzikwa, T. Uniform, Binary Functionalization of a Metal–Organic Framework Material. *Inorg. Chem.* **2019**, *58* (14), 8906–8909. https://doi.org/10.1021/acs.inorgchem.9b00838.

(2) Shahrokhinia, A.; Biswas, P.; Reuther, J. F. Orthogonal Synthesis and Modification of Polymer Materials. *J. Polym. Sci.* **2021**, *59* (16), 1748–1786. https://doi.org/10.1002/pol.20210345.

(3) Baran, P. S.; Richter, J. M. Direct Coupling of Indoles with Carbonyl Compounds: Short, Enantioselective, Gram-Scale Synthetic Entry into the Hapalindole and Fischerindole Alkaloid Families. *J. Am. Chem. Soc.* **2004**, *126* (24), 7450–7451. https://doi.org/10.1021/ja047874w.

(4) Zhang, Y.; Üçüncü, M.; Gambardella, A.; Baibek, A.; Geng, J.; Zhang, S.; Clavadetscher, J.; Litzen, I.; Bradley, M.; Lilienkampf, A. Bioorthogonal Swarming: In Situ Generation of Dendrimers. *J. Am. Chem. Soc.* **2020**, *142* (52), 21615–21621. https://doi.org/10.1021/jacs.0c07869.

(5) Tonga, M.; Yesilbag Tonga, G.; Seber, G.; Gok, O.; Sanyal, A. Dendronized Polystyrene via Orthogonal Double-Click Reactions. *J. Polym. Sci. Part Polym. Chem.* **2013**, *51* (23), 5029–5037. https://doi.org/10.1002/pola.26933.

(6) Castro, V.; Rodríguez, H.; Albericio, F. CuAAC: An Efficient Click Chemistry Reaction on Solid Phase. *ACS Comb. Sci.* **2016**, *18* (1), 1–14. https://doi.org/10.1021/acscombsci.5b00087.

(7) Samarakoon, K.; Yazdanparast, M.; Day, V. W.; Gadzikwa, T. Uniform and Simultaneous Orthogonal Functionalization of a Metal-Organic Framework Material. **2020** 5, 804-808. https://doi.org/10.26434/chemrxiv.11482893.v2.

(8) Garibay, S. J.; Wang, Z.; Tanabe, K. K.; Cohen, S. M. Postsynthetic Modification: A Versatile Approach Toward Multifunctional Metal-Organic Frameworks. *Inorg. Chem.* **2009**, *48* (15), 7341–7349. https://doi.org/10.1021/ic900796n.

(9) Dugan, E.; Wang, Z.; Okamura, M.; Medina, A.; Cohen, S. M. Covalent Modification of a Metal–Organic Framework with Isocyanates: Probing Substrate Scope and Reactivity. *Chem. Commun.* **2008**, No. 29, 3366–3368. https://doi.org/10.1039/B806150E.

(10) Bernt, S.; Guillerm, V.; Serre, C.; Stock, N. Direct Covalent Post-Synthetic Chemical Modification of Cr-MIL-101 Using Nitrating Acid. *Chem. Commun.* **2011**, *47* (10), 2838–2840. https://doi.org/10.1039/C0CC04526H.

(11) A. Gotthardt, M.; Grosjean, S.; S. Brunner, T.; Kotzel, J.; M. Gänzler, A.; Wolf, S.; Bräse, S.; Kleist, W. Synthesis and Post-Synthetic Modification of Amine-, Alkyne-, Azide- and Nitro-Functionalized Metal–Organic Frameworks Based on DUT-5. *Dalton Trans.* **2015**, *44* (38), 16802–16809. https://doi.org/10.1039/C5DT02276B.

(12) Yi, X.-C.; Xi, F.-G.; Qi, Y.; Gao, E.-Q. Synthesis and Click Modification of an Azido-Functionalized Zr(IV) Metal–Organic Framework and a Catalytic Study. *RSC Adv.* **2014**, *5* (2), 893–900. https://doi.org/10.1039/C4RA09883H.

(13) Dong, X.-W.; Liu, T.; Hu, Y.-Z.; Liu, X.-Y.; Che, C.-M. Urea Postmodified in a Metal–Organic Framework as a Catalytically Active Hydrogen-Bond-Donating Heterogeneous Catalyst. *Chem. Commun.* **2013**, *49* (70), 7681–7683. https://doi.org/10.1039/C3CC42531B.

(14) *Data Collection: SMART Software in APEX2 V2014.11-0 Suite. Bruker-AXS, 5465 E. Cheryl Parkway, Madison, WI 53711-5373 USA.*

(15) *Data Reduction: SAINT Software in APEX2 V2014.11-0 Suite. Bruker-AXS, 5465 E. Cheryl Parkway, Madison, WI 53711-5373 USA.*

(16) *Refinement: SHELXTL Software in APEX2 V2014.11-0 Suite. Bruker-AXS, 5465 E. Cheryl Parkway, Madison, WI 53711-5373 USA.*

Chapter 5 - Enzyme-inspired Metal-Organic Framework Materials Based Chiral Brønsted Acid Catalysts

5.1. Introduction

Chapters 3 and 4 discussed two proofs of concept developed to generate uniformly multifunctionalized MOF pores. The two strategies fill the gap in existing literature where none of the previous efforts were able to achieve uniform multifunctionalization of a MOF interior. In this chapter, our aim is to design a solid-state organocatalyst to demonstrate the practical application of our strategies. Herein, we designed a heterogenous chiral Brønsted acid catalyst to perform the asymmetric epoxide ring opening reaction.

According to IUPAC a Brønsted acids are defined as "molecular entity capable of donating hydron (proton) to a base (i.e., a hydron donor") or the corresponding chemical species". They are widely used in industrial catalysis to convert biomass into valuable fine-chemical and petrochemical products.[1–4] Traditional homogeneous acids play an important role in catalyzing chemical reactions at the industrial scale though they suffer from high toxicity and corrosion issues. Therefore much attention has been paid to developing solid-state Brønsted acid catalysts due to their ease of separation, lower corrosion, and easy handling.[1,5,6]

A wide range of solid Brønsted acid catalysts have been developed over the past decades. Heteropolyacids,[7] phosphates,[8] acidic resins[9] and sulfated metal oxides[10] are a few examples. However, their catalytic activity is limited due to their low surface area and porosity. Mesoporous silica and zeolites have emerged as better alternatives to address these issues, but they suffer from poor designability, tunability and controllability.[11] Therefore metal-organic framework (MOF) materials have gained much attention as a potential solid state catalysts because of their high

tunabilty, porosity and surface area. By taking advantage of their modifiable structure, Brønsted acid groups have been successfully incorporated into MOF pores.[11,12] Through the incorporation of Brønsted acids on the MOF scaffold one can heterogenize homogeneous catalysts and gain the advantages of both homogeneous and heterogenous systems to improve both activity and selectivity.[13]

Carboxylic acids are a common functional group found in a large pool of organic compounds. Carboxylic acids as Brønsted acid catalysts are not well-studied most likely due to their weaker acidity compared to well-known phosphonic acid catalysts.[14] However, a key consideration with Brønsted acid catalysis is to choose a catalyst with appropriate acidity, as higher acidity can cause substrate decomposition. Therefore, it is beneficial to develop weaker-Brønsted acids to catalyze organic reactions. Similarly chiral carboxylic acids are widely used as organocatalysts in asymmetric catalysis. Figure **5.1** shows some common chiral Brønsted acids found in literature. But fine-tuning these catalysts is a daunting process because all the groups are attached to the same molecular scaffold. Therefore, it is necessary to developing chiral Brønsted acid catalyst systems that can be modified systematically if necessary.

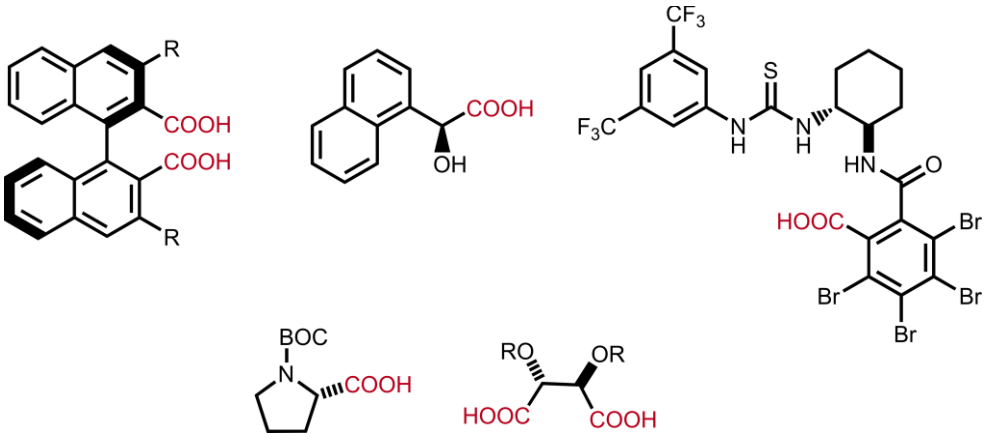

Figure 5.1 Pool of chiral Brønsted acids.[15]

5.2. Synthetic strategy

To achieve such a systematically modifiable chiral Brønsted acid catalyst, we propose the use of our previously implemented method of uniform binary functionalization of a MOF material. Using the strategy, it is possible to introduce both Brønsted acid group and chiral group uniformly through independent post-synthetic modification (PSM) strategy. In a report by Cohen et. al., they demonstrated the creation of heterogenous Brønsted acid catalysts through the post-synthetic modification of a MOF structure that bears pendent -NH_2 groups.[16] They performed nucleophilic ring opening reactions with different cyclic anhydrides which resulted in free COOH groups.

By taking the advantage of the nucleophilic -NH_2 group in **KSU-1** we introduce a carboxylic acid through the nucleophilic ring opening reaction of cyclic anhydrides, and we introduced a chiral group through the -OH to achieve "chiral- Brønsted acid" catalyst (Figure **5.2**).

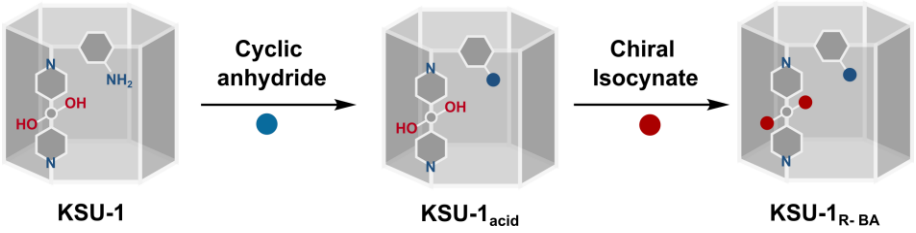

Figure 5.2. Synthetic strategy to introduce a Brønsted acid and a chiral group to **KSU-1**.

In order to generate a pool of catalysts we use three different cyclic anhydrides, which possess different acid strengths due to their chemical structure (Figure **5.3 A).** In order to introduce chirality into the MOF framework the -OH group is reacted with a chiral isocyanate: (R)-(+)-α-Methylbenzyl isocyanate to form a chiral carbamate (Figure **5.3 B)**. To test the catalytic activity of the resulting material the asymmetric epoxide ring opening reaction will be investigated.

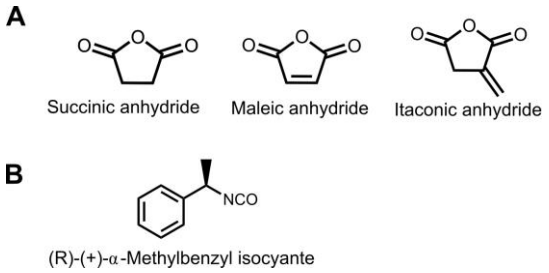

Figure 5.3 Pool of A. Cyclic anhydrides B. Chiral isocyanates.

5.3. Post-synthesis modification of KSU-1 to generate chiral Brønsted acid catalyst

To generate the **KSU-1** based chiral Brønsted acid catalyst, first the -NH_2 group in **KSU-1** was reacted with 0.2 M solution of cyclic anhydride in $CHCl_3$ at room temperature over 12 hours (Figure **5.4**). After the reaction the MOF material was exchanged with fresh $CHCl_3$ a few times and finally washed with DMF and stored in DMF until further use. It is necessary to carefully monitor the reaction to prevent the reaction between the -OH group and the cyclic anhydride. The proton nuclear magnetic resonance (^{1}H-NMR) spectroscopy confirmed quantitative conversions of the -NH_2.groups in the reactions with all three anhydrides. Initial ^{1}H-NMR peaks correspond to BDC-NH_2 had shifted as the reaction progressed and at the complete conversion, all three peaks at 7.26 ppm, 7.54 ppm and 7.85 ppm had moved to 7.66 ppm, 9.00 ppm and 8.03 ppm respectively (Figure **5.5**).

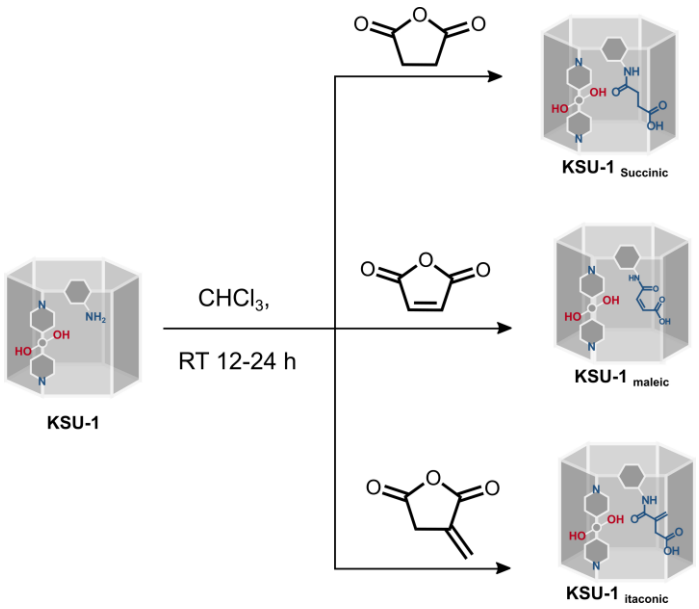

Figure 5.4. Installation of Brønsted acids into **KSU-1** through cyclic anhydride ring opening reactions.

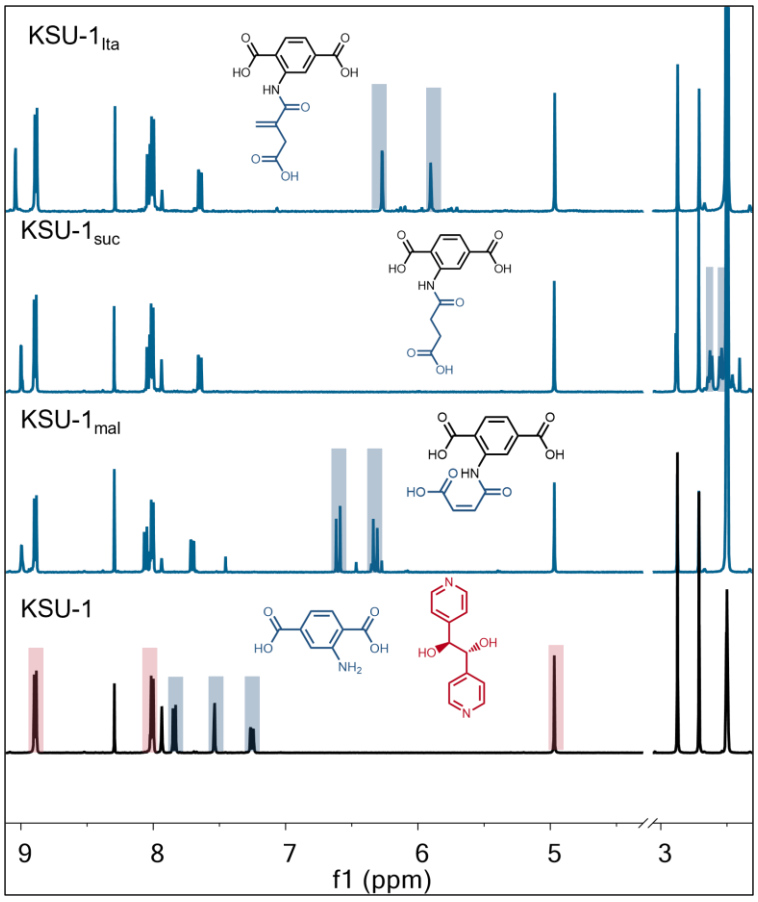

Figure 5.5. ^{1}H-NMR of **KSU-1$_{acid}$** after digesting the MOF samples in d_6-DMSO/D_2SO_4 mixture

The crystallinity of the material was confirmed by the powder x-ray crystallography (PXRD) and thermogravimetric analysis (TGA) was performed after soaking the material in DMF for two days. The TGA traces that **KSU-1$_{maleic}$**, **KSU-1$_{succinic}$** and **KSU-1$_{itaconic}$** lost 49.5%, 46.5% and 57.2% masses as the solvent respectively.

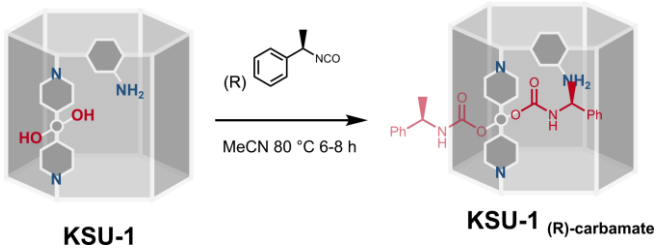

Figure 5.6. Functionalization of **KSU-1** with a chiral isocyanate**.**

In a change to our original plan, to synthesize the chiral Brønsted catalysts, **KSU-1** was reacted with the chiral isocyanate first. Pricilla Matseketsa, a graduate student from the Gadzikwa lab found that the -OH group of the **KSU-1** unexpectedly reacts with certain isocyanates leaving the more nucleophilic -NH_2 unreacted. Therefore, the same reaction conditions were applied to synthesize chiral **KSU-1$_{R\text{-}carbamate}$** (Figure **5.6**). **KSU-1** was incubated in a 0.2 M solution of the chiral isocyanate prepared in acetonitrile at 80 °C for 6-8 h, and the reaction was monitored by ^{1}H-NMR. Upon successful reaction, formation of **KSU-1$_{R\text{-}carbamate}$**, the initial peak corresponding to protons alpha to the -OH groups (at 4.9 ppm) completely disappeared, and two new doublets appeared around 6.23 ppm and the new aromatic protons appeared as two sets (Figure **5.7)**. The reason is that DPG molecule is no longer *meso* (R,S) compound but is now a diastereomer due to the installation of a chiral group..

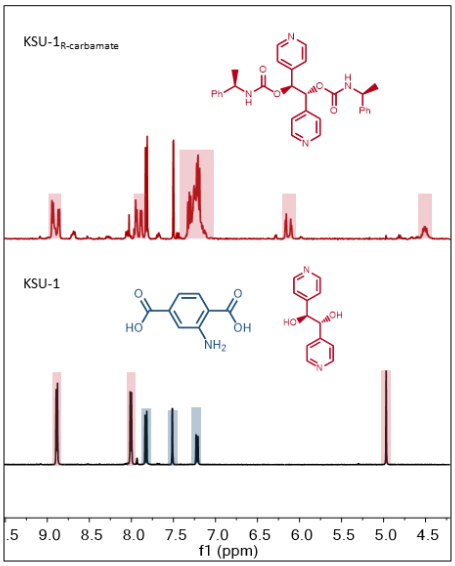

Figure 5.7. ^{1}H-NMR of **KSU-1$_{R\text{-}carbamate}$** digested in d_6-DMSO/D_2SO_4 mixture**.**

After successful synthesis of **KSU-1$_{R\text{-}carabamate}$**, the material was then reacted with the three different cyclic anhydrides to install carboxylic acid groups. **KSU-1$_{R\text{-}carbamate}$** (Figure **5.8**) were incubated in 0.2 M solutions of the respective cyclic anhydrides in $CHCl_3$ and left on the shaker for up to 24 h until reaction went to completion. It was also found that reacting the **KSU-1**$_{acid}$ with chiral isocyanate was much slower. The reactions were monitored through ^{1}H-NMR (Figure **5.9**). and the successful conversion of **KSU-1$_{R\text{-}carbamate}$** to **KSU-1$_{R\text{-}BA}$** was confirmed by the complete shift of peaks corresponding to BDC-NH_2.

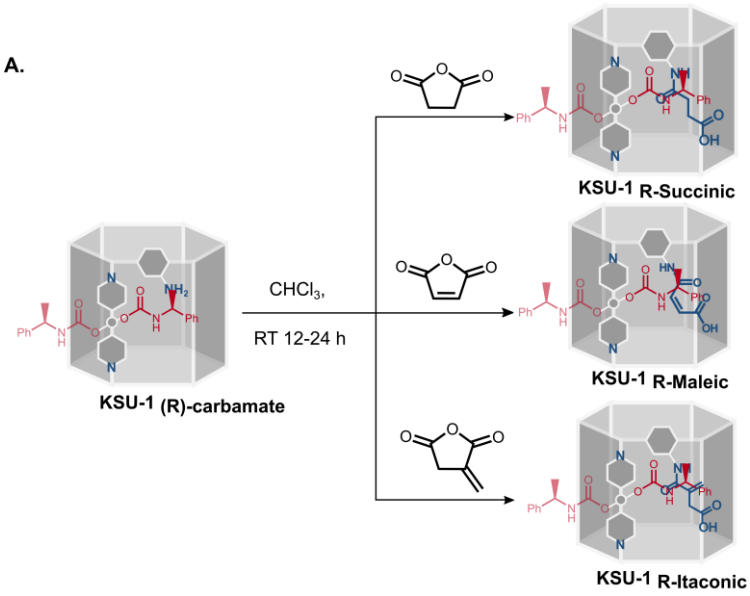

Figure 5.8. Functionalization of **KSU-1$_{R\text{-}carbamate}$** with cyclic anhydrides.

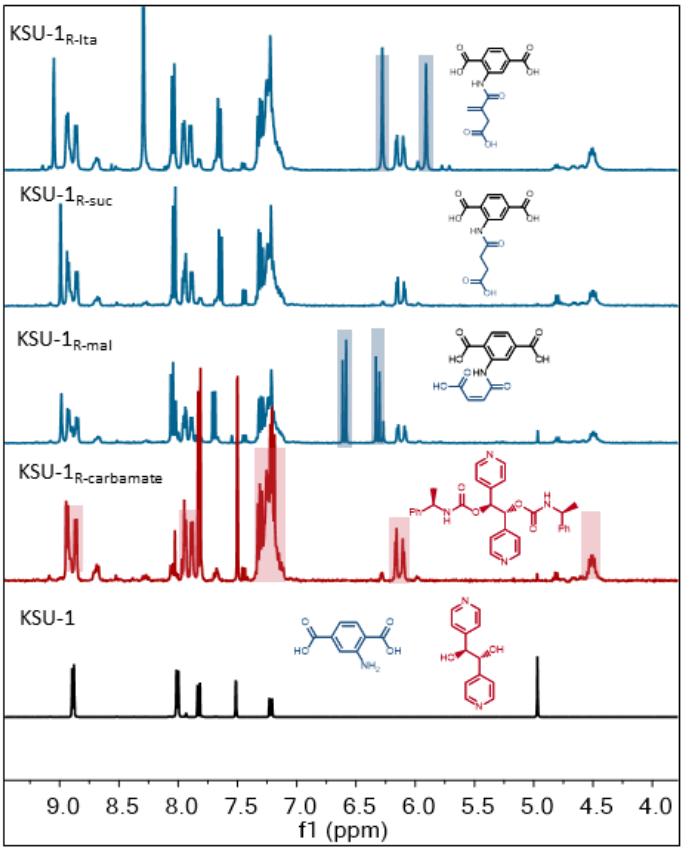

Figure 5.9. ^{1}H-NMRs of series of **KSU-1$_{R\text{-}BA}$** digested in a d_6-DMSO/D_2SO_4 mixture**.**

PXRD of the bifunctionalized materials (Figure **5.10**) confirmed that the material retained their crystallinity and TGA (Figure **5.11**) confirmed that the material possessed solvent accessible pore volume even after the second functionalization.

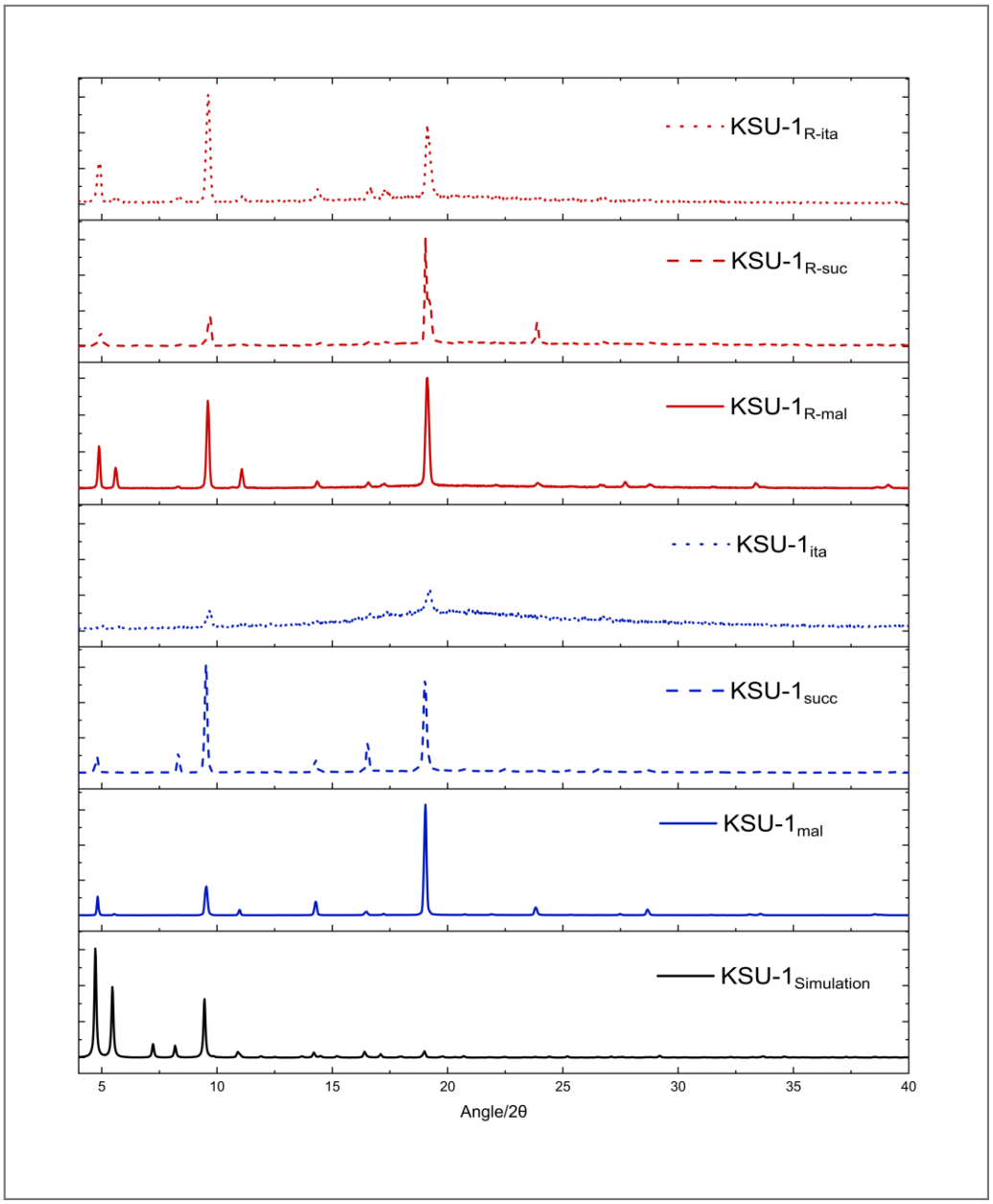

Figure 5.10. PXRD data for functionalized **KSU-1** materials.

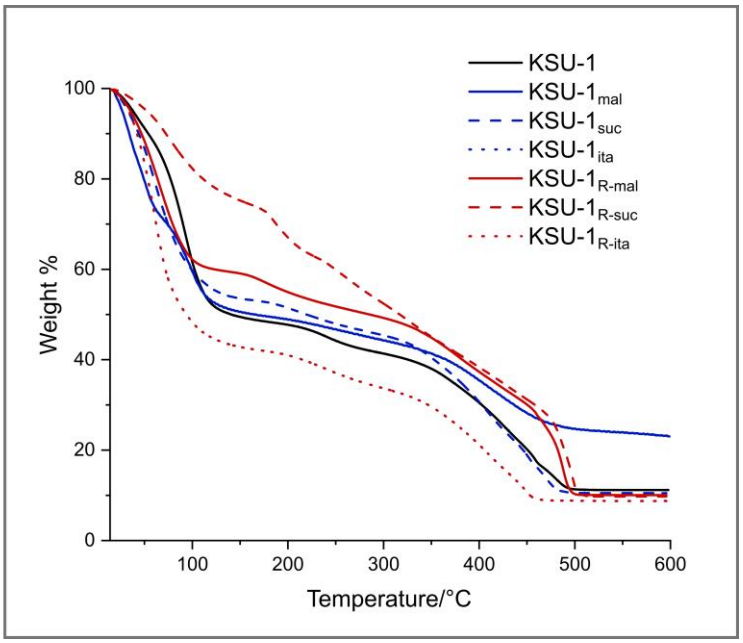

Figure 5.11. TGA data for functionalized **KSU-1** materials.

5.4. Catalytic activity of Brønsted acid catalyst

In order to test the catalytic activity of the series of **KSU-1$_{R\text{-}BA}$**, the methanolysis of epoxides was chosen. Initial catalysis experiments were performed using cis-1,2 epoxybutane. A 1 dram vial was charged with the catalysts (20 mol%), methanol (stored in 3Å molecular sieves) and finally with the epoxide. The reaction was left on the shaker at 25 °C for 24 h before taking an aliquot to analyze through ^{1}H-NMR. Conversions were calculated with respect to the methyl groups of the starting material and the product.

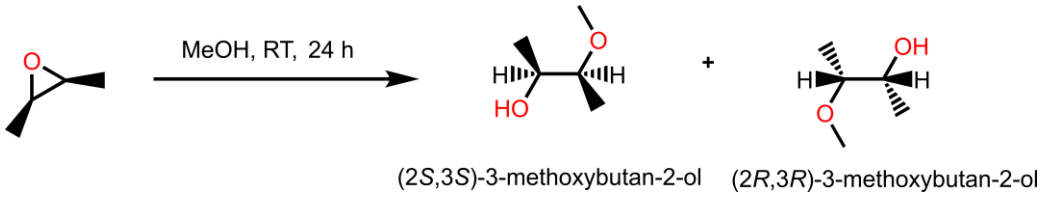

Figure 5.12. Methanolysis of *cis* 2,3-epoxybutane.

Control experiments were conducted in the absence of catalysts and they did not show any conversions. In the presence of **KSU-1** the reaction was slow and gave <1% conversion. In the presence of three different **KSU-1**$_{\mathbf{acid}}$ as the catalyst the reaction progressed in the following order: **KSU-1**$_{\mathbf{maleic}}$ showed higher conversion while **KSU-1**$_{\mathbf{succinic}}$ and **KSU-1**$_{\mathbf{itaconic}}$ had almost similar conversions (Figure **5.12** and **5.13**). These results strongly suggested that carboxylic acid groups acted as Brønsted acid catalysts during the epoxidation of the cis-2,3 epoxybutane. Higher catalytic activity of the maleic acid is attributed to its strong acidity; the conjugate base of maleic acid has higher stability due to conjugation to the C=C double bond which results higher acidity.[16] Yet overall the reaction conversions were low compared to what was reported by Cohen et al. Since our primary intension of this work is not to achieve higher conversion but to demonstrate the applicability of our previously developed concept of uniform independent binary functionalization to achieve enzyme-like complexity we decided to move forward with our results.

After establishing the catalytic behaviors of each of the **KSU-1**$_{\mathbf{acid}}$, the next step was to investigate the possibility of achieving enantioselectivity of the reaction using **KSU-1**$_{\mathbf{R\text{-}BA}}$. Our hypothesis was that after installing the chiral groups to **KSU-1**$_{\mathbf{acid}}$, catalytic reactions should favor one enantiomer over the other. Catalytic reactions were carried out in the presence of 20 mol % of each **KSU-1**$_{\mathbf{R\text{-}BA}}$ at room temperature for 24 h and aliquots were analyzed using ^{1}H-NMR after dilution with $CDCl_3$. Overall, the reaction conversions were lower compared to monofunctionalized catalysts which can be attributed to the slower diffusion of the substrate molecules through the more crowded MOF pores. Surprisingly, the reaction conversions with the bifunctionalized catalysts were the opposite of what we observed with **KSU-1**$_{\mathbf{acid}}$ (Figure **5.12** and **5.13**). Average conversions suggested that **KSU-1**$_{\mathbf{R\text{-}itaconic}}$ was a better catalyst compared to than **KSU-1**$_{\mathbf{R\text{-}maleic}}$ and **KSU-1**$_{\mathbf{R\text{-}succinic}}$.

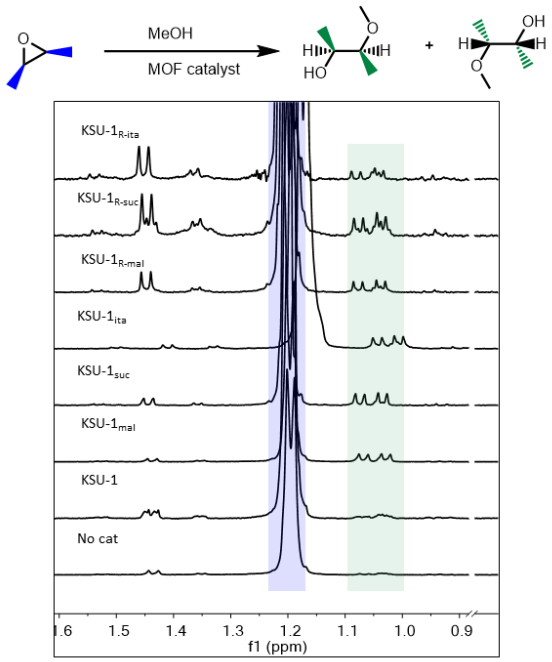

Figure 5.13. Partial ^{1}H-NMR of aliquots from the catalytic reaction diluted in $CDCl_3$.

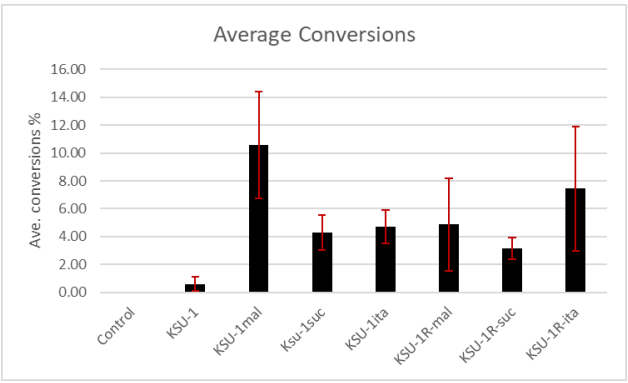

Figure 5.14. Average conversions with each catalyst after 24 h at RT**.**

In order to determine the enantioselectivity of the reaction, the reaction mixtures need to be analyzed by chiral high performance liquid chromatography (HPLC) or chiral gas chromatography (GC). It is also possible to extend this work not only to introduce a chiral group to **KSU-1$_{acid}$** but also hydrophobic group or hydrophilic group[17,18] into MOF through the -OH group of the DPG and see how it affects the epoxidation reaction.

5.5. Conclusion

In conclusion our goal was to demonstrate the applicability of our implemented strategy of uniform independent binary functionalization of a MOF material to fine tune the catalytic behavior of a MOF material. We have successfully synthesized chiral Brønsted acid catalysts through two step independent functionalization of a well-defined MOF **KSU-1**. During the catalysis experiments **KSU-1$_{acid}$** acted as Brønsted acid catalysts for the epoxidation of cis 2,3-epoxybutane. Upon introducing the chiral group to the **KSU-1$_{acid}$**, overall catalytic activity of the material was diminished yet we expect that it will result some enantioselectivity in the epoxidation reaction. Chiral HPLC or GC experiments needed to be done to determine the %ee of the products.

5.6. Experimental

Materials

All chemicals were used as received from commercial sources unless otherwise noted. Meso-*α*,*β*-di(4-pyridyl) glycol (DPG), maleic anhydride, (R)-(+)-α-Methylbenzyl isocyanate were purchased from TCI. Sulfuric acid-*d*$_2$ (D_2SO_4, 98 wt.% in D_2O, 99.5+% atom D), 2-aminoterephthalic acid (BDC-NH_2), succinic anhydride, itaconic anhydride and cis 2,3-epoxybutane were purchased from Aldrich. *N*,*N*-dimethylformamide (DMF), Chloroform ($CHCl_3$),and Acetonitrile (MeCN), Methanol (MeOH) were purchased from Fisher Scientific, and zinc nitrate hexahydrate from Strem Chemicals and 1,4-Diazabicyclo[2.2.2]octane (DABCO) were purchased from Oakwood Products. Dimethyl sulfoxide-*d*$_6$ (*d*$_6$-DMSO, 99.9 atom % D) was purchased from Cambridge Isotopes Laboratories.

Synthetic procedures

Synthesis of KSU-1.[20] $Zn(NO_3)_2 \cdot 6H_2O$ (95.2 mg, 0.32 mmol), **DPG** (106 mg. 0.49 mmol), and DMF (80 mL) were combined in a 500 mL Florence flask. The flask was heated at 60 °C in a 500 mL heating block until the solution became clear. A solution of **BDC-NH_2** (90.6 mg, 0.50 mmol) in DMF (20 mL) was added, and the flask incubated at 60 °C. After 48 h, the flask was removed from the heating block and left at room temperature for 48 h. Pale yellow crystals (40 mg, 35% yield) of the product were collected by filtration after several ~30 min washings with DMF.

General procedure for the synthesis of KSU-1anhydrides

Following a modified literature procedure,[16] **KSU-1** (15-20 mg, 0.0283 mmol, ca. 0.566 mmol equiv of $-NH_2$) was transferred into a into a 20 mL scintillation vial. The vial was charged with 8 mL of a 0.2 M solution of cyclic anhydride (56 equiv.) in $CHCl_3$ (stored in 3Å molecular sieves), and the mixture was left at room temperature for 12-24 h with continuous mixing on a Corning LSE Low Speed Orbital Shaker. The MOF material was then transferred to a new scintillation vial containing fresh $CHCl_3$ and mixed for ~30 min. The $CHCl_3$ was exchanged with fresh $CHCl_3$ 3 times, and then fresh DMF a further 3 times and stored under DMF.

General procedure for the synthesis of KSU-1$_{\text{chiral carbamate}}$

Following a modified literature procedure,[21] **KSU-1** (15-20 mg, 0.0283 mmol, ca. 0.566 mmol equiv of $-OH$) was transferred into a into a 20 mL scintillation vial. The vial was charged with 2 mL of a 0.2 M solution of chiral isocyanates (56 equiv.) in MeCN (stored in 3Å molecular sieves), and the mixture was left at 80°C for 6-8 h with continuous mixing on a Corning LSE Low Speed Orbital Shaker. The MOF material was then transferred to a new scintillation vial containing fresh MeCN and mixed for ~30 min. The MeCN was exchanged with fresh MeCN 3 times, and then fresh DMF a further 3 times and stored under DMF.

General procedure for the synthesis of KSU-1$_{\text{chiral BA}}$

KSU-1$_{\text{chiral carbamate}}$ (15-20 mg, 0.0149 mmol, ca. 0.0299 mmol equiv of $-NH_2$) was transferred into a into a 20 mL scintillation vial. The vial was charged with 8 mL of a 0.2 M solution of cyclic anhydride (53 equiv.) in $CHCl_3$ (stored in 3Å molecular sieves), and the mixture was left at room temperature for 12-24 h with continuous mixing on a Corning LSE Low Speed Orbital Shaker. The MOF material was then transferred to a new scintillation vial containing fresh $CHCl_3$ and mixed for ~30 min. The $CHCl_3$ was exchanged with fresh $CHCl_3$ 3 times, and then fresh DMF a further 3 times and stored under DMF.

Catalysis experiment

Followed a modified literature procedure.[16] In a typical experiment, crystalline solids that were stored in DMF were filtered through vacuum filtration and weighed (20 mol % BDC ligand) after considering the amount of DMF in the pores. Then it was transferred to a 4 ml scintillation vial charged with the epoxide substrate (145 mM, 7 µL) and MeOH (550 µL). Vials were left at room temperature for 24 h with continuous mixing on a Corning LSE Low Speed Orbital Shaker and 50 µL aliquot was taken and used for the 1H-NMR analysis after diluting with 500 µL of $CDCl_3$.

5.7. Characterization

Powder X-ray diffraction (PXRD)

Powder patterns were recorded on a Bruker AXS D8 Advance Phaser diffractometer with Cu Kα radiation ($\lambda = 1.5418$ Å) over a range of $5° < 2\theta < 40°$ in 0.02° steps with a 0.5 s counting time per step. Samples were collected from the bottom of the reaction vial as a thick suspension in DMF and spread on a Si-Einkristalle plate immediately before PXRD measurements.

Thermogravimetric analysis (TGA)

TGA was performed on a TGA-Q50 interfaced with a PC using TA Universal Analysis software. Samples were heated at a rate of 10 ºC/min under a nitrogen atmosphere. All samples were extensively solvent exchanged with fresh DMF prior to analysis.

Proton nuclear magnetic resonance (^{1}H NMR)

Spectra were recorded on a Brucker 400MHz NMR spectrometer (400 MHz for ^{1}H). NMR chemical shifts are reported in ppm against a residual solvent resonance as the internal standard (δ(d_6-DMSO) = 2.5 ppm or δ($CDCl_3$) = 7.26)). In a typical analysis, MOF materials stored in DMF were solvent exchanged with $CHCl_3$, isolated by vacuum filtration, and then evacuated in a vacuum oven at 80 °C overnight. Evacuated MOF samples (~8 mg) were transferred into an NMR tube and d_6-DMSO (0.6 mL) was added. Subsequently, D_2SO_4 (0.010 mL, 98% w/w in D_2O) was also added. The tubes were capped and sonicated until all the solid was dissolved (~ 1 min).

5.8. References

(1) Huang, Y.-B.; Fu, Y. Hydrolysis of Cellulose to Glucose by Solid Acid Catalysts. *Green Chem.* **2013**, *15* (5), 1095–1111. https://doi.org/10.1039/C3GC40136G.

(2) Liu, F.; Huang, K.; Zheng, A.; Xiao, F.-S.; Dai, S. Hydrophobic Solid Acids and Their Catalytic Applications in Green and Sustainable Chemistry. *ACS Catal.* **2018**, *8* (1), 372–391. https://doi.org/10.1021/acscatal.7b03369.

(3) Wang, P.; Zhao, Y.; Liu, J. Versatile Design and Synthesis of Mesoporous Sulfonic Acid Catalysts. *Sci. Bull.* **2018**, *63* (4), 252–266. https://doi.org/10.1016/j.scib.2018.01.017.

(4) Su, F.; Guo, Y. Advancements in Solid Acid Catalysts for Biodiesel Production. *Green Chem.* **2014**, *16* (6), 2934–2957. https://doi.org/10.1039/C3GC42333F.

(5) Gupta, P.; Paul, S. Solid Acids: Green Alternatives for Acid Catalysis. *Catal. Today* **2014**, *236*, 153–170. https://doi.org/10.1016/j.cattod.2014.04.010.

(6) Hattori, H. Solid Acid Catalysts: Roles in Chemical Industries and New Concepts. *Top. Catal.* **2010**, *53* (7), 432–438. https://doi.org/10.1007/s11244-010-9469-9.

(7) Atia, H.; Armbruster, U.; Martin, A. Dehydration of Glycerol in Gas Phase Using Heteropolyacid Catalysts as Active Compounds. *J. Catal.* **2008**, *258* (1), 71–82. https://doi.org/10.1016/j.jcat.2008.05.027.

(8) Moffat, J. B. Phosphates as Catalysts. *Catal. Rev.* **1978**, *18* (2), 199–258. https://doi.org/10.1080/03602457808081868.

(9) Siril, P. F.; Cross, H. E.; Brown, D. R. New Polystyrene Sulfonic Acid Resin Catalysts with Enhanced Acidic and Catalytic Properties. *J. Mol. Catal. Chem.* **2008**, *279* (1), 63–68. https://doi.org/10.1016/j.molcata.2007.10.001.

(10) Arata, K. Organic Syntheses Catalyzed by Superacidic Metal Oxides: Sulfated Zirconia and Related Compounds. *Green Chem.* **2009**, *11* (11), 1719–1728. https://doi.org/10.1039/B822795K.

(11) Gong, W.; Liu, Y.; Li, H.; Cui, Y. Metal-Organic Frameworks as Solid Brønsted Acid Catalysts for Advanced Organic Transformations. *Coord. Chem. Rev.* **2020**, *420*, 213400. https://doi.org/10.1016/j.ccr.2020.213400.

(12) Jiang, J.; Yaghi, O. M. Brønsted Acidity in Metal–Organic Frameworks. *Chem. Rev.* **2015**, *115* (14), 6966–6997. https://doi.org/10.1021/acs.chemrev.5b00221.

(13) Kumar, S.; Mohan, B.; Tao, Z.; You, H.; Ren, P. Incorporation of Homogeneous Organometallic Catalysts into Metal–Organic Frameworks for Advanced Heterogenization: A Review. *Catal. Sci. Technol.* **2021**, *11* (17), 5734–5771. https://doi.org/10.1039/D1CY00663K.

(14) Min, C.; Seidel, D. Asymmetric Brønsted Acid Catalysis with Chiral Carboxylic Acids. *Chem. Soc. Rev.* **2017**, *46* (19), 5889–5902. https://doi.org/10.1039/C6CS00239K.

(15) Cheon, C. H.; Yamamoto, H. Super Brønsted Acid Catalysis. *Chem. Commun.* **2011**, *47* (11), 3043–3056. https://doi.org/10.1039/C0CC04867D.

(16) Garibay, S. J.; Wang, Z.; Cohen, S. M. Evaluation of Heterogeneous Metal−Organic Framework Organocatalysts Prepared by Postsynthetic Modification. *Inorg. Chem.* **2010**, *49* (17), 8086–8091. https://doi.org/10.1021/ic1011549.

(17) Miura, H.; Kameyama, S.; Komori, D.; Shishido, T. Quantitative Evaluation of the Effect of the Hydrophobicity of the Environment Surrounding Brønsted Acid Sites on Their Catalytic Activity for the Hydrolysis of Organic Molecules. *J. Am. Chem. Soc.* **2019**, *141* (4), 1636–1645. https://doi.org/10.1021/jacs.8b11471.

(18) Decarpigny, C.; Ponchel, A.; Monflier, E.; Bleta, R. Effect of Functional Group on the Catalytic Activity of Lipase B from Candida Antarctica Immobilized in a Silica-Reinforced Pluronic F127/α-Cyclodextrin Hydrogel. *Gels* **2022**, *8* (1), 3. https://doi.org/10.3390/gels8010003.

(19) Chandra, B. P.; Wu, Z.; Ntim, S. A.; Rao, G. N.; Mitra, S. The Effect of Functional Group Polarity in Palladium Immobilized Multiwalled Carbon Nanotube Catalysis: Application in Carbon–Carbon Coupling Reaction. *Appl. Sci.* **2018**, *8* (9), 1511. https://doi.org/10.3390/app8091511.

(20) Samarakoon, K. P.; Satterfield, C. S.; McCoy, M. C.; Pivaral-Urbina, D. A.; Islamoglu, T.; Day, V. W.; Gadzikwa, T. Uniform, Binary Functionalization of a Metal–Organic Framework Material. *Inorg. Chem.* **2019**, *58* (14), 8906–8909. https://doi.org/10.1021/acs.inorgchem.9b00838.

(21) Samarakoon, K.; Yazdanparast, M.; Day, V. W.; Gadzikwa, T. Uniform and Simultaneous Orthogonal Functionalization of a Metal-Organic Framework Material. **2020**. https://doi.org/10.26434/chemrxiv.11482893.v2.